Endothelial cells serve as a cardiac progenitor population in the adult heart during homeostasis and contribute to repair after ischemic injury

By

Bryan Adam Fioret

Dissertation

Submitted to the Faculty of the

Graduate School of Vanderbilt University

in partial fulfillment of the requirements

for the degree of

DOCTOR OF PHILOSOPHY

In

Pharmacology

August, 2014

Nashville, Tennessee

Approved:

Professor Antonis K. Hatzopoulos

Professor Christopher B. Brown

Professor H. Scott Baldwin

Professor Joey V. Barnett

Professor Douglas B. Sawyer

To my parents, Rhonda and Phil, my brother, Dan, and my wife, Katherine.

I would not be who I am or where I am, without each of you.

ACKNOWLEDGEMENTS

This work would not have been possible without the financial support of the Vanderbilt Interdisciplinary Graduate Program, Training in Pharmacological Sciences Grant fellowship T32GM007628, an American Heart Association pre-doctoral fellowship 11PRE7600210, the HHMI/VUMC-Certificate Program in Molecular Medicine, and NIH grants U01HL100398 and R01HL083958.

I am deeply grateful to my mentor, Antonis Hatzopoulos, who has had tremendous positive influence in shaping my scientific mindset and skillsets as a graduate student and young scientist. Antonis has shown patience and understanding, especially during my early years in the lab, and helped me to develop into the scientist I am today. I have benefited greatly from our in-depth conversations, on countless occasions, and have experienced the scientific process first-hand through Antonis' guidance. Antonis has created a positive and supportive environment to perform scientific research, and has consistently encouraged me to improve as a researcher and scientist. I've also come to appreciate the importance of a correct bracket during NCAA March Madness, and the unparalleled taste of a free lunch awarded to the victor.

To my committee, I am greatly appreciative of your time and valuable scientific insight, which has helped to guide and strengthen my research. I would like to thank Chris Brown, Ph.D., for his efforts spent serving as chair of my committee during my years as a graduate student. I have benefited significantly from his experimental expertise and scientific knowledge. I greatly appreciate the time and support of Dr. Scott Baldwin, who has been a tremendous driving force behind the success and direction of my thesis work. I truly appreciate his contributions, particularly during committee

meetings, and respect his knowledge of the field. Dr. Joey Barnett has been a wonderful collaborator and mentor. His enthusiasm for Pharmacology was one of the reasons I joined the department, and I am grateful for the time spent discussing both my thesis project and our TGFβR3 collaboration. I would like to thank Dr. Douglas Sawyer for his clinical expertise and time spent as my clinical mentor within the Certificate Program in Molecular Medicine. Observing the human side of cardiovascular disease, away from the lab bench and from the perspective of the patient and family, creates meaning and relevance for the work we do. Finally, to the unofficial sixth member of my committee, I am grateful for the expertise of Dr. Ela Knapik. She has provided important feedback about my project at crucial junctions, which helped to guide it into the work it is today.

I have tremendously enjoyed my time within the Hatzopoulos Laboratory, and appreciated working alongside its members, both past and present. I am deeply grateful for the pioneering work performed by Omo Aisagbonhi which laid the groundwork for my current project. I thoroughly enjoyed my time in the lab spent with past members: Joel Walthall, Meena Rai, Jianyong Hu, Amrita Mukherjee, Andy Schoenhard, Vineeta Tanwar, Jeremy Heimfeld, and Mitch Funke. And I will miss the companionship of the current members, Jeff Bylund, David Paik, and Lehanna Sanders, after I move on from Vanderbilt. I also would like to acknowledge Paige DeBenedittis, Leshana Saint-Jean, and Kevin Tompkins, of the Baldwin lab, who have been of great help to my work by providing reagents, experimental animals, and sound scientific advice.

I would not have made it to this point without the love and support of my family, and I am forever grateful for each of them. My parents, Phil and Rhonda, have provided endless support and encouragement, and chocolate chip muffins. My other set of

parents, Denise and Alan, have been wonderful and have made Nashville feel like it's just down the road from Louisville. My brother Dan is a life-long companion and constant friend. And, perhaps most importantly, my wife Katherine has been invaluable with the support and encouragement she has provided me since the day we met.

Alright, now let's talk science.

TABLE OF CONTENTS

Page

LIST OF FIGURES

Figure **Page**

Chapter I

Chapter II

Chapter III

Chapter IV

Chapter V

Chapter VI

LIST OF TABLES

Table **Page**

LIST OF ABBREVIATIONS

AngII	Angiotensin II
ASC	Adult Stem Cell
β-Gal	Beta-Galactosidase
BM	Bone Marrow
BMP	Bone Morphogenetic Protein
BSA	Bovine Serum Albumin
CSC	Cardiac Stem Cell
CM	Cardiomyocyte
Col IV	Collagen IV
Cre	Cre Recombinase
cTnT	Cardiac Troponin T
Cx43	Connexin 43
Cy	Cyanine
DAPI	4’,6-Diamidino-2-Phenylindole
EC	Endothelial Cell
ECM	Extracellular Matrix
EMT	Epithelial-To-Mesenchymal Transition
EndMT	Endothelial-To-Mesenchymal Transition
ESC	Embryonic Stem Cell
ER^T	Estrogen Receptor-Tamoxifen Sensitive
FSP1	Fibroblast Specific Protein 1
H&E	Hematoxylin and Eosin
HSC	Hematopoietic Stem Cell
HFSC	Hair Follicle Stem Cell
ICAM-1	Intercellular Adhesion Molecule-1
IF	Immunofluorescence
IHC	Immunohistochemistry
ISC	Intestinal Stem Cell
Lgr5	Leucine-Rich Repeat-Containing GPCR5
MCEC	Murine Cardiac Endothelial Cell

MI	Myocardial Infarction
mg	Milligram
mL	Milliliter
mM	Millimolar
µl	Microliter
nGFP	Nuclear Green Fluorescent Protein
NSC	Neural Stem Cell
PBS	Phosphate Buffered Saline
PECAM-1 (CD31)	Platelet Endothelial Cell Adhesion Molecule
PFA	Paraformaldehyde
qRT-PCR	Quantitative Reverse Transcriptase Polymerase Chain Reaction
RFP	Red Fluorescent Protein
ROSA (R26R)	Reverse Orientation Splice Acceptor
Sca1	Stem Cell Antigen-1
SCL	Stem Cell Leukemia
αSMA	Alpha Smooth Muscle Actin
TAC	Trans-Aortic Constriction
TGFβ	Transforming Growth Factor Beta
Tie1	Tyrosine kinase with immunoglobulin-like and EGF-like domains 1
TNFα	Tumor Necrosis Factor Alpha
TX-100	Triton X-100
VCAM-1	Vascular Cell Adhesion Molecule-1
VE-Cadherin	Vascular Endothelial Cadherin
VEGF	Vascular Endothelial Growth Factor
VEGFR2	Vascular Endothelial Growth Factor Receptor 2
vWF	von Willibrand Factor
X-gal (BCIG)	5-bromo-4-chloro-3-indolyl-β-D-galactopyranoside
YFP	Yellow Fluorescent Protein

CHAPTER I

INTRODUCTION

Cardiac repair after ischemic injury

An estimated seventeen million people die each year due to cardiovascular disease, and the most common cause of death is myocardial infarction (MI) (Go *et al*., 2013). MI occurs when atherosclerotic plaque rupture and subsequent platelet aggregation form a coronary thrombus which occludes the coronary artery. The ensuing ischemia and lack of oxygen causes cardiomyocyte (CM) necrosis within minutes of the occlusion (Frangogiannis, 2012). While recent studies indicate the adult myocardium is capable of regenerating cardiac tissue, the heart lacks a robust regenerative response to replace the substantial amount of cardiac tissue that is lost after a severe ischemic injury (Uchida *et al*., 2013; Laflamme and Murry, 2011). Consequently, the heart naturally repairs the injured area with a collagenous scar which impedes cardiac contractility and can cause adverse remodeling.

During ischemia, a lack of oxygen impedes oxidative phosphorylation and leads to the depletion of adenosine triphosphate (ATP). Consequently, cardiomyocyte ion pumps fail to function, the levels of intracellular calcium [Ca^{2+}] rise, and mitochondrial Ca^{2+} accumulation occurs (Murphy and Steenbergen, 2008). The ischemic injury is often exacerbated by reperfusion and the generation of reactive oxygen species (ROS). ROS are generated as oxygen returns to the cells during reperfusion and, coupled with mitochondrial matrix Ca^{2+} overload, opens the mitochondrial permeability transition

pore. This process induces activation of mitochondrial apoptotic pathways, such as caspases, and exhausts the cell of its ATP. Cell death and rupture of the plasma membrane occur due to disrupted ion homeostasis, lack of ATP, ROS accumulation, and intracellular proteolysis.

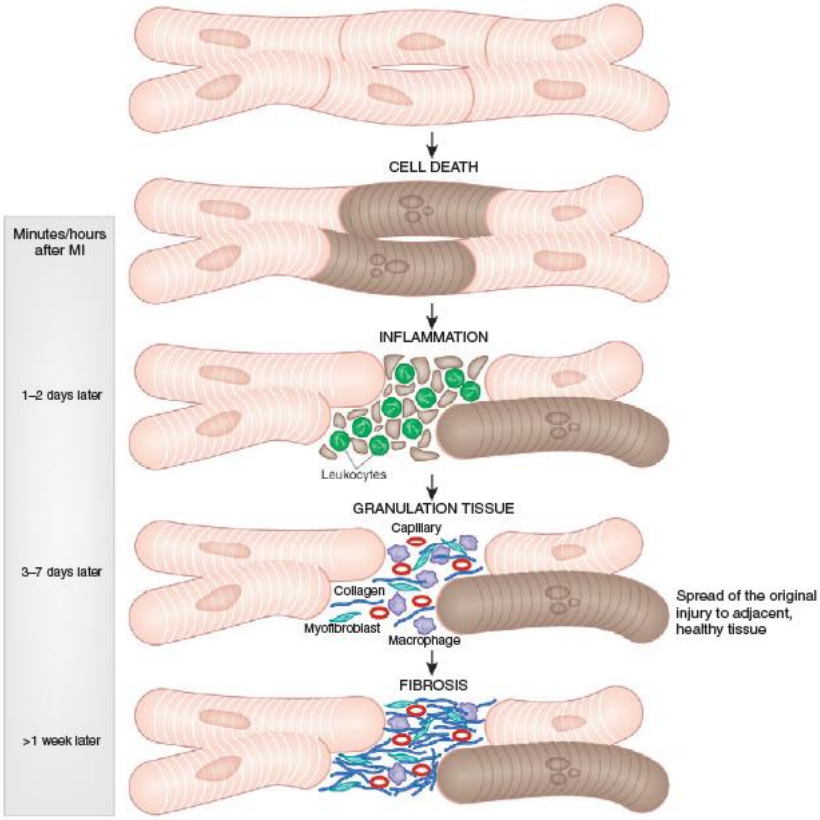

Figure 1. Key stages of repair after ischemic cardiac injury. After occlusion of a coronary artery, cell death occurs within minutes. The necrotic debris released from rupture of the cardiac cells induces an inflammatory phase, which progresses into a reparative granulation tissue phase after several days. Neovascularization and collagen deposition occur over the next several weeks until a dense scar (fibrosis) has replaced the lost tissue. Figure from Boudoulas and Hatzopoulos (2009).

An inflammatory response is then triggered by the remaining surviving cells as they are exposed to the surrounding necrotic debris and toxic mediators (**Figure 1**, from Boudoulas and Hatzopoulos, 2009**)**. This initial immune response begins the process of infarct healing after cardiac ischemic injury. Chemokines such as interleukin (IL)-1,

monocyte chemoattractant protein-1 (MCP-1), and tumor necrosis factor-α (TNF-α) attract circulating leukocytes to the infarct (Frangogiannis, 2008). Cytokines stimulate endothelial cells (ECs) to upregulate expression of E-selectin, intercellular adhesion molecule-1 (ICAM-1), and vascular cell adhesion molecule-1 (VCAM-1), which promotes adhesion between ECs and infiltrating leukocytes. Extravasation of leukocytes from the microvasculature to the site of injury occurs to remove dead cells and debris from the infarct. Neutrophils and monocytes also transmigrate into the infarcted myocardium through integrin-mediated interaction with ECs and clear the injury of cells and matrix debris. Monocytes mature into macrophages which, over time, also clear the injury to leave enlarged capillaries throughout sparse amounts of surviving cardiac tissue.

The inflammatory phase of infarct healing switches to a granulation tissue deposition phase within three to four days after the injury, (**Figure 1**) and is mediated in part by transforming growth factor-β (TGF-β) (Frangogiannis, 2014). Fibroblasts and ECs begin to proliferate and replace the inflammatory blood cells. Angiogenic and fibrogenic growth factors, secreted by leukocytes, promote neo-vascularization and synthesis of extracellular matrix (ECM) proteins, respectively. Fibroblasts differentiate into myofibroblasts, which are nonvascular, α-smooth muscle actin (αSMA) positive, interstitial cells that transiently appear after MI and deposit collagen. Myofibroblast proliferation within the healing wound produces ECM and forms a microvascular network (Frangogiannis, 2014).

Ultimately, myofibroblasts, macrophages, and new blood vessels comprise the granulation tissue of the infarct within 7 days post-MI. The neovessels formed are

required for delivery of oxygen and nutrient-rich blood to the proliferative cells of the infarct. Angiogenic growth factors such as vascular endothelial growth factor (VEGF) and angiopoietins (Ang)-1 and Ang-2 are released to modulate angiogenesis.

Maturation of the granulation tissue occurs within weeks of the injury, and the tissue develops into a dense collagen-based scar. By this time in the repair phase, the majority of myofibroblasts cease to deposit collagen and undergo apoptosis. The dense collagen-rich scar contains mature vessels surrounded with mural cells. Due to the significant cellular and molecular changes that occur in response to MI, the infarcted left ventricle may also undergo dilative remodeling to compensate for the reduced contractile capacity, and experience electrical instability in response to the infarction. The adverse cardiac remodeling, and systolic dysfunction resulting from the ischemic injury, may cause heart failure or arrhythmias, leading to death.

Endothelial-to-mesenchymal transition contributes to cardiac repair

Scar formation, which occurs with deposition of collagen from myofibroblasts, is necessary to heal the wound and provide stability to the infarcted ventricular wall. However, excessive amounts of dense, collagenous scar can impede efficient electromechanical coupling between surviving regions of CMs. Multiple origins of cardiac fibroblasts which contribute to scar formation have been proposed, and include resident cardiac fibroblasts, bone marrow-derived fibroblasts and endothelial cell-derived fibroblasts (Zeisberg and Kalluri, 2010). In addition, fibroblasts may also derive from the epicardium, or the mesenchymal cells that surround ECs in microvessels and

capillaries, known as pericytes; but these putative sources have yet to be confirmed with fate-mapping studies (Zeisberg and Kalluri, 2010).

Epithelial-to-mesenchymal transition (EMT) is a well-characterized process in which epithelial cells lose their intrinsic characteristics and begin to express mesenchymal, myofibroblast markers (Thiery *et al*., 2009). However, studies have shown a role for the endothelium in generation of cardiac fibroblasts, through a process known as endothelial-to-mesenchymal transition (EndMT) (Zeisberg *et al*., 2007; Aisagbonhi *et al*., 2011). EndMT is a similar, more recently discovered process, which instead involves a mesenchymal transition of ECs (Boudoulas and Hatzopoulos, 2009). During EndMT, ECs down-regulate expression of endothelial genes, including vascular endothelial Cadherin (VE-Cadherin), platelet endothelial cell adhesion molecule (PECAM-1, or CD31), von Willebrand Factor (vWF), and the angiopoietin receptor tyrosine kinases, Tie1 and Tie2 (Ghosh *et al*., 2012; Garcia *et al*., 2012). Concurrent with down-regulation of EC markers, the trans-differentiating cells begin to express mesenchymal markers such as α-smooth muscle actin (αSMA) and Vimentin, and acquire more migratory and invasive properties.

Myofibroblasts derived from EndMT may generate up to 35% of subepicardial infarct myofibroblasts (Aisagbonhi *et al*., 2011), and represent a significant, and only recently discovered, proportion of contributing repair cells. Consequently, studies investigating the cellular and molecular mechanisms of EndMT as it relates to repair post-MI are warranted, and may provide new treatments to limit excessive deposition of collagen and minimize maladaptive fibrosis following ischemic injury.

EndMT connects angiogenesis and fibrosis after myocardial infarction

An increasing number of studies implicate both EMT and EndMT as important processes for generation of myofibroblasts which contribute to fibrosis (Wynn, 2008; Boudoulas and Hatzopoulos, 2009). Notably, these processes are not restricted to a particular organ, and contribute to repair in numerous organs throughout the body. For instance, EndMT has been implicated in lung, kidney, and cardiac fibrosis (Arciniegas *et al*., 2007; Wada *et al*., 2011; Goumans *et al*., 2008). In the lung, hypoxia-induced pulmonary vascular remodeling has been shown to induce a transdifferentiation of pulmonary arteriolar ECs into smooth muscle-like cells (Zhu *et al*., 2006). Significant damage to the kidney activates resident fibroblasts, pericytes, bone marrow-derived cells, epithelial cells, and endothelial cells, which all contribute to fibrosis. In the kidney, ECs have been shown to undergo EndMT and contribute to tubulointerstitial fibrosis. Similarly, in the adult mouse heart, pressure overload, chronic allograft rejection, or ischemic injuries such as MI, induce EndMT which generates myofibroblasts that deposit collagen and contribute to scar formation during repair (Zeisberg *et al*., 2007).

In addition to generating myofibroblasts during tissue repair, EndMT also contributes to neovascularization during repair after ischemic injury. The process of vessel branching during revascularization of injured tissue requires that ECs develop a mesenchymal phenotype (Gerhardt *et al*., 2003). Furthermore, inhibition of the EndMT-associated gene Vimentin has been shown to reduce angiogenesis in tumor cells (Lahat *et al*., 2010). The anti-angiogenic effects were observed in proliferating ECs, with minimal consequence to non-proliferating ECs. Similarly, suppression of VEGF and VEGFR2 in prostate tumors inhibited tumor angiogenesis and progression of

mesenchymal transition required for local invasion and metastasis (Singh *et al*., 2008). These studies support the idea that EndMT is necessary for cell migration and angiogenesis during periods of tissue repair, particularly after ischemic injury.

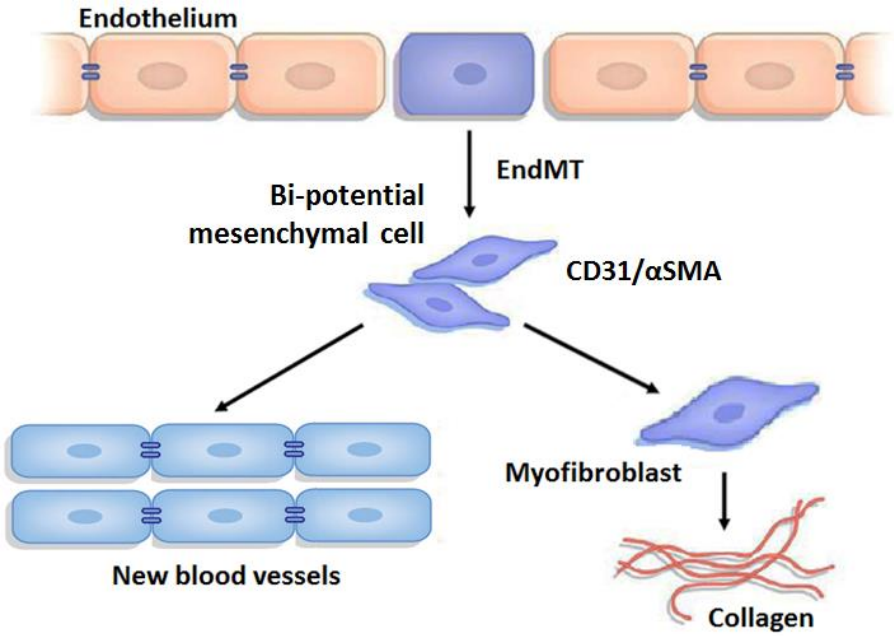

Figure 2. Angiogenesis and fibrosis are connected through EndMT. After injury, local and systemic mediators induce endothelial cells to undergo EndMT. These cells remove from the vasculature and down-regulate expression of CD31, while simultaneously upregulating expression of the mesenchymal marker αSMA. The resulting bipotent mesenchymal cells either generate new blood vessels (neovascularization) or form myofibroblasts, which deposit collagen. Figure modified from Aisagbonhi *et al*., 2011.

EndMT has been observed in the production of myofibroblasts which contribute to cardiac fibrosis, and implicated in angiogenesis, specifically during vessel branching. Thus, EndMT may connect the beneficial neovascularization and detrimental fibrosis which occurs during cardiac repair after ischemic injury (**Figure 2**, from Aisagbonhi *et al*., 2011). This connection may provide the opportunity to improve the course of cardiac repair post-MI by temporal manipulation of ECs and myofibroblasts. EndMT may be a general post-injury repair mechanism providing a novel therapeutic target to bolster the

beneficial angiogenic response or minimize maladaptive fibrosis, and ultimately improve cardiac repair post-infarction.

Endothelial cell plasticity

The studies above show ECs contain the potential to become mesenchymal cells, and indicate mature ECs are not terminally differentiated. This cellular plasticity of adult ECs is likely retained from their multi-lineage potential as observed during heart formation. Understanding the contribution of the vasculature during cardiac development will provide insight into the plasticity of the endothelium in the adult heart.

Throughout embryogenesis, epithelial and endothelial mesenchymal transitions are critical processes for tissue development. Both EMT and EndMT are necessary to generate the mesenchymal cells which will give rise to the heart (Boudoulas and Hatzopoulos, 2009). During gastrulation, the primitive ectoderm forms the mesoderm through EMT, and a subset of mesodermal cells then give rise to cardiovascular progenitors (Moorman *et al*., 2007). The mesodermal/mesenchymal cells in the lateral plate near the foregut begin to express the early cardiac regulatory genes *Nkx2-5*, *Gata4* and *Mef2c*. Subsequently, endocardial cells derived from the inner cardiac tube undergo EndMT, migrate into the surrounding cardiac jelly, and form the endocardial cushions (Person *et al*., 2005). This tissue eventually matures into the heart valves. Two additional EMTs occur to create the cardiac neural crest cells (which migrate to the heart and form the aortico-pulmonary septum), and the epicardial-derived progenitor cells (EPDCs; which differentiate into interstitial and perivascular fibroblasts, and smooth muscle cells, of the developing blood vessels) (Snider *et al*., 2007) (Winter and Gittenberger-de Groot, 2007).

After birth, EMT and EndMT contribute to adult tissue homeostasis. However, the contribution of EndMT to regeneration of the adult heart remains to be determined. Interestingly, adult cells that have undergone EMT appear to develop stem cell characteristics (Mani *et al*., 2008). Furthermore, evidence indicates EMT of tumor epithelial cells generates cells with properties of stem cells, such as a proliferative ability for self-renewal and increased migratory capacity (Hollier *et al*., 2009). Based on these studies, it is probable that EndMT is involved with maintenance of cardiac homeostasis and is necessary for cell and tissue regeneration, using the vasculature as an initial progenitor source. From these initial findings, I hypothesize that endothelial cells contribute to the maintenance of cardiac tissue during homeostasis through mechanisms of EndMT.

The role of cardiac stem and progenitor cells in the adult heart

Before exploring the hypothesis that ECs contribute to regeneration of cardiac tissue, it is first necessary to understand the numerous, putative cardiac stem and progenitor cells which have been identified in the adult heart. Fish and some amphibian species possess a greater cardiac regenerative potential than their mammalian counterparts (Laflamme and Murry, 2011). Traditionally, the mammalian heart was thought of as a post-mitotic organ without intrinsic mechanisms to replace cardiomyocytes. Under this model, CM number was determined shortly after birth, and no additional CMs appeared to be generated within the adult heart (Beltrami *et al*., 2001; Leri *et al*., 2011). However, an increasing number of studies have indicated the existence of cardiac stem cell (CSC) populations, endogenous to the adult myocardium

(Bearzi *et al*., 2007; Martin-Puig *et al*., 2008; Segers and Lee, 2008; Uchida *et al*., 2013). Recent studies documented moderate annual CM renewal rates in the adult mammalian heart, averaging from 0.4% to 1% (Bergmann *et al*., 2009) (Murry and Lee, 2009). To date, each putative population has varied expression of surface markers, unique or unknown origins, self-renewal capabilities, and cardiac potential (Aguirre *et al*., 2013).

The origins of cardiac tissue renewal mechanisms have been actively pursued, leading to the identification of several distinct cardiac cell types with stem cell characteristics proposed to contribute to maintenance of the adult mammalian heart (Boudoulas and Hatzopoulos, 2009). One such population consists of cells that form cardiospheres in suspension and differentiate to CMs, endothelial cells (ECs), and smooth muscle cells (SMCs) (Messina *et al*., 2004; Smith *et al*., 2007).

Cardiac stem cells (CSCs) also include c-Kit expressing cells, which generate CMs, ECs and SMCs after injury (Beltrami *et al*., 2003; Rota *et al*., 2008; Ellison *et al*., 2013). A different CSC type consists of Side Population (SP) cells (Hierlihy *et al*., 2002; Martin *et al*., 2004; Mouquet *et al*., 2005). The potential of SP cells to differentiate to cardiac cells is higher in the subgroup that expresses Stem cell antigen 1 (Sca1) (Pfister *et al*., 2005).

$Sca1^+$ cells independently isolated from adult cardiac tissue express early regulators of cardiac differentiation such as Gata4 and, when stimulated, Nkx2.5 and sarcomeric proteins (Oh *et al*., 2003). $Sca1^+$ cells home to infarcted myocardium, yielding CMs around the injury area and improving cardiac function (Oh *et al*., 2003; (Wang *et al*., 2006). Recent transcriptional profiling suggests $c\text{-}Kit^+$ cells represent a

less differentiated phenotype, whereas SP and $Sca1^{+}$ cells are more committed to the cardiac lineage (Dey *et al*., 2013).

Lessons from *bona fide* adult stem cells

In the heart, little is known about the origins of cardiac stem cells or the structural organization of their niche. By contrast, adult organs including the hair follicles, gut, bone marrow (BM), and brain, harbor adult stem cells (ASCs) in specialized niches, allowing for spatial and temporal regulation of the renewal process (Li and Clevers, 2010; Fuentealba *et al*., 2012). These niches support quiescent stem cell populations that, upon stimulation, give rise to transient amplifying progenitors which differentiate to mature, tissue-specific cell types (**Figure 3**, modified from Li and Clevers, 2010; and Fuentealba *et al*., 2012).

The hair follicle bulge serves as a niche for hair follicle stem cells (HFSCs; **Figure 3A**). HFSCs exist in a quiescent state in the bulge region and active proliferating state in the hair germ (dermal papilla, DP), and are capable of generating all lineages of the hair (Li and Clevers, 2010; Tumbar, 2004). These two unique regions allow the HFSC niche to restrict HFSC growth and differentiation until replenishment of cells is

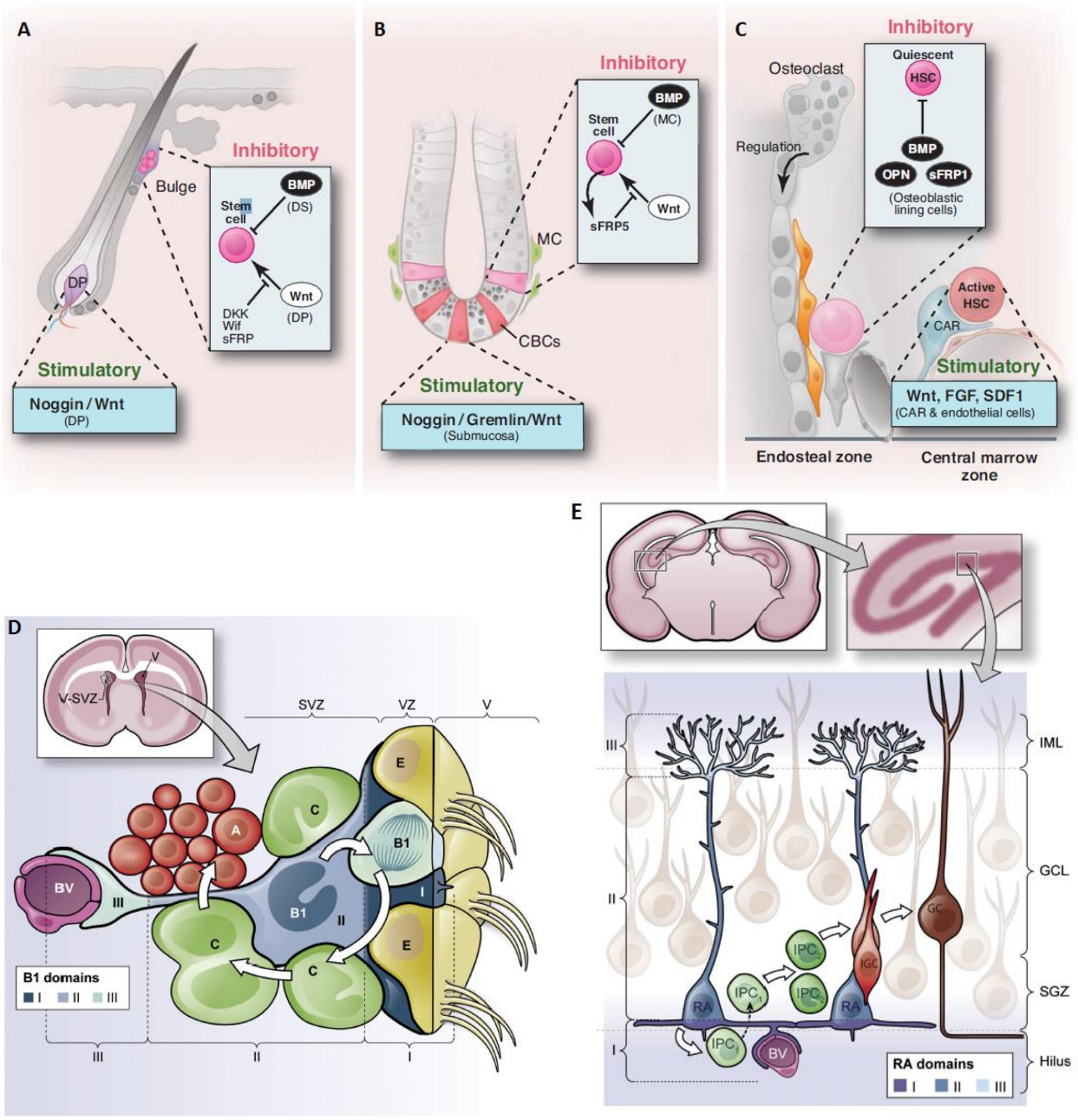

Figure 3. Adult stem cell niches in the hair follicle, bone marrow, gut, and brain. The adult stem cells of the (A) hair follicles (hair follicle stem cells), (B) gut (intestinal stem cells), (C) bone marrow (bone marrow stem cells), (D) ventricular-subventricular zone (V-SVZ) of the brain (neural stem cells, NSCs) and (E) subgranular zone (SGZ) of the brain (NSCs), are unique clusters of undifferentiated cells which reside in the specialized tissue-specific niches of their respective organ. They have the ability to self-renew and to differentiate into some or all of the mature cells of the organ in which they reside (Scadden, 2006). They are also known as somatic stem cells, or stem cells of the body, to distinguish them from germ cells involved in reproduction. Figure modified from Li and Clevers, 2010; and Fuentealba *et al*., 2012.

required. The stem cell marker Leucine-rich repeat-containing GPCR5 (Lgr5) is expressed in the bulge and hair germ, and can be used to sub-classify these populations of cells. The canonical Wnt, Noggin, and BMP signaling pathways are critical regulators of the bulge HFSC niche, controlling cell proliferation and quiescence. The proteins DKK, Wif, and sFRP are canonical Wnt pathway antagonists.

The intestinal stem cell (ISC) niche is located at the bottom of the intestinal Crypts of Lieberkühn (crypts), which are small recesses within the epithelial lining of the small intestine and colon (**Figure 3B**). Both of these regions of the gastrointestinal (GI) tract contain crypts, however only the small intestine contains villi (Moore and Lemischka, 2006; Jiang and Edgar, 2012). The ISC niche generates all cells of the small intestine, and this occurs as ISCs mature as they migrate upwards into the villi. Two populations of ISCs exist within the crypt niche of the small intestine, both of which are multipotent and capable of self-renewal. The first, at the +4 position from the crypt base, is a quiescent population of slow cycling, label-retaining cells, adjacent to mesenchymal cells (MCs) (Li and Clevers, 2010). This population is marked by Bmi-1, mTert, and Hopx (Sangiorgi and Capecchi, 2008). The second ISC population termed crypt-based columnar cells (CBCs) is found at the bottom of the crypt, interspersed between supportive Paneth cells, and marked by Lgr5, CD133, and Sox9 (Jiang and Edgar, 2012; Tian *et al*., 2011). Similar to the HFSC niche, the canonical Wnt and BMP signaling pathways regulate cell proliferation and quiescence.

Within the BM, the hematopoietic stem cell (HSC) niche consists of two general sites: (1) a quiescent, osteoblastic niche at the endosteum, and a (2) proliferative, vascular niche in the central marrow **(Figure 3C**) (Nakamura-Ishizu and Suda, 2012).

Within the endosteal niche, osteoblast (OB) support cells and osteoblastic lining cells reside along the endosteum. Osteoclasts (OCLs) and macrophages exert structural and regulatory roles within the endosteal niche. OCLs form cavities in the bone in which HSCs reside. Maintenance of HSC quiescence within the endosteal niche is mediated by osteopontin (OPN), BMP signaling, and repression of canonical Wnt signaling via sFRP-1, (Li and Clevers, 2010). In the central marrow niche, to maintain blood cell homeostasis, quiescent long term-HSCs within the endosteal niche migrate to the sinusoids of the vascular niche in the central marrow, and become rapidly cycling short term-HSCs. BM sinusoidal endothelial cells line the lumen of these vessels and express vascular endothelial growth factor receptor-2 (Nakamura-Ishizu and Suda, 2012). Perivascular CXCL12-abundant reticular (CAR) cells provide structural support to the sinusoids at the central marrow. Regulation in the vascular niche is achieved by a balance of canonical Wnt, Fibroblast Growth Factor (FGF), Notch, SDF1, and BMP signaling.

Adult neurogenesis has best been characterized within neural stem cell (NSC) niches located in the ventricular-subventricular zone (V-SVZ) of the lateral ventricles and subgranular zone (SGZ) of the dentate gyrus (Decimo *et al*., 2012). During neural development, radial glial cells give rise to a group of astroglial-like cells, known as B1 cells, which persist in the adult brain and function as NSCs (Fuentealba *et al*., 2012). Neurogenesis within the V-SVZ utilizes these B1 cells, located in the walls of the lateral ventricles, which extend through this region to contact blood vessels within the SVZ (**Figure 3D**) (Fuentealba *et al*., 2012). B1 cells are induced to generate a subpopulation of transient amplifying cells, also known as intermediate progenitor cells (IPCs), or type

C cells. These TACs divide briefly and then become neuroblasts (type A cells) which, in rodents, migrate along the rostral migratory stream to the olfactory bulb and mature into interneurons (Kriegstein and Alvarez-Buylla, 2009). A second NSC niche exists in the subgranular zone of the dentate gyrus (DG), within the hippocampus (**Figure 3E**) (Fuentealba *et al*., 2012). The DG is composed of several layers, with the SGZ located at the bottom, directly above the hilus (a structure where blood vessels and nerves enter). The granule cell layer (GCL) and inner molecular layer (IML) exists above the SGZ. In the SGZ, astroglial cells, known as radial astrocytes (RAs) or type 1 progenitors, serve as the neural stem cell. When induced, RAs generate transient amplifying progenitors known as intermediate progenitor cells -1 and -2 (IPC_1, IPC_2) or type 2a and 2b, respectively. Once generated, IPC_1 cells quickly develop into proliferating IPC_2 cells, characterized by expression of the early neuronal marker, doublecortin (Lugert *et al*., 2012). IPC_2 cells then develop into immature granule cells (IGCs) which become mature granule cells (GCs) and extend axons into both the hilus and inner molecular layer of the dentate gyrus.

ASCs primarily differ from their embryonic stem cell (ESC) counterparts in both their origins and lineage differentiation capabilities. ESCs, derived from the inner cell mass of the blastocyst, are pluripotent and capable of differentiating into the three germ layers of the embryo (endoderm, mesoderm and ectoderm) and generating all embryonic and somatic cell types (Thomson *et al*., 1998). Unlike ESCs whose origins are clearly defined, the origins of ASC populations, particularly those in the heart, are still uncertain. ASC differentiation potential is also more limited (multipotent, instead of

pluripotent) and generally lineage restricted to the cell types of their host organ (Jones and Wagers, 2008).

ASC populations are maintained through symmetric cell divisions, in which two identical daughter stem cells are generated. They are also capable of generating multipotent progenitors with limited self-renewal capacity through asymmetric division (Jones and Wagers, 2008). One of the primary characteristics of ASCs is their ability to self-renew indefinitely. Consequently, they play a vital role in the maintenance of organ homeostasis by replacing dying cells lost to wear-and-tear, and also serve as a regenerative cell source after tissue damage or disease (Jones and Wagers, 2008).

The number of organs in which ASCs have been identified and characterized is continuously growing. When studying putative cardiac stem cell populations, common themes observed with ASCs of other organs (i.e.: bone marrow, hair follicles, gut, and brain) can be used as an initial framework for generating testable hypotheses. However, even with these more extensively characterized stem cell populations, questions remain regarding the mediators which regulate their proliferation, differentiation, and fate. Consequently, significant effort has been applied towards understanding the regulatory signals and the regions in which they reside: the stem cell niche.

Adult stem cell niches

The adult stem cell niche is an intricate, tissue-specific structure, responsible for maintenance of resident ASC populations, and regulation of their differentiation throughout the lifetime of an organism. This remarkable process occurs in numerous organs, and often makes use of similar structural, cellular, molecular, and transcriptional

themes (Scadden, 2006; Li and Clevers, 2010). While each niche is unique, they all support their resident stem cell using a combination of stromal support cells, soluble mediators, ECM and cell adhesion components, neuronal innervation, and vascular networks (**Figure 3**). The integration of numerous regional and systemic factors ultimately regulates ASC activity in a spatial and temporal manner (Jones and Wagers, 2008). Cellular and molecular methods to manipulate each tissue-specific stem cell population (BM, hair follicle, gut, brain, cardiac, etc.) will likely be achieved most optimally through regulation of their niches.

Ultimately, maintenance of adult stem cells occurs through regulation of quiescent (slow-cycling) and active (rapidly proliferating) populations (Li and Clevers, 2010). Support cells within the niche control these opposing processes through common molecular signaling pathways, such as canonical Wnt, Noggin, or BMP pathway mediators, which stimulate or inhibit stem cell proliferation and differentiation. Niche stem cells are responsive to secreted factors through various receptors, and when induced to proliferate, either generate identical daughter cells or precursors destined to become mature cells of the organ. This niche-mediated regulation of ASCs is crucial for maintenance of the tissue, and repair after damage.

Summary and Hypothesis

The information obtained from studies of stem cells and their niches in the BM, hair follicle, gut, and specific regions of the brain, can be extrapolated to predict characteristics of cardiac stem cells and their putative niche. It is likely that a CSC niche will contain quiescent and rapid populations of cells, maintained by support cells and

mediated by one or more of the signaling pathways described previously. Furthermore, previous studies demonstrate that after acute ischemic injury in the adult heart, endothelial-to-mesenchymal transition produces bipotent cells that generate both endothelial cells and myofibroblasts during scar formation (Aisagbonhi *et al*., 2011). Other groups have documented the ability of adult ECs to generate multipotent stem-like cells via EndMT in organs such as the bone, demonstrating EC plasticity and the ability to differentiate to alternative cell types (Medici *et al*., 2010). Based on these findings, and increasing evidence that the adult heart harbors an endogenous population of CPCs, I hypothesized that ECs serve as cardiac progenitors and contribute to the maintenance of cardiac tissue during homeostasis.

CHAPTER II

ENDOTHELIAL CELL LINEAGE TRACING LABELS CARDIOMYOCYTES IN THE ADULT HEART

INTRODUCTION

Although it is becoming increasingly evident that cardiac stem or progenitor populations exist, there is currently a debate about the regenerative ability of the adult myocardium (Kajstura *et al*., 2012). What is clear is that after injury, any natural regenerative ability of endogenous cells is inadequate to restore lost cardiac tissue. Instead, the myocardial response to infarction leads to scar formation, left ventricular remodeling, and heart failure.

While reports suggest that adult ECs contribute to cardiac fibrosis and mesenchymal cells after injury (Aisagbonhi *et al*., 2011; Zeisberg *et al*., 2007; Chen *et al*., 2012), studies in the vertebrate embryo indicate they also contain regenerative potential. For example, during development, misspecification of the embryonic endothelium to a cardiac fate is observed with knockout of the transcriptional regulator, stem cell leukemia (SCL) (Van Handel *et al*., 2012). SCL-/- mouse embryos display beating CMs in endothelial tissues, which derived from hemogenic endothelium and the endocardium. This study indicates SCL as a master regulator during heart development, suppressing cardiogenesis in favor of inducing hemogenic endothelium to endothelial and hematopoietic fate.

Thus, evidence increasingly indicates that adult ECs retain a degree of plasticity, and appear to possess properties of progenitor cells. These cells may serve as a new potential target to improve cardiac recovery after ischemic injury. Before manipulating them after injury however, it is first necessary to characterize their contribution to cardiac homeostasis (in the uninjured heart) and determine to what degree, if any, adult ECs exhibit cardiogenic potential. To study the fate of ECs in the adult heart, constitutive and inducible fate mapping strategies were used to track cells expressing endothelial genes in the adult mouse heart.

EXPERIMENTAL METHODS

Animals

ECs and their progeny were genetically labeled using Cre-LoxP recombination tools to activate expression of β-galactosidase (β-gal) or various fluorescent proteins under the control of the ubiquitously active *ROSA* gene locus (Soriano, 1999). Three independent transgenic mouse lines were used to direct constitutive or inducible Cre recombinase activity specifically in ECs: the Tie1-Cre and VE-Cadherin-Cre lines (Gustafsson *et al*., 2001; Alva *et al*., 2006) and the endothelial-SCL-Cre-ER^T line, which drives a Tamoxifen-inducible Cre-ER^T recombinase under control of the 5' endothelial-specific enhancer of the stem cell leukemia (*SCL*) gene locus (Göthert *et al*., 2004). The EC-specific Cre lines were crossed to R26R*stopLacZ* (Soriano, 1999) or R26R*stopYFP* (Srinivas *et al*., 2001) mice to generate double transgenics. The Tie1-Cre mouse line was also bred with the multi-fluorescent reporter R26R*stopConfetti* (Snippert *et al*.,

2010). Finally, transgenic mice expressing β-gal directly under the Tie1 promoter (Korhonen *et al*., 1995) were used to assess Tie1 expression in cardiac tissue.

Whole mount β-gal activity staining assay

Whole mouse hearts were isolated into cold 1X phosphate-buffered saline (PBS) and fixed for 1 hr at 4°C in 1X PBS containing 2% paraformaldehyde (PFA). After fixation, hearts were washed thrice with 1X PBS for 15 min each, and placed overnight (O/N) at 30°C in X-gal staining solution (1 mg/ml X-gal, 5 mM potassium ferro- and ferricyanate, 2 mM magnesium chloride, and 0.02% NP-40 in 1X PBS). Whole-mount hearts were photographed, stored in 10% phosphate buffered formalin at room temperature (RT) O/N and embedded in paraffin for sectioning.

Immuno- and epi- fluorescence

For cryosectioning, freshly isolated hearts were perfused with 1X PBS, bisected transversely, and fixed in 4% PFA dissolved in 1X PBS for 2 hrs at RT. Hearts were rinsed three times in 0.1% TX-100 solution in 1X PBS for 5 min each, embedded in Optimal Cutting Temperature compound (OCT; VWR), sectioned and stored at -70^{o}C. Slides were thawed at RT and rehydrated in 1X PBS for 30 min to remove OCT. Sections were washed twice in 0.1% TX-100 solution for 3 min each, and permeabilized in 0.5% TX-100 solution for 20 min at RT. Sections were then blocked in 0.1% TX-100 solution containing 2% BSA and 10% normal goat serum (Sigma) for 30 min at RT, and

incubated with primary antibodies O/N at 4^{o}C. Afterwards, slides were washed four times in 1X PBS for 10 min each, incubated with secondary antibodies in blocking solution for 1 hr at RT, washed four times in 1X PBS for 10 min each, and mounted with VECTASHIELD fluorescent mounting medium (Vector Laboratories). Antibody sources and dilutions are included in **Table 2 (Appendix).**

Imaging and 3-D Reconstruction

A series of confocal images (z-stack) were acquired sequentially on 100µm cardiac sections. Image stacks were attained for each channel using an LSM 710 META inverted microscope (Zeiss). Images were maximally projected using ZEN or ImageJ software and reconstructed into 3-D Z-series using Imaris (Bitplane) image analysis software.

Quantification of endothelial-derived CMs per volume of cardiac tissue

Cardiac cross-sections from End-SCL-CreER^{T}-LacZ mice, previously stained with X-gal for β-gal activity and counterstained with hematoxylin/eosin (H&E), were analyzed to determine the number of labeled CMs per volume of cardiac tissue. Transverse cardiac sections were imaged (Nikon AZ-100M widefield) and the average area was calculated using the Region Measurements function of MetaMorph Image Analysis Software. The µm/pixel calibration value was used to convert pixels into area of tissue in µm^2. Volume of total cardiac tissue in µm^3 was calculated by multiplying the area

obtained per section by the 10 μm thickness of tissue for each slide. A total of 352 slides (with 4 separate sections per slide; total of 1,408 sections) were imaged to analyze and estimate global cardiac CM labeling in the End-SCL-CreER^T-LacZ pulse-chase (N=17 mice) lineage tracing experiments.

Tamoxifen Preparation and Administration

For pulse-chase experiments, Cre recombinase was induced in adult, male End-SCL-CreER^T-LacZ and End-SCL-CreER^T-YFP mice by five intra-peritoneal injections of 3 mg Tamoxifen Free Base (MP Biomedicals) every other day for 9 days. Tamoxifen was suspended at 100 mg/ml in ethanol and mixed with sunflower oil to a final concentration of 10 mg/ml (10% ethanol). The fifth and last injection was set as 'Day 0' for pulse-chase experiments. A continuous 0.8% Tamoxifen chow diet (Harlan) was administered using Tamoxifen citrate salt in sucrose. Tamoxifen chow was freely available to the mice with average consumption of ~1 pellet/mouse/day.

Immunohistochemistry

Paraffin-embedded hearts were cut in 10μm sections. For antibody staining, sections were deparaffinized through Histo-Clear and graded alcohols per standard protocol. Antigen retrieval was performed by heating slides to 95^{o}C in a solution of 10mM Sodium Citrate (Reveal Decloaker RTU, Biocare) for 30 min. Sections were washed three times in 1X PBS for 5 min each. Endogenous peroxidase activity was

quenched by immersing slides in 0.3% peroxidase dissolved in 1X PBS for 10 min at RT. Sections were blocked in 2% BSA for 1 hr at RT, and stained O/N at 4^{o}C with primary antibodies, cTnT (Abcam, Ab10214; 1:800) in blocking solution. Slides were washed three times in 1X PBS for 5 min each and then processed using the Anti-Mouse Ig Horseradish Peroxidase detection kit (BD Biosciences). Slides were counterstained with Hematoxylin and Eosin (H&E), dehydrated, and mounted in Cytoseal-60 (Fisher).

Epifluorescence analysis

We documented epifluorescence in sections from Tie1-Cre-Confetti mice with direct excitation at 488nm, 515nm, and 561nm to activate nGFP, YFP and RFP, respectively. Sections were stained with DAPI (1:5000).

Analysis of regional YFP^{+} CM location and global YFP^{+} CM percentage

Cardiac cross sections of Tie1-Cre-YFP mice were analyzed to determine the regional location of YFP^{+} CM clusters, by visualization with direct excitation at 515nm. Hearts were bisected transversely at the mid-region, and embedded with the cut sides facing the same direction. This allowed for sections to concurrently progress towards the base and apex. An average of fifty 10µm sections per heart (one every 10 sections) were imaged, covering approximately 5000µm of tissue. Numbers of YFP^{+} CMs were recorded throughout these sections. To calculate the percentage of total YFP^{+} CMs, the number of recorded YFP^{+} CMs per imaged cardiac tissue was adjusted to total heart

size and divided by $8x10^6$, the approximate total number of CMs in the adult mouse heart (Adler *et al*., 1996; Doevendans *et al*., 1998).

Probability calculation of single cell origin of CM clusters in Confetti mice

Given that Cre-recombinase activity is cell-autonomous, we assume that each CM has been labeled independently of Cre activity in neighboring cells. Based on all observed fluorescent CM labeling, we calculated that the proportion of red, yellow, and green fluorescent CMs in the analyzed cardiac sections are 0.46, 0.23, and 0.31, respectively. Therefore, the probability for each cluster of a given size to have CMs of the same color has been calculated using the formula:

$P = P_R^{\#} + P_Y^{\#} + P_G^{\#}$, where P_R, P_Y, and P_G are the probabilities (0.46, 0.23, and 0.31) of seeing a RFP^+, YFP^+, or $nGFP^+$ cardiomyocyte, respectively; and # is the total number of CMs in the cluster. Calculated values have been included in **Table 1**. Given that each cluster is independent (i.e., the colors of the labeled CMs in one cluster are not influenced by the labeled colors of CMs in another cluster), then the probability that all 26 analyzed clusters never have mixing of colors (i.e., never more than one color per cluster) is 5.8×10^{-36}.

Bone marrow engraftment

Bone marrow engraftment was performed as described previously (Vinh *et al*., 2010), using bone marrow from CAG-EGFP transgenic mice (Okabe *et al*., 1997)

engrafted into C57Bl/6 wild type recipient mice. Cardiac tissue of recipient mice was analyzed 10 weeks after engraftment. All animal procedures were carried out with the approval of the Institutional Animal Care and Use Committee.

Statistical analysis

All values were reported as mean +/- S.D. Statistical significance was assessed by Student's unpaired two-tailed *t*-test for all statistical analysis comparisons. Statistical significance was expressed as follows: *$p < 0.05$; **$p < 0.01$.

RESULTS

Endothelial fate mapping strategy

To investigate the potential role of the endothelium for maintenance of the normal, uninjured adult heart, we analyzed cell fate in the hearts of 3-5 month-old Tie1-Cre-LacZ or Tie1-Cre-YFP mice, generated by crossing Tie1-Cre mice to ROSA-β-galactosidase (LacZ) or ROSA-Enhanced Yellow Fluorescence Protein (YFP) reporter mice, respectively (Gustafsson *et al.*, 2001; Soriano, 1999; Srinivas *et al.*, 2001) (**Figure 4**). In double transgenic animals, the ubiquitous *Rosa26* promoter constitutively drives reporter gene expression in ECs and their progeny.

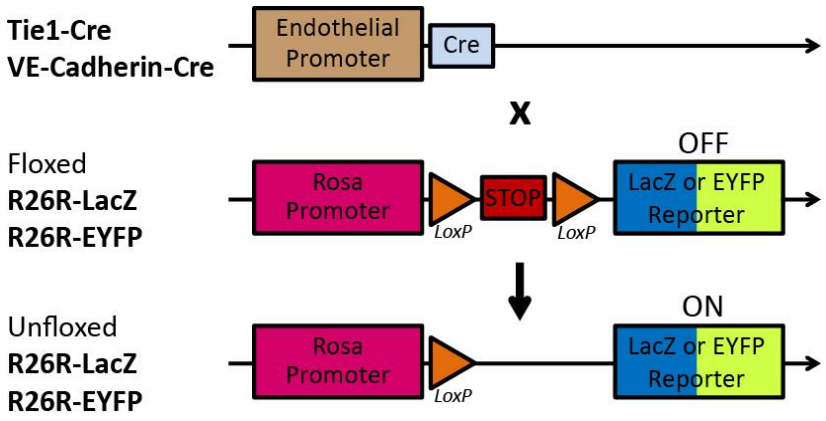

Figure 4. Endothelial cell lineage tracing strategy. Schematic drawing of gene loci used for EC lineage tracing and fate mapping. Transgenic mice expressing Tie1-Cre or VE-Cadherin-Cre were crossed with R26R-LacZ or R26R-EYFP mice to generate double transgenic lines.

Endothelial-specific Tie1 and VE-Cadherin expression labels patches of CMs

Tie1-Cre-LacZ hearts were stained with X-gal to visualize β-gal activity and thus Tie1$^+$ cells and their derivatives. In addition to marking ECs as expected, we detected labeled cells of non-endothelial appearance that were organized in clusters (**Figure 5A**). Histological analysis showed the β-gal$^+$ clusters were CMs, based on morphology and co-staining for cardiac Troponin T (**Figure 5B**). To exclude that CM staining was due to aberrant β-gal activity in CMs, we stained cardiac tissue sections from Tie1-Cre-YFP mice with antibodies recognizing YFP and the CM marker α-Actinin. Immunofluorescence (IF) analysis showed robust EC staining, but also revealed the presence of YFP$^+$ CMs with proper sarcomeric structures (**Figure 5C**). EC-derived CMs in sections appeared in clusters, in agreement with the pattern observed in whole-mount images.

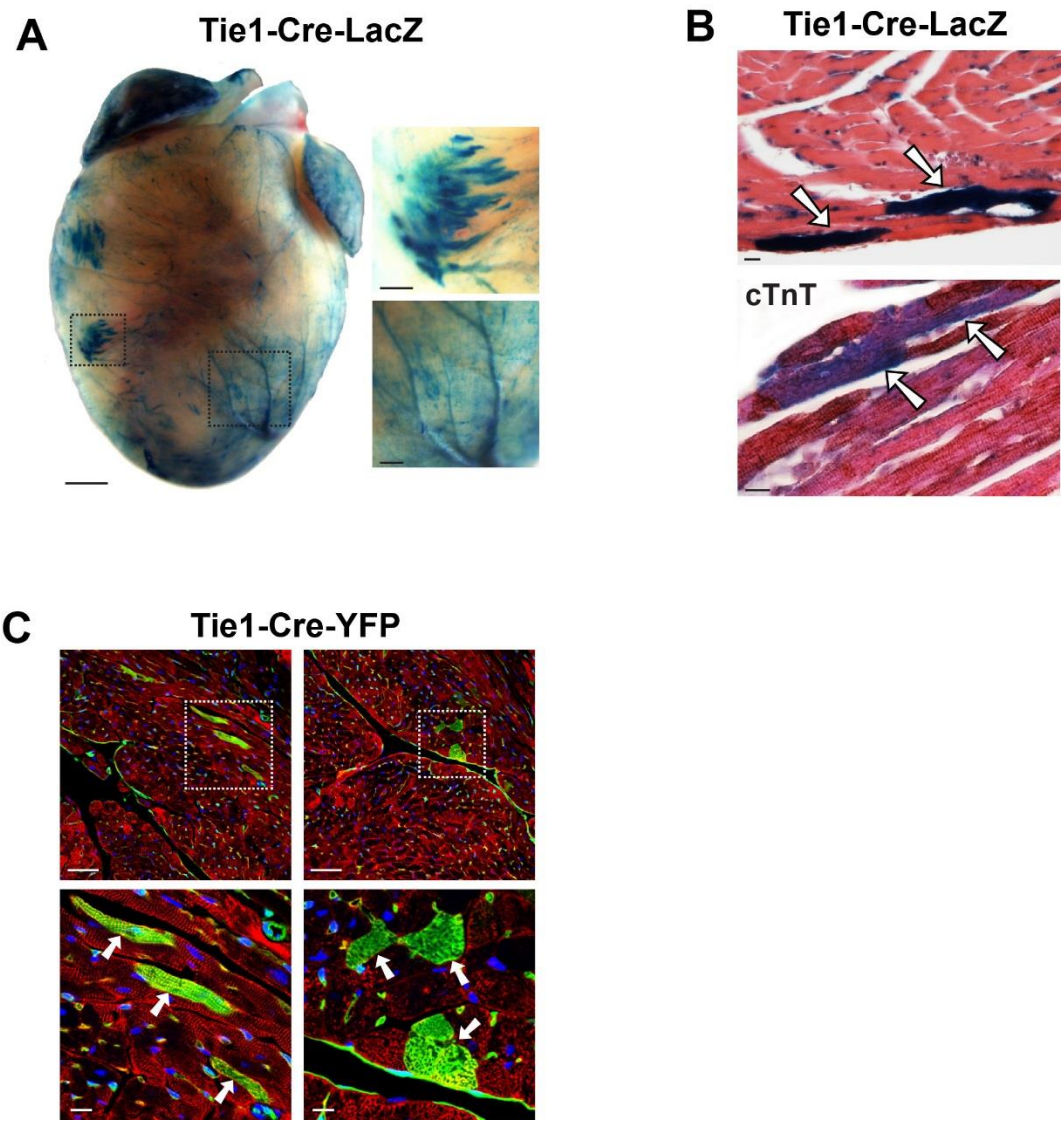

Figure 5. Endothelial-specific *Tie1* promoter expression labels patches of cardiomyocytes. (A) Whole mount X-gal staining of hearts from 3 month old Tie1-Cre-LacZ mice shows EC labeling and clusters of non-ECs in the ventricles. Right panels represent boxed areas showing a cluster of labeled non-ECs (upper panel) and ECs (lower panel). Scale bars 1mm in original image, 250µm in insets. **(B)** Upper panel: Histological analysis of X-gal-stained cardiac tissue sections from Tie1-Cre-LacZ mice shows CM staining (arrows). Lower panel: labeled non-ECs co-stain for cardiac Troponin T (cTnT; arrows). Scale bars 10µm. **(C)** IF analysis of cardiac tissue from Tie1-Cre-YFP mice stained for YFP (green) shows ECs and CMs, the latter co-stained for α-Actinin (red). YFP^+ CMs (arrows) are shown sectioned longitudinally (left) and transversely (right). DAPI (blue) was used for nuclear counter-staining. Lower panels depict boxed areas to depict sarcomeric structures in YFP^+ CMs. Scale bars 50µm (top panels), 10µm (bottom panels).

To eliminate the possibility that CM staining was due to ectopic Tie1 promoter activity in cardiac cells, we used mice expressing β-*gal* directly under the Tie1 promoter to mark ECs, but not their progeny (Korhonen *et al*., 1995). Histological analysis at 2 days, 2 weeks, 1 month, and 2 months of age detected exclusive EC labeling, without β-gal^{+} CMs (**Figure 6**). These results indicate the labeled CMs observed in Tie1-Cre-LacZ and Tie1-Cre-YFP hearts are progeny of Tie-1^{+} cells and not due to ectopic Tie1 expression in CMs.

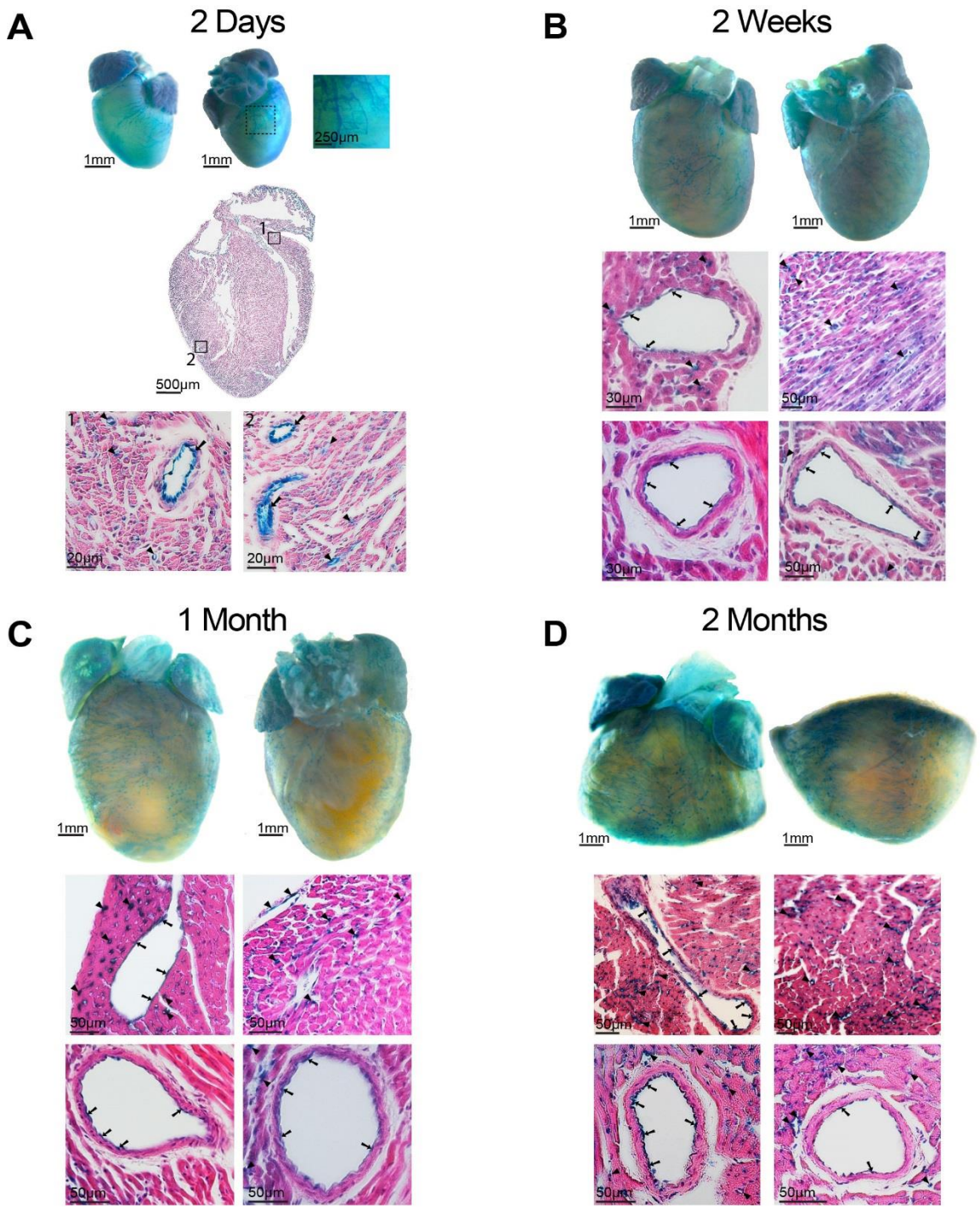

Figure 6. Lack of cardiomyocyte labeling in the absence of Cre recombinase. (**A-D, top panels**) Whole mount X-gal staining of Tie1-LacZ transgenic hearts at 2 days (A), 2 weeks (B), 1 month (C) and 2 months (D) depicts widespread labeling of blood vessels, but no labeling of cardiac tissue. (**A-D**, **bottom panels**) Histological analysis of Tie1-LacZ cardiac tissue sections shows prominent labeling of ECs, but no labeling of CMs, at each of the four time points, precluding aberrant *Tie1* promoter activity in adult CMs. Arrows indicate coronary artery and vein ECs, arrowheads denote microvasculature.

To further confirm that ECs give rise to CMs, we used an independent mouse line with endothelial-specific Cre expression under the control of the Vascular Endothelial (VE)-Cadherin gene transcription regulatory elements (Alva *et al*., 2006) (**Figure 4**). The VE-Cadherin promoter-based labeling produced comparable results to the Tie1-Cre-LacZ or Tie1-Cre-YFP mice. Specifically, histological sections obtained from 3-5 month-old VE-Cadherin-Cre crossed to ROSA-LacZ (VE-Cadherin-Cre-LacZ) or ROSA-YFP (VE-Cadherin-Cre-YFP) hearts showed labeling of both ECs and CMs (**Figure 7**).

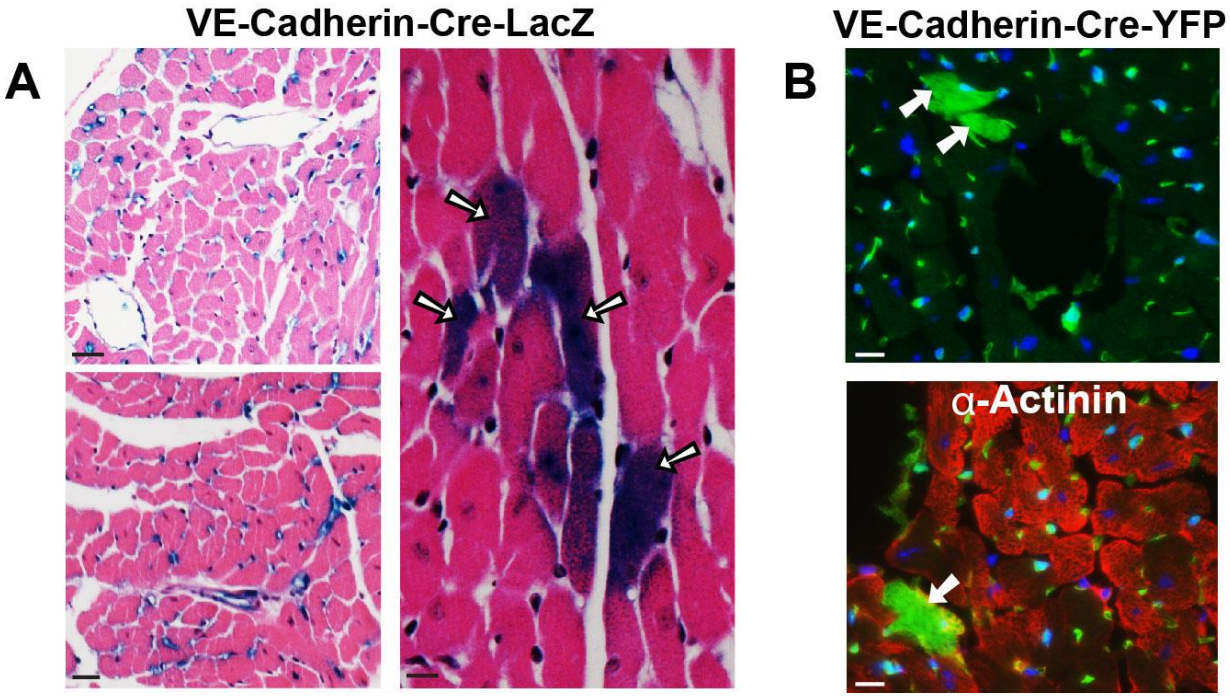

Figure 7. Endothelial-specific VE-Cadherin expression labels patches of CMs. (A) Histological analysis of *X-gal*-stained cardiac tissue from VE-Cadherin-Cre-LacZ mice shows staining of ECs (left panels). A labeled CM cluster is highlighted in the right image. Scale bars 25µm (left panels), 10µm (right panel). **(B)** IF analysis of cardiac tissue from VE-Cadherin-Cre-YFP mice co-stained for YFP (top and bottom, green) and α-Actinin (bottom; red). DAPI (blue) was used for nuclear counter-staining. Scale bars 10µm.

IF analysis showed EC-derived, YFP^{+} CMs were surrounded by normal basal membrane (Collagen IV staining), properly expressed cell-adhesion membrane molecules (N-Cadherin), and formed gap junctions (Connexin 43) among themselves, as well as non-EC derived CMs, suggesting they are functionally integrated with neighboring YFP$^{(-)}$ CMs (**Figure 8**). Taken together, our results show that in adult mice fate mapping using endothelial genetic labeling yields cells with functional and structural properties of CMs.

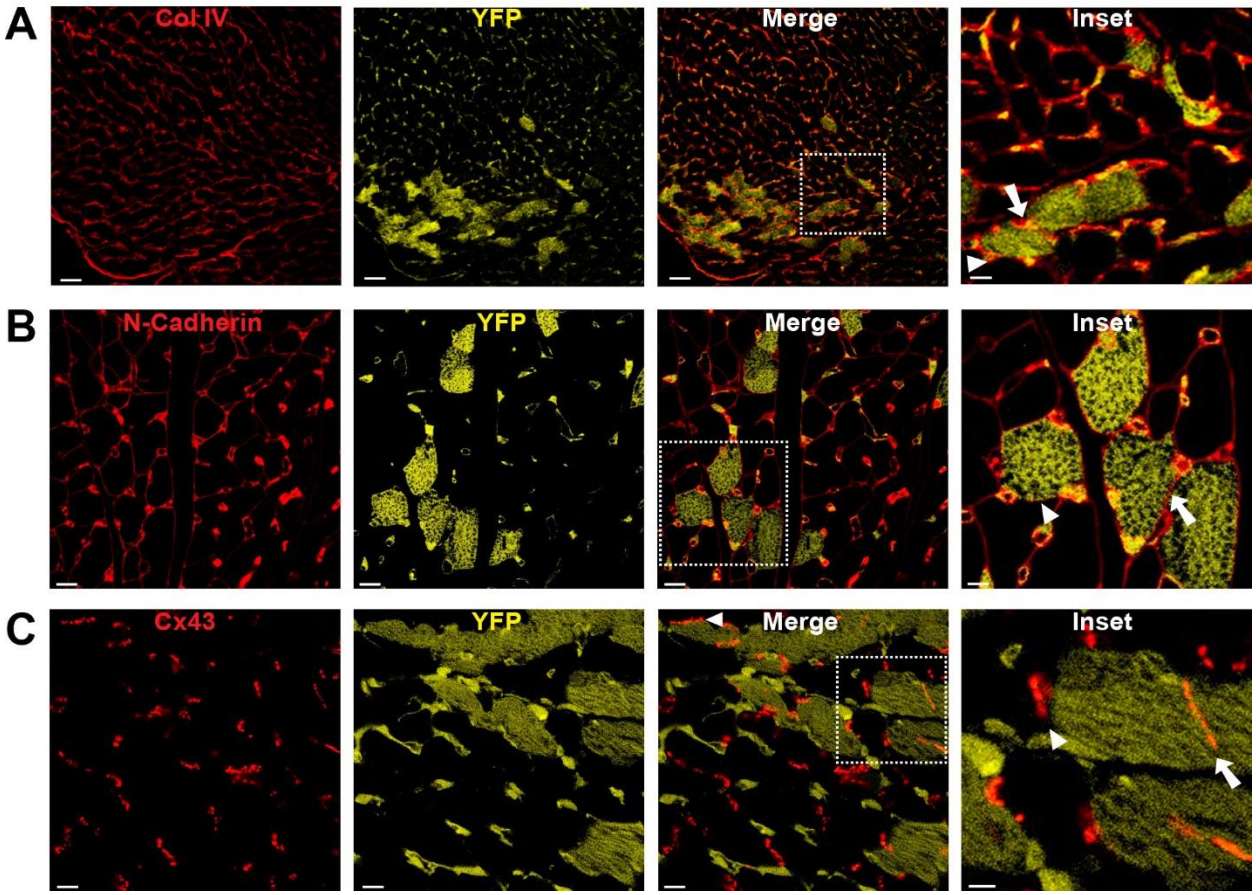

Figure 8. Functional and structural characterization of YFP^{+} CMs. (A-C) IF analysis of cardiac tissue from Tie1-Cre-YFP mice indicating YFP (yellow) and basal membrane Collagen IV (**A**; Col IV, red), membrane cell adhesion protein N-cadherin (**B**; red) and gap junction protein Connexin 43 in intercalated discs (**C**; Cx43, red). YFP antibody marks both ECs and EC-derived CMs. Higher magnification inserts are shown in the right panels. Arrows indicate adjacent YFP^{+}/YFP^{+} CMs, arrowheads indicate adjacent YFP^{+}/YFP^{-} CMs. Scale bars 30μm (A) and 10μm (B,C) in original images, and 10μm (A) and 5μm (B,C) in insets.

Endothelial-derived myocytes first appear 2 weeks after birth

During development, mesodermal progenitor cells, which differentiate to ECs, CMs, and SMCs, also express the endothelial-specific gene *Vascular Endothelial Growth Factor Receptor 2* (*Vegfr2, or Flk-1*; (Kattman *et al*., 2006). This raised the possibility that the labeled CM clusters in the adult heart are derived from early embryonic cells with endothelial characteristics. To distinguish whether EC-derived CMs are of embryonic or adult origin, we used End-SCL-CreER^T mice with inducible Cre recombinase expression under the control of the 5$^{'}$ endothelial-specific enhancer of the *Stem Cell Leukemia* (*SCL*) gene (Göthert *et al.*, 2004). End-SCL-CreER^T mice were crossed to the ROSA-LacZ or ROSA-YFP reporter lines to generate End-SCL-CreER^T-LacZ or End-SCL-CreER^T-YFP mice, respectively. These double transgenic mice allow for specific labeling of mature ECs after tamoxifen induction of Cre-recombinase activity.

End-SCL-CreER^T-LacZ and End-SCL-CreER^T-YFP adult mice were continuously fed a diet containing 0.8% tamoxifen to tag and lineage trace ECs. Whole-mount staining with X-gal and histological analysis of End-SCL-CreER^T-LacZ hearts after 6 weeks of tamoxifen diet showed EC as well as CM labeling (**Figure 9A,B**), similar to the constitutively active endothelial-specific Cre models described in **Figures 5 and 7**. Labeling of CMs, which co-stained for sarcomeric α-Actinin, was also observed after 12 weeks on tamoxifen (**Figure 9C**).

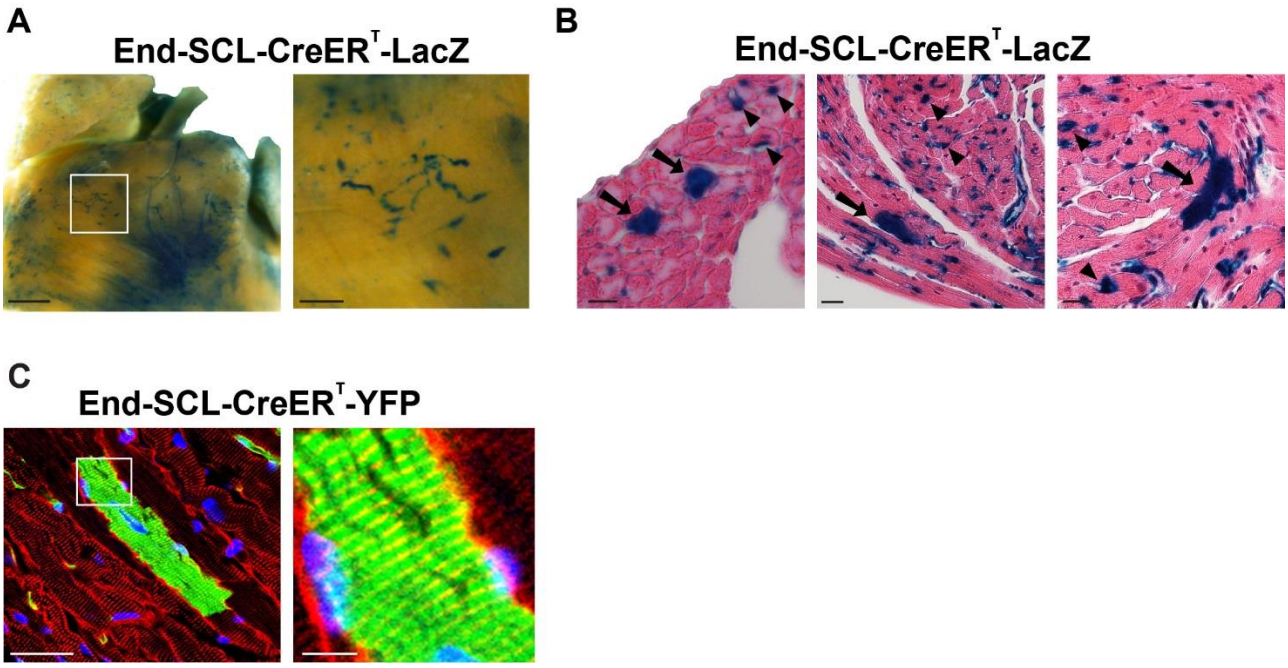

Figure 9. Endothelial-specific End-SCL-CreER^T expression labels patches of CMs in the adult heart. (A,B) Images of X-gal stained hearts from 5 month old End-SCL-CreER^T-LacZ mice, fed tamoxifen chow for 6 weeks to induce Cre recombinase in adult ECs and their progeny. Whole mount staining in A shows EC and CM labeling. Scale bar 1mm in original image, 250µm in inset. Histological sections in B depict labeled CMs (arrows) and ECs (representative arrowheads). Scale bars 20µm. **(C)** Labeling of cardiac ECs and CMs in End-SCL-CreER^T-YFP double transgenic line after 12 weeks of tamoxifen diet. Sections stained for YFP (green) and α-Actinin (red). Right panel: magnification of boxed area highlights sarcomeric structures in YFP$^+$ CM. Scale bars 10µm (left), 50µm (right).

Of note, we did not detect CM labeling, and found extremely rare EC labeling (<1%), in control End-SCL-CreER^T-LacZ mice without tamoxifen administration, indicating tight regulation of inducible Cre recombinase activity. No labeled cells were present in ROSA-STOP-LacZ mice on tamoxifen (**Figure 10**).

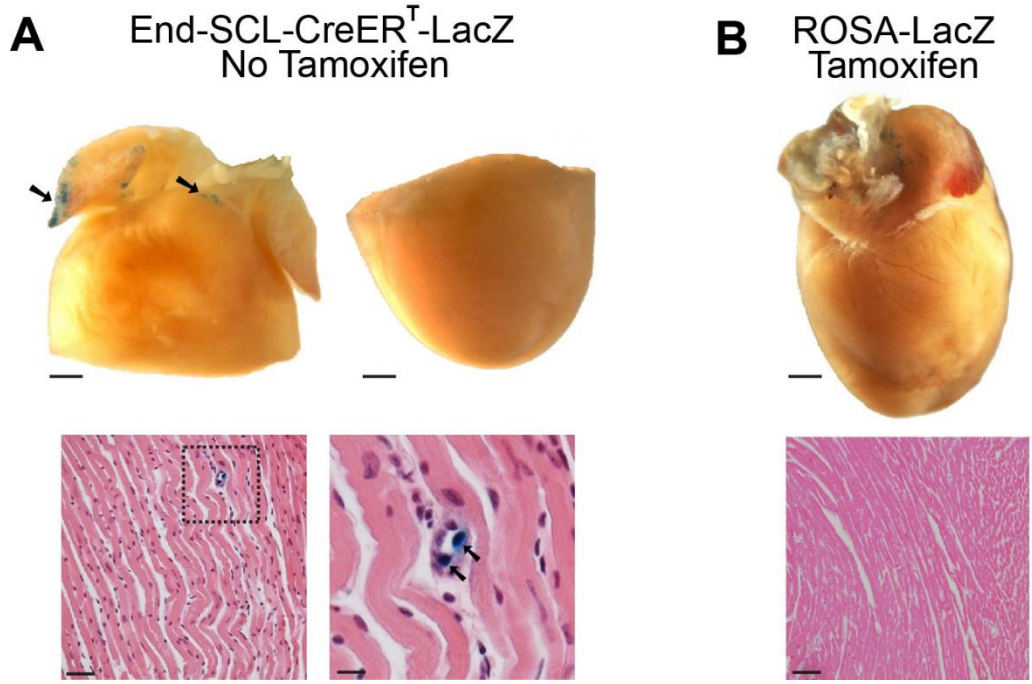

Figure 10. Cardiomyocyte labeling in EC lineage tracing depends on endothelial Cre expression. (A) Whole mount X-gal staining of hearts from End-SCL-CreER^T-LacZ mice without tamoxifen administration shows minimal EC labeling (<1%; arrows) and no CM labeling, demonstrating tight and specific regulation of Cre recombinase activity. Scale bars 1mm in top panels, 20µm in bottom left panel, 5µm in bottom right panel. **(B)** Whole mount X-gal staining of single ROSA-STOP-LacZ transgenic hearts demonstrates lack of aberrant β-galactosidase activity without the presence of Cre recombinase. Scale bar 1mm in top panel, 50µm in bottom panel.

To test whether the observed CM staining is due to ectopic activity of the Tie1 or Endothelial-SCL promoter/enhancer elements in non-ECs, we stained cardiac tissue sections from Tie1-Cre-YFP and End-SCL-CreER^T-YFP mice with antibodies recognizing Cre protein. IF analysis showed that Cre expression is restricted to ECs, supporting an endothelial origin of labeled CMs (**Figure 11A,B**). We confirmed the endothelial specificity of Tie1 expression by co-staining cardiac sections from Tie1-Cre-YFP mice for Tie1 and α-Actinin. Furthermore, we did not detect co-labeling of Tie1 in YFP$^+$ or YFP$^-$ CMs, showing that CMs do not express Tie1 (**Figure 11C**). Collectively,

these results indicate the observed labeling is not due to 1) leaky activity of the inducible Cre fusion protein, 2) expression of β-gal and YFP without Cre activity, or 3) aberrant Tie1 or Cre expression in CMs.

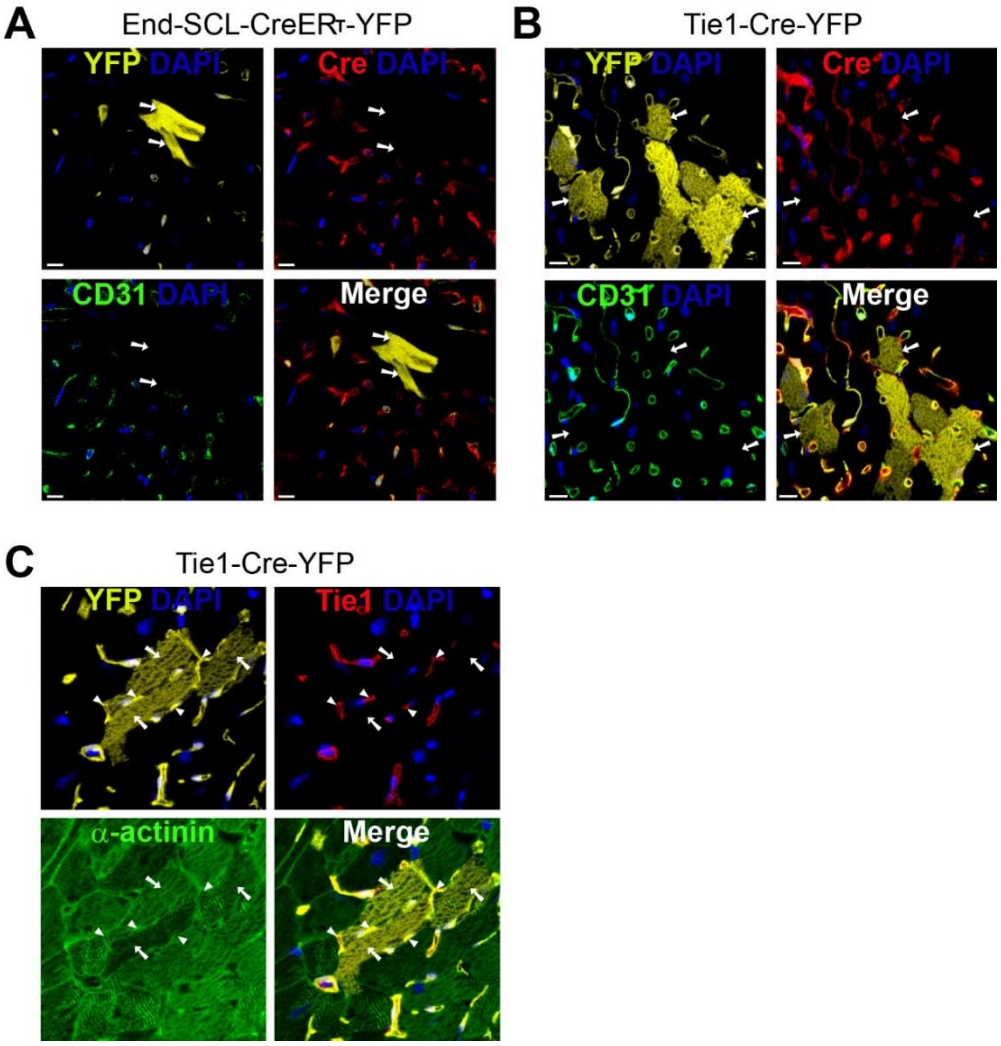

Figure 11. Cre and Tie1 expression are restricted to cardiac endothelial cells. (A,B) IF analysis of cardiac sections from End-SCL-CreER^{T}-YFP and Tie1-Cre-YFP mice with antibodies recognizing Cre recombinase protein (red), CD31 (green), and YFP (yellow) illustrates Cre recombinase expression is restricted to CD31+ ECs, and does not mark CMs. Arrows indicate examples of YFP+ CMs which do not express Cre recombinase. Scale bars, 10μm. **(C)** Analysis of cardiac tissue sections from Tie1-Cre-YFP mice with antibodies recognizing the endothelial marker Tie1 (red), and mature CM marker α-Actinin (green), indicate Tie1 expression is restricted to ECs and is not present in CMs. Arrows point to examples of Tie1-, α-Actinin+ CMs; arrowheads indicate Tie1+ ECs. Scale bars, 10μm.

To further exclude the possibility that EC-derived CMs are marked during development, we isolated and stained hearts from neonatal and young Tie1-Cre-LacZ mice with X-gal. Staining of hearts from perinatal day P2, weanling (P14) and young adult (2 months) mice indicated that while cardiac vasculature was labeled at each time point (**Figure 12A-D**; also **Figure 6**), CM clusters first appeared within the postnatal heart by 2 weeks of age (**Figure 12C,D**).

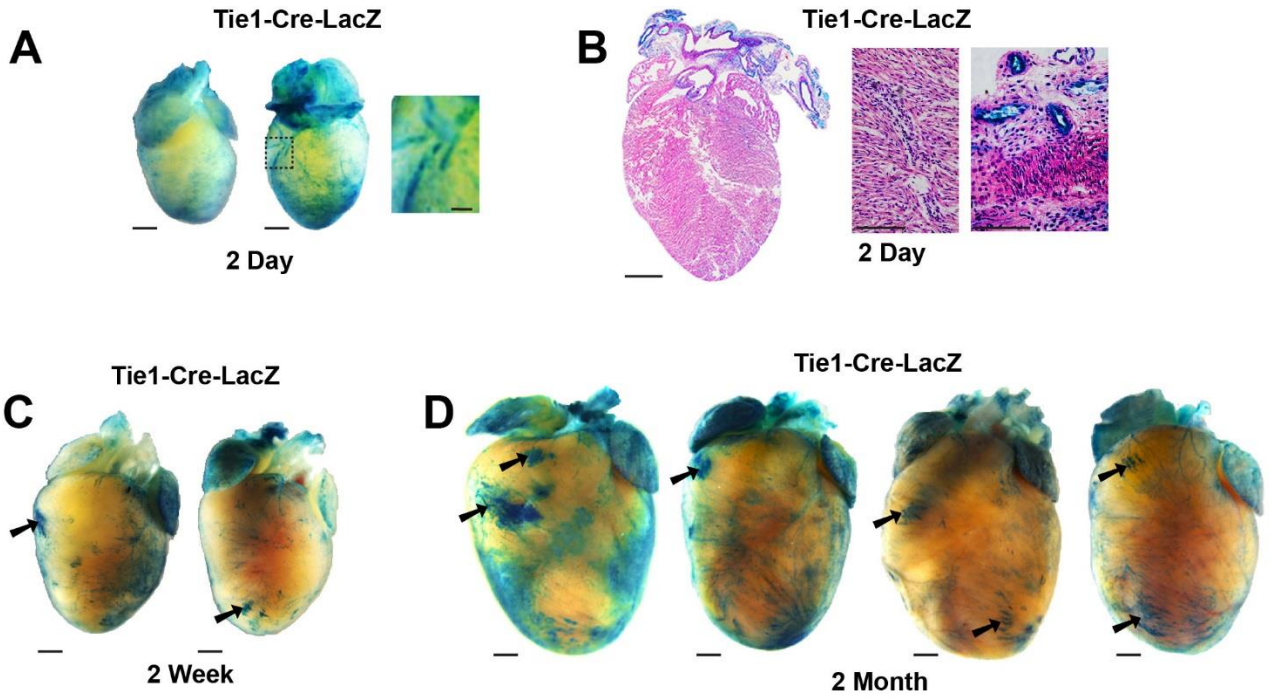

Figure 12. Endothelial-derived cardiomyocytes appear in the adult heart. (A,B) Whole mount images (A) and sections (B) of X-gal stained neonatal hearts from 2 day old Tie1-Cre-LacZ mice shows EC, but not CM labeling. Scale bars 1mm in original images, 250µm in magnified areas. **(C,D)** X-gal staining of hearts from weanling (2 weeks) and young adult (2 months) mice show EC-derived CM clusters appear around 2 weeks of age. Scale bars 1mm.

In summary, three independent, constitutive (Tie1, VE-Cadherin) or inducible (End-SCL) endothelial-specific promoters, with two independent reporters (LacZ, YFP) were used that all showed similar labeling of ECs and CM clusters. Thus, the data support the idea that a subset of CMs in the adult mouse heart is postnatally derived from ECs.

Clusters of endothelial-derived cardiomyocytes originate from single cells

The clustering of EC-derived CMs suggested they were clonally related. To test this model, the Tie1-Cre line was crossed to the ROSA-Confetti multi-fluorescent reporter to generate Tie1-Cre-Confetti mice. The Confetti line carries four distinct fluorescent protein genes (red, yellow, nuclear green and membrane-bound cyan) in the ROSA locus (Snippert *et al*., 2010). The fluorescent protein coding sequences are organized in tandem among alternating *LoxP* sites in a way that recombination of the ROSA-Confetti allele leads to stochastic expression of RFP, YFP, nuclear GFP (nGFP) or membrane CFP (mCFP).

The confetti construct is designed such that random recombination activates only one of the fluorescent protein genes, allowing stochastic labeling of each targeted cell and its descendants with a single color (**Figure 13**). As a result, this fate mapping strategy can distinguish whether cells in a cluster are clonally related (i.e., generated from a single, labeled progenitor cell), or if each cell in a cluster has been independently derived. In the first case, the entire cluster should have CMs of one color; if the latter is true, individual clusters should consist of cells expressing different colors (Greif *et al*., 2012).

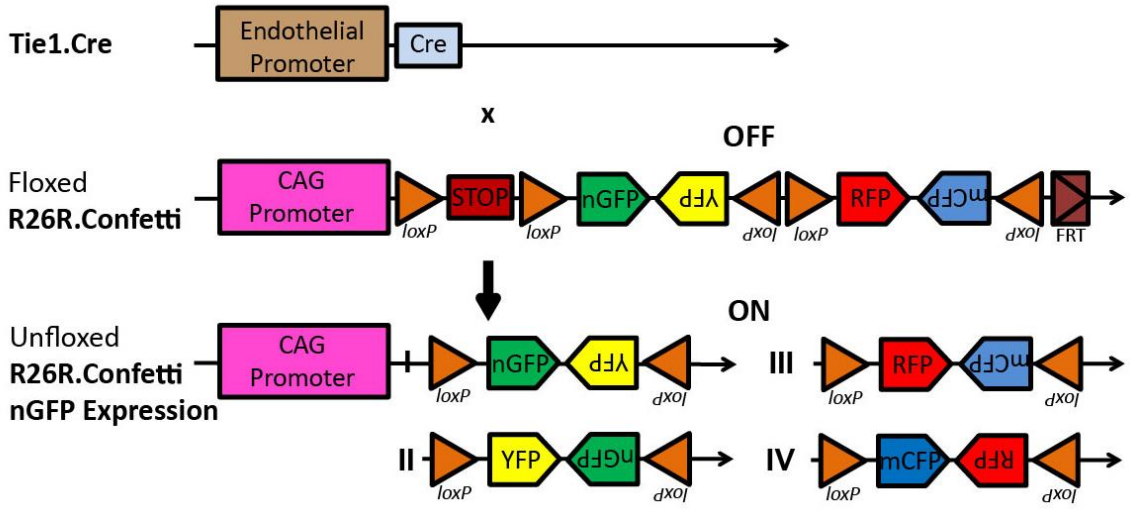

Figure 13. Schematic drawing of the ROSA-Confetti reporter gene locus. Stochastic expression of either mCFP, nGFP, YFP, or RFP occurs with Cre-mediated recombination at one of the *loxP* sites of the Confetti gene construct. The *Tie1* promoter drives expression of a constitutively active Cre recombinase.

Epifluorescence examination of cardiac sections from adult Tie1-Cre-Confetti mice detected ECs expressing RFP, YFP and nGFP in equal proportions (**Figure 14)**; in our hands, expression of mCFP in cardiac sections was too weak to reliably detect; therefore we focused further analysis on RFP, YFP, and nGFP). Among labeled CMs, each individual cluster was marked by expression of the same single fluorescent protein (**Figure 15)**.

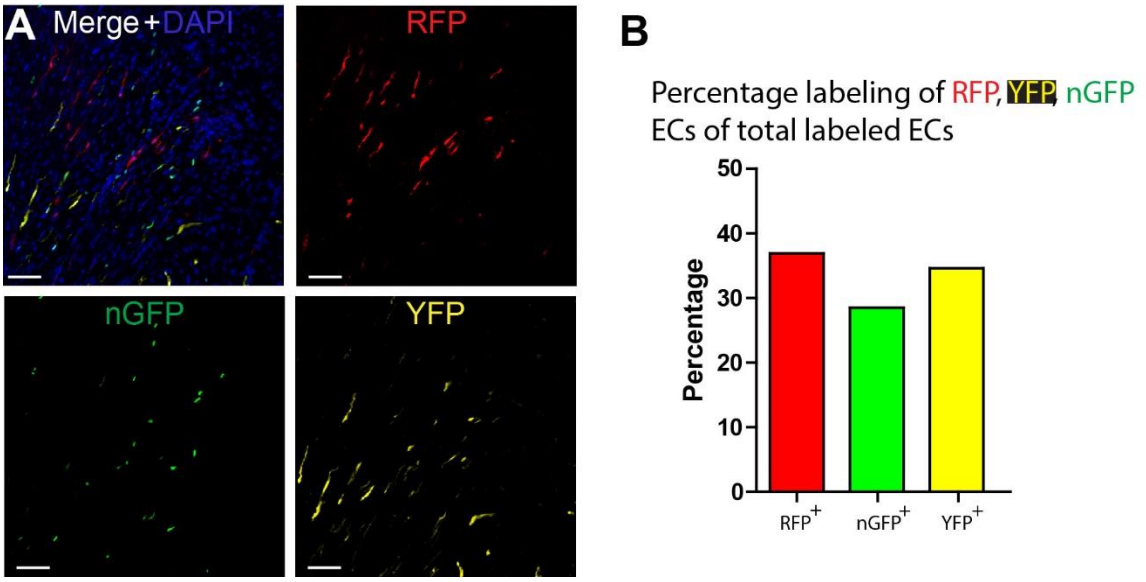

Figure 14. Quantitative analysis of red, yellow, and green fluorescent protein expressing endothelial cells in stochastic lineage tracing. (A) Epifluorescence examination of transverse cardiac section from adult Tie1-Cre-Confetti mouse illustrates EC labeling with the analyzed RFP, nGFP, and YFP fluorescent proteins. Scale bars 50µm. **(B)** Quantification of ECs marked with epifluorescence in Tie1-Cre-Confetti mice shows equivalent ratios of RFP^+, $nGFP^+$, and YFP^+ ECs. Percentages of RFP, nGFP and YFP expressing ECs were quantified by counting the number of individually fluorescent ECs as a percentage of the total fluorescent EC population in a given visual field (N=4 mice, n=8 total visual fields).

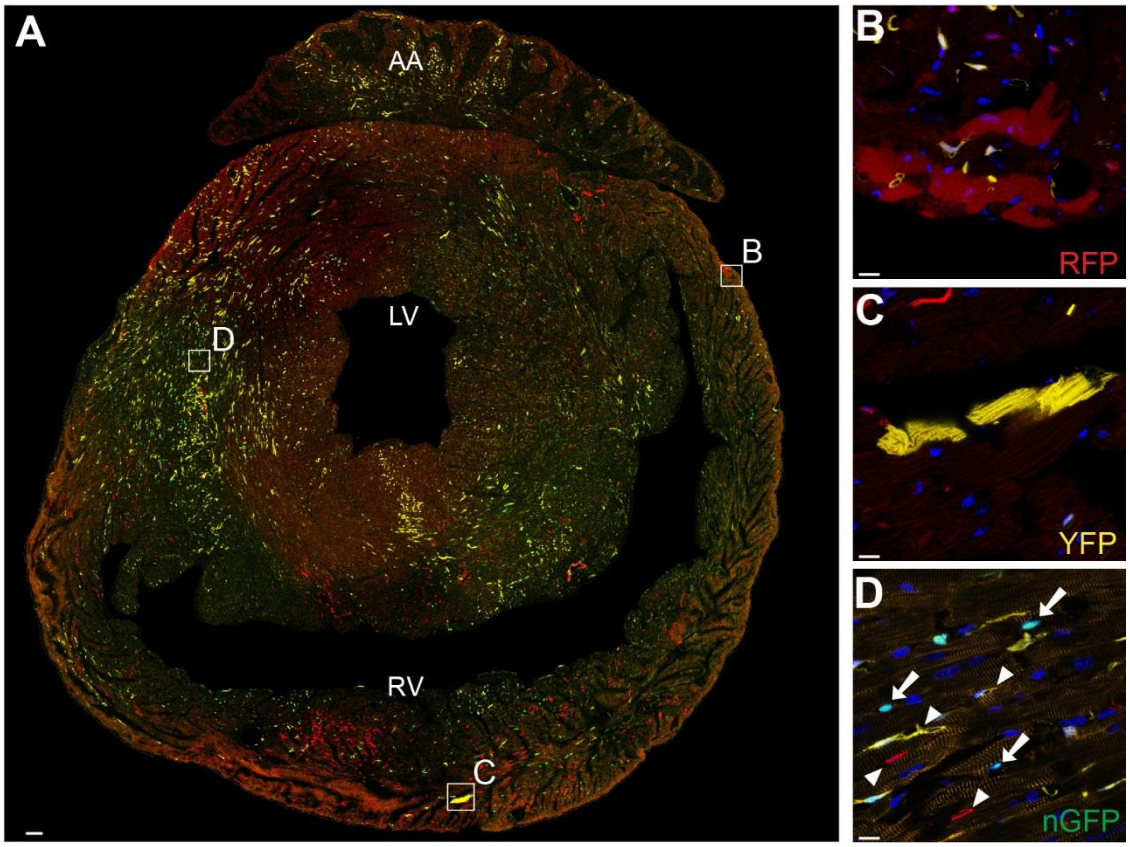

Figure 15. Each CM in a cluster expresses the same fluorescent color in Tie1-Cre-Confetti mice. (A-D) Epifluorescence analysis for RFP, YFP and nGFP expression in transverse cardiac sections from adult Tie1-Cre-Confetti mice depicts ECs and CMs expressing RFP, YFP and nGFP. CM clusters marked in boxed areas in A are magnified in B-D. Individual CMs in each cluster express the same fluorescent protein. Scale bars 100µm in A, 10µm in B-D.

To calculate the probability (P) that each cluster would randomly consist of CMs expressing the same fluorescent protein *without* being derived from a single cell, we recorded the size and color of CM clusters with ≥3 cells in sections of three independent Tie1-Cre-Confetti mouse hearts (**Table 1**). The probability that the observed labeling patterns in this analyzed set of CMs are due to random recombination events is $P<10^{-36}$, indicating that labeled CMs in each cluster are not independently derived, but originate from a single cell.

Cluster #	# RFP+ CMs	# YFP+ CMs	# nGFP+ CMs	Probability, P
1	12			0.0001
2	8			0.002
3	7			0.005
4	6			0.011
5	6			0.011
6	4			0.057
7	3			0.139
8	3			0.139
9	3			0.139
10		4		0.057
11		4		0.057
12		3		0.139
13		3		0.139
14		3		0.139
15		3		0.139
16		3		0.139
17		3		0.139
18			5	0.024
19			5	0.024
20			4	0.057
21			4	0.057
22			4	0.057
23			4	0.057
24			3	0.139
25			3	0.139
26			3	0.139
# CMs:	52	26	35	
Proportion of Total:	0.46	0.23	0.31	

Table 1. Quantitative analysis of red, yellow, and green fluorescent protein expressing cardiomyocytes in stochastic lineage tracing. The table indicates the calculated probability values for observing clusters of single color labeled CMs. Percentages of RFP, nGFP, and YFP expressing CM clusters were determined by counting the number of single-color labeled CMs in each distinct cluster and comparing with the total number of fluorescently labeled CMs (N=4 mice, n=26 separate CM clusters).

Using 3-D reconstruction images, we documented that in many instances individual CM clusters were marked by a different fluorescent color than neighboring microvasculature, suggesting CM labeling was not due to fusion with ECs (**Figure 16**). Furthermore, CMs in the same cluster were not always contiguous but often interspersed with unlabeled CMs, a pattern also observed in other organs that might be indicative of tissue repair in the adult versus *de novo* development in the embryo (Kopinke *et al*., 2011; Bowman *et al*., 2013).

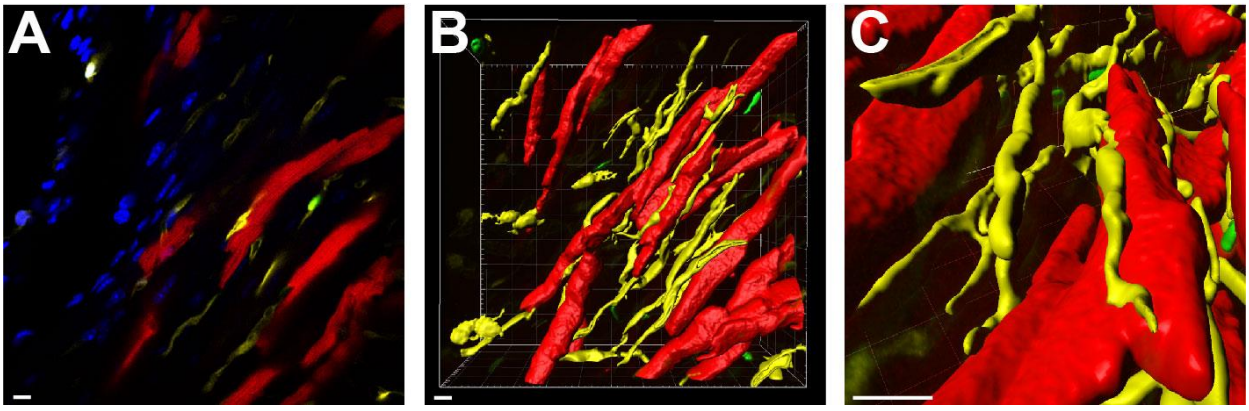

Figure 16. 3-D reconstruction of a representative CM cluster. (A) Single image from within the serial section plane. Each CM expresses RFP; adjacent ECs express YFP; DAPI is shown in blue. Scale bar 10μm. **(B,C)** Compilation of z-stack images is used to recreate the 3-dimensional RFP^+ CM cluster. Surrounding YFP^+ and $nGFP^+$ vasculature indicates a lack of endothelial cell fusion with adjacent CMs. Scale bars 10μm.

Collectively, the staining patterns in Tie1-Cre-Confetti mice indicate that each labeled CM cluster has originated from a single parental cell expressing EC markers. It is also possible that rare, proliferating CMs transiently express endothelial markers, and thus become labeled before expansion to form clusters.

Cardiac myocyte progeny of endothelial cells are regionally restricted

Whole-mount heart staining indicated EC-derived CM clusters were localized in specific areas (**Figures 5 and 12**). To determine overall distribution patterns throughout right and left ventricles, we systematically mapped the location of CM progeny following EC lineage tracing. Complete sets of serial transverse cardiac tissue sections from five Tie1-Cre-YFP mice were analyzed using confocal microscopy.

The results revealed clusters of labeled CMs were present in both left and right ventricles, most frequently around coronary blood vessels in subepicardial regions (**Figure 17 A,B**). The locations of clusters containing ≥4 YFP^+ CMs were placed in a diagram of four heart planes from base to apex. We found YFP^+ CM clusters were primarily localized in three regions of the heart: the anterior free wall of the right ventricle; the junction areas between right and left ventricles and adjacent septum; and the lateral free posterior wall of the left ventricle (**Figure 17C**).

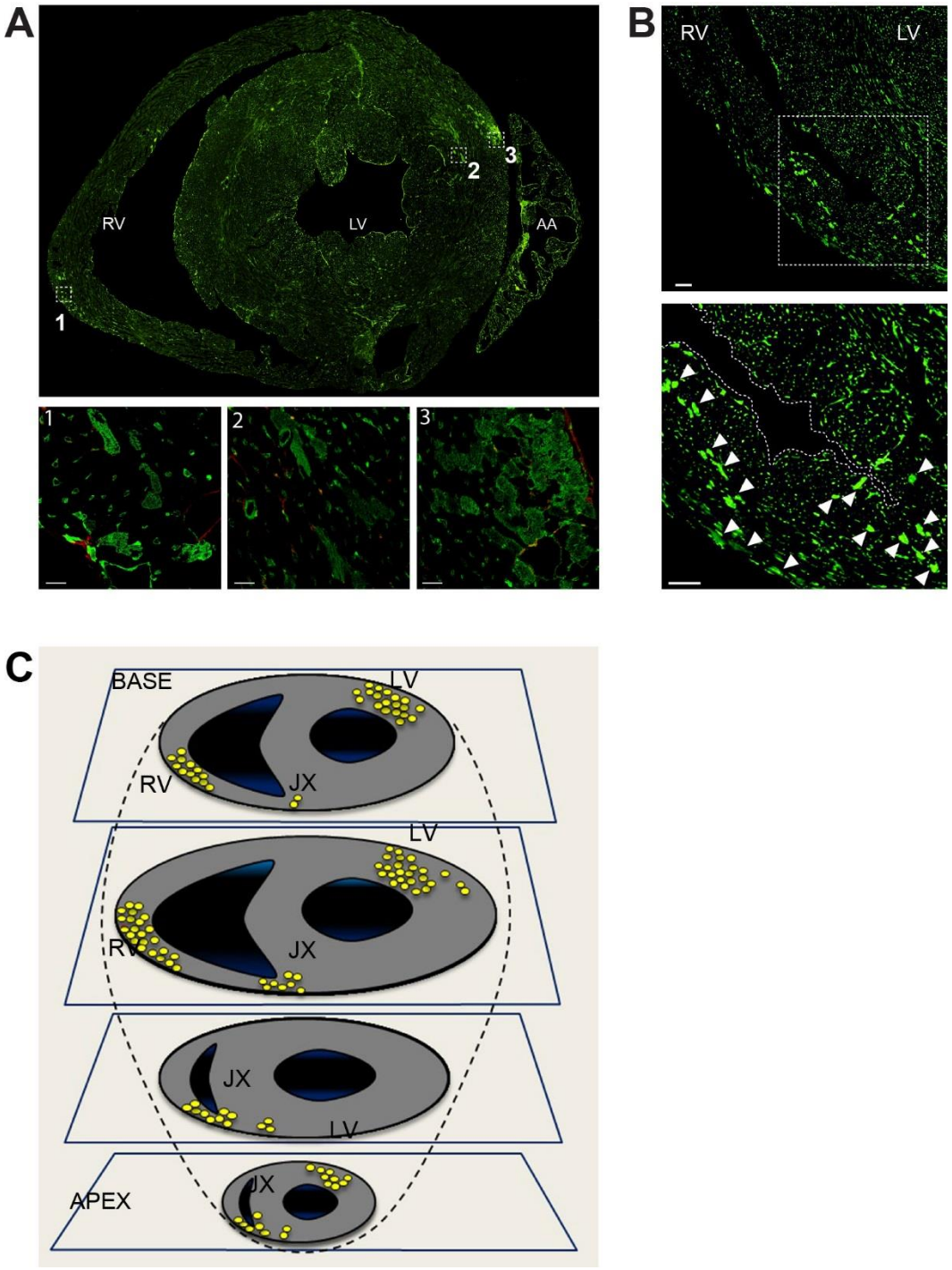

Figure 17. Endothelial-derived cardiomyocytes are localized to three specific heart areas. (A) Transverse cardiac section from adult Tie1-Cre-YFP mice stained for YFP reveals EC-derived YFP$^+$ CMs are found in both left and right ventricles, most frequently in perivascular (insets 1,2,3) and subepicardial (insets 1,3) areas. Scale bars 500µm in original image, 10µm in insets. **(B)** Clusters of CMs are also localized at the junction of the left and right ventricles and adjacent septum. Scale bars 50µm. **(C)** Schematic drawing depicting the location of all clusters ≥4 YFP$^+$ CMs identified in serial sections of 5 Tie1-Cre-YFP mice. Abbreviations: AA, atrial appendage; RV, right ventricle; LV, left ventricle; JX, junction; L, lumen.

Each cluster consisted of up to 50 CMs. 60% of the observed clusters were in the left ventricle with the remaining 40% equally distributed in the right ventricle and junction areas. Furthermore, left ventricle clusters consisted on average of twice as many cells per cluster than those in the right ventricle (**Figure 18A,B**).

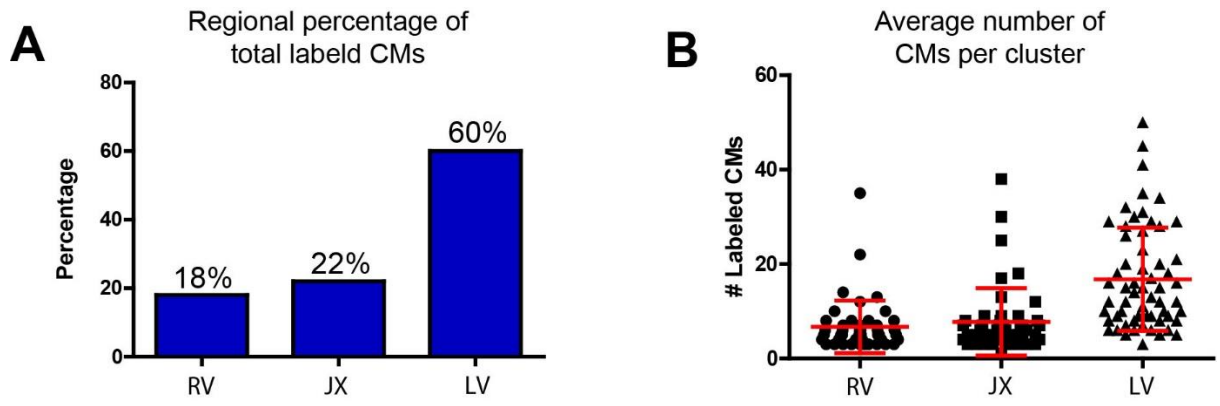

Figure 18. Quantitative analysis of the three cardiac regions where labeled CMs are observed. (A) Quantification of CM cluster locations shows 60% are present in the left ventricle and the remaining 40% in the right ventricle and junction areas. **(B)** Quantification of CM number in each cluster shows clusters in the left ventricle are on average double in size compared to clusters in the right ventricle. Abbreviations: RV, right ventricle; LV, left ventricle; JX, junction; L, lumen.

Taking into account the number of clusters in each heart and the number of cells per cluster, we calculated the total number of YFP^+ CMs represent ~0.3% of the approximately 8 million CMs in the mouse heart (Adler *et al*., 1996; Doevendans *et al*., 1998). These data indicate that in both ventricles, cardiogenic endothelium seeds specific cardiac areas, representing a relatively small fraction of the CM population.

Pulse labeling of endothelial cells leads to rapid long-term CM labeling

To test whether ECs are the originating cells, or represent an intermediate, transient step in the cardiogenic process, we pulsed-chased ECs using the inducible End-SCL-CreER^T-LacZ mouse described above. Adult mice were given a series of closely spaced tamoxifen injections ('pulse') and hearts were isolated at various time-points after the final injection ('chase') (**Figure 19A**). Hearts were then stained with X-gal to visualize labeled CMs in transverse sections. Analysis of cardiac tissue sections immediately (i.e., 1 day after the end of the pulse), and 3-days later showed exclusive labeling of ECs, whereas labeled CMs appeared one week after the pulse and persisted up to 12 weeks, the last time point examined (**Figure 19B**).

The number of labeled CMs per volume of cardiac tissue was quantified for each of the time-points. The data indicate labeled CMs appeared in low numbers one week after the pulse, increased over a period of 3 weeks, and remained relatively constant at least up to 12 weeks (**Figure 19C**).

These results suggest cells labeled by EC-specific Cre expression represent an originating cell rather than a transient subpopulation in the CM generation process, since in the latter case CM numbers would decline after a single pulse. Alternatively, it is likely EC-derived CMs have long life spans beyond the examined 12-week period. In either case, the duration required to achieve maximum CM labeling after the pulse suggests the process is efficient and reaches a steady state within approximately 3 weeks.

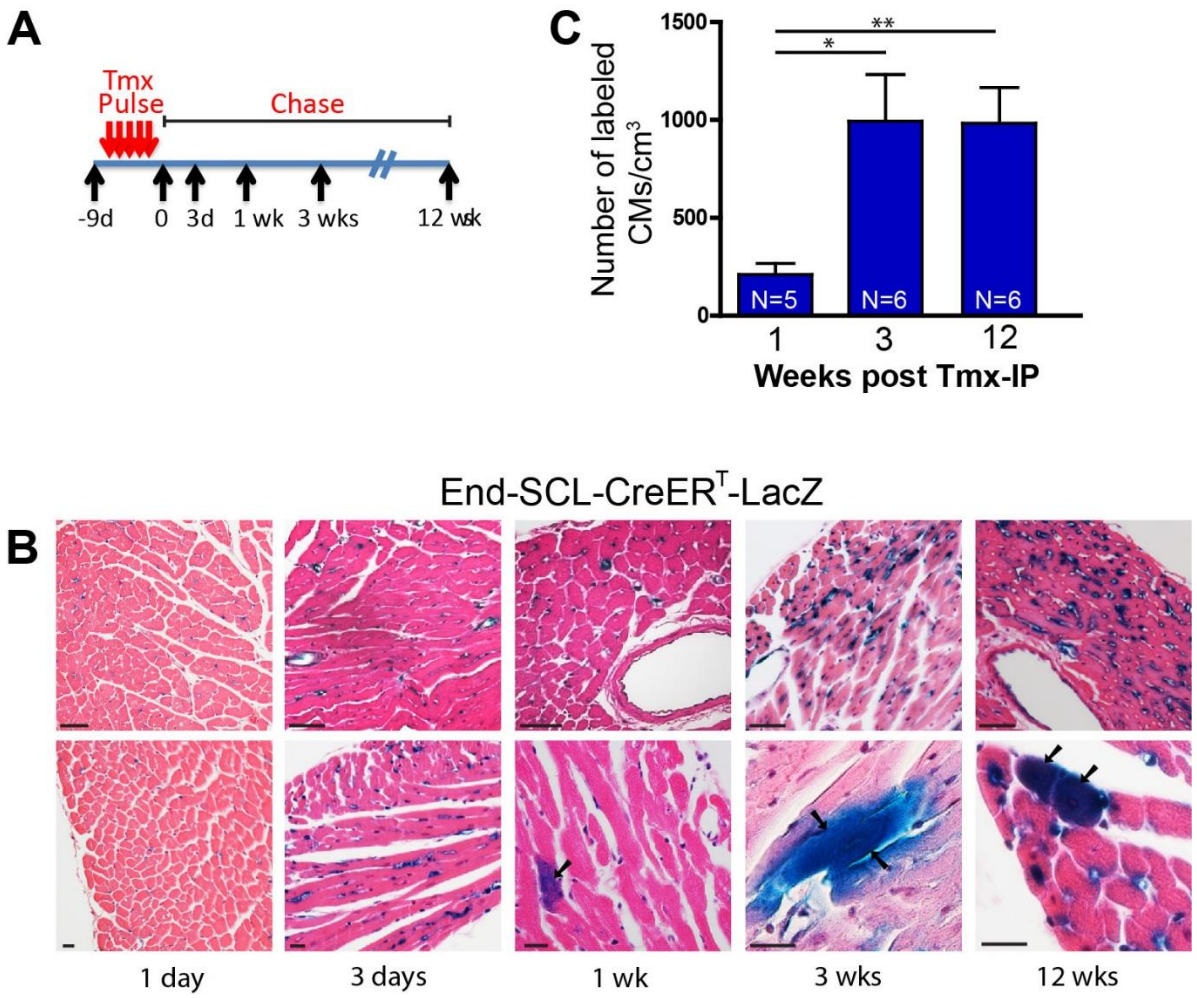

Figure 19. Pulse-chase labeling of ECs leads to rapid long-term labeling of CM progeny. (A) Schematic drawing of the pulse-labeling experimental design. **(B)** Histological analysis of hearts stained with X-gal and counter-stained with Hematoxylin and Eosin to visualize ECs and labeled CMs in transverse sections at indicated time points. After a 1- and 3-day chase, labeling of only cardiac ECs was observed, whereas labeled CMs appeared by one week after the pulse and persisted at 3 months. Arrows indicate X-gal$^+$ CMs. Scale bars 50μm (upper), 20μm (lower panels). **(C)** Quantification of CM numbers at different chase time points shows maximum CM labeling within 3 weeks which remains constant thereafter. N indicates number of mice used for analysis. Values reported as mean +/- S.D. *$p < 0.05$; **$p < 0.01$.

Bone marrow-derived cells do not contribute to CMs in the adult heart

The SCL gene, as well as Tie1 and VE-Cadherin, are also expressed in hematopoietic stem cells (HSCs), raising the possibility that labeled CMs are of bone marrow origin. One advantage of the SCL 5' enhancer is that it is not expressed in adult HSCs (Göthert *et al.*, 2004), which suggests labeled CMs are derived from ECs and not bone marrow cells.

To directly test whether HSCs contribute CMs in the adult heart, we used a method independent of lineage tracing. Specifically, we analyzed cardiac tissues from mice transplanted with fluorescently tagged bone marrow cells (**Figure 20**). IF analysis showed bone marrow derived cells present in the adult heart were primarily F4/80$^+$ macrophages and FSP-1$^+$ fibroblasts, with no labeling of CMs, consistent with previous studies (Murry *et al*., 2004). The results of the transplantation studies excluded that labeled CM clusters are derived from HSCs.

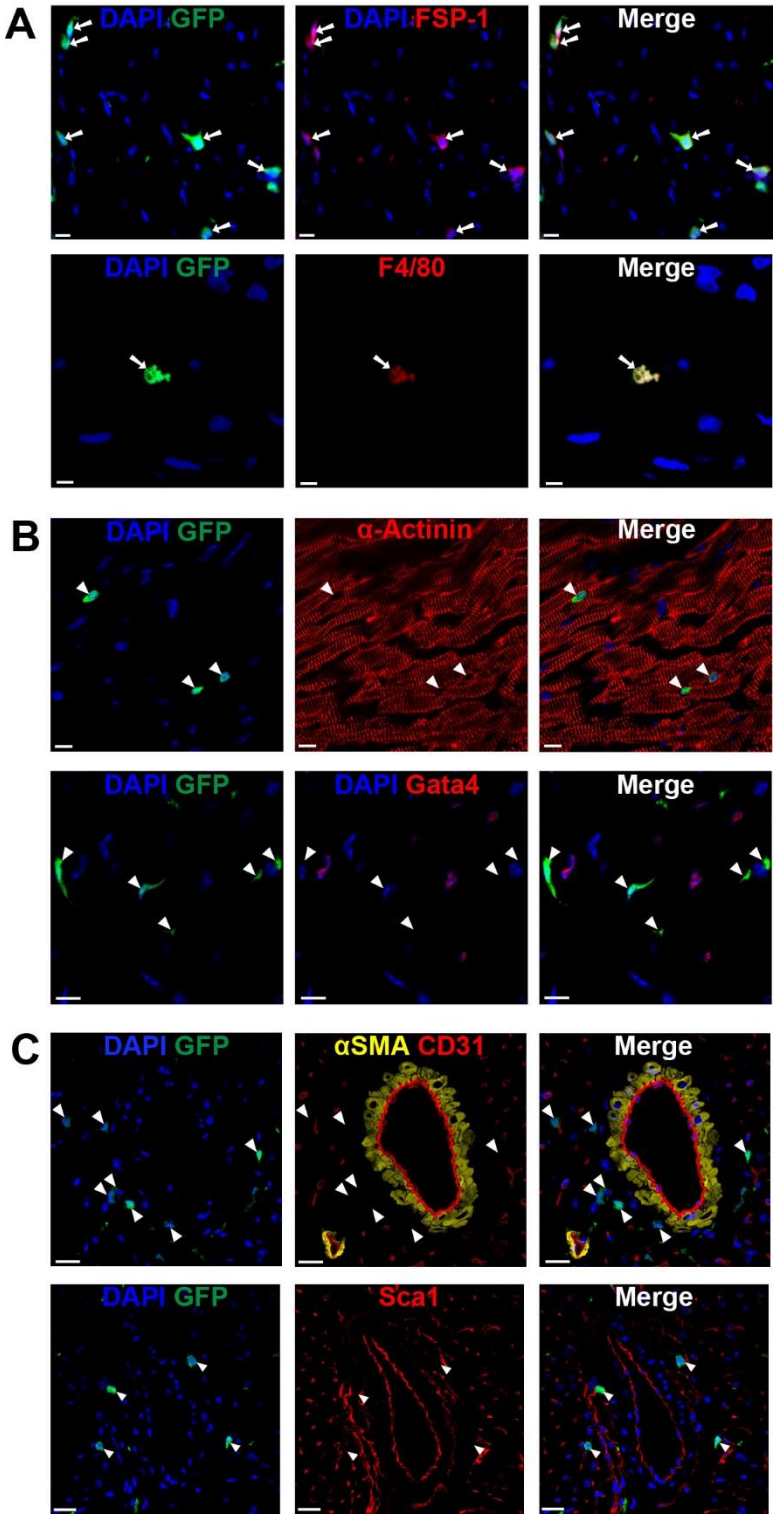

Figure 20. Analysis of heart tissue in mice after fluorescently labeled bone marrow transplantation. Bone marrow (BM) from CAG-EGFP transgenic mice was engrafted into wild type recipient mice. Fluorescent BM-derived cells were observed in cardiac sections only after BM engraftment. **(A)** GFP^+ BM-derived cells in cardiac sections co-stain with the fibroblast marker FSP-1 (top panels) and the macrophage marker F4/80 (bottom panels). Arrows indicate overlap of BM-derived GFP^+ cells with FSP-1 and F4/80. Scale bars 10μm in top panels, 5μm in bottom panels. **(B)** GFP^+ BM-derived mononuclear cells (arrowheads) do not costain with the mature CM marker α-Actinin (top panels), or the early cardiac marker Gata4 (bottom panels). Scale bars 10μm. **(C)** Similarly, GFP^+ BM-derived cells (arrowheads) in the proximity of coronary vessels do not costain with the smooth muscle marker αSMA or endothelial cell marker CD31 (top panels), or the cardiac stem cell surface marker Sca1 (bottom panels). Scale bars 20μm.

DISCUSSION

We have used Cre/Lox technology to generate a fate map of vascular cells in the healthy, adult heart. Our data show ECs retain cardiogenic potential in the adult heart, similar to the differentiation capacity of cardiovascular progenitor cells during the early stages of cardiac development, the EC-based cardiogenic process is rapid, but restricted to specific areas of the myocardium, and approximately 0.3% of the adult heart is comprised of endothelial-derived CMs.

Although the classical role of ECs is to ensure proper functioning of the inner wall in blood vessels, evidence increasingly points to a more direct and active role of ECs in organ development, homeostasis, and tissue repair. ECs display exceptional differentiation potential and plasticity during development and disease. During development, ECs in the ventral wall of the dorsal aorta transform to budding blood cells and migrate to hematopoietic organs, ultimately residing in the bone marrow (Lancrin *et al*., 2009). This particular type of EC is called the hemogenic endothelium. In the adult, besides the angiogenic response of ECs to build new blood vessels after ischemia, they also undergo mesenchymal transition after injury (EndMT), producing SMA^+ myofibroblasts in the heart, lung and kidney, supporting a fibrogenic potential of ECs (Zeisberg *et al*., 2007; Arciniegas *et al*., 2007; Zeisberg *et al*., 2008; Aisagbonhi *et al*., 2011; Chen *et al*., 2012).

These results indicate ECs also have cardiogenic potential in the adult. This notion is compatible with embryonic development when all three types of cardiovascular cells (ECs, SMCs, and CMs) are derived from multipotent progenitor cells expressing EC markers such as VEGFR2 (or Flk-1; Kattman *et al*., 2006). Furthermore, inactivation

of SCL/TAL1 can transform vasculature to cardiac cells, turning the yolk sac from a hematopoietic tissue to a contracting sheet of CMs (Van Handel *et al*., 2012). This striking outcome suggests, at least early in development, EC to CM transition can be accomplished by switching off a single transcriptional regulator.

Additionally, the data show EC-derived CMs represent a small number of the total cardiac cell pool and are confined to specific areas. The first observation likely reflects the slow rate of cardiac renewal necessary during cardiac homeostasis, a fact also supported by the low number of new CMs generated annually in the human and mouse hearts (Bergmann *et al*., 2009; Murry and Lee, 2009). The second suggests renewal may take place in specific sites characterized by high attrition rates due to work overload or structural constrains.

Since the heart is constantly contracting, areas of the myocardium which are under greater strain may require localized regeneration. In support of the possibility that localized renewal of CMs occurs in the adult heart, clinical studies showed cardiac tissue fibrosis often appears in the perivascular space, or the insertion points between ventricles (Biernacka and Frangogiannis, 2011; Karamitsos and Neubauer, 2013). These areas of the myocardium are sites that contain the majority of the labeled clusters we identified in the mouse hearts.

In summary, endothelial lineage tracing in the adult mouse, using three independent constitutive or inducible promoters, all indicate CMs are derived from an endothelial population. This physiological process may occur through asymmetric division of a vascular stem or progenitor population, or direct de-differentiation of

endothelial cells. Thus far, the data show that lineage tracing using separate endothelial promoters labels both ECs and CMs, and further suggests that ECs serve as an originating source of CMs. It is likely that an intermediate population, transiently present during the cellular transition between endothelial progenitor and mature cardiomyocyte, also exists in the adult heart. Locating this putative population, and characterizing its role in the cardiogenic process, is a necessary step in generating a complete model to describe the cardiogenic capability of ECs under conditions of cardiac homeostasis.

CHAPTER III

CORONARY ARTERIES SERVE AS THE SITE OF THE CARDIAC STEM CELL NICHE

INTRODUCTION

The concept of a niche for cells was first proposed in 1978 based on studies involving hematopoietic stem cells (Schofield, 1978). Contradictory data indicated apparent limitless renewal of stem cells, but a finite life-span of spleen colony-forming cells, which were believed to be HSCs themselves (Schofield, 1978). To reconcile this discrepancy, the idea of a stem cell niche was proposed to explain how stem cells were regulated to continuously self-renew, but also generate differentiated progeny which do not persist indefinitely and have various rates of turnover.

Today, the stem cell (SC) niche is more fully defined as a unique, tissue-specific, regulatory microenvironment responsible for enabling and controlling stem cell self-renewal while balancing internal and external molecular signals for maintenance or repair of host tissue (Scadden, 2006). An increasing number of studies have identified a wide variety of tissue-specific stem cells, each with their own unique niche (Jones and Wagers, 2008). Studying the relationship between these stem cells and their niche environment will provide a better understanding of maintenance of organ homeostasis, or repair of damaged tissue in the adult.

The brain was once viewed as a post-mitotic organ, with little to no mechanisms for neurogenesis after birth. However, the discovery of specialized niches in the lateral ventricles (V-SVZ) and hippocampus (SGZ) which continue to undergo neurogenesis, provided strong evidence that even adult organs considered to lack regenerative potential, still had this capability. This localized regenerative ability of the brain may provide clues into the heart, another organ which was classically considered to lack regenerative potential.

Increasing evidence indicates the heart contains one or more resident populations of cardiac stem cells. However, each putative population has a distinct expression of surface markers, unique or unknown origins, and varied cardiogenic potential. While recent studies show that CSC populations generate new cardiomyocytes in the heart, there is still considerable debate about the actual regenerative ability of the myocardium over the lifetime of an individual.

These putative cell populations must be characterized to understand their contribution to the heart, and how the integration of different signals culminates to affect their function and turnover within the niche. It is also necessary to understand the source and location of the CSC populations to establish consensus within the field. Finally, it is important to reconcile these CSC progenitors with the cardiogenic endothelial population I have identified through endothelial lineage tracing.

EXPERIMENTAL METHODS

Animals

The Tie1-Cre line (Gustafsson *et al*., 2001) and the Tamoxifen-inducible endothelial-SCL-Cre-ER^T line (Göthert *et al*., 2004) were crossed to R26R*stopLacZ* (Soriano, 1999) or R26R*stopYFP* (Srinivas *et al*., 2001) mice to generate double transgenics as described in the previous Chapter. The Tie1-Cre mouse line was also bred with the multi-fluorescent reporter R26R*stopConfetti* (Snippert *et al*., 2010).

Whole mount β-gal activity staining assay

Whole mouse hearts were isolated and X-gal stained as described in the previous Chapter.

Immuno- and epi- fluorescence

Freshly isolated hearts were prepared for cryosectioning as described in the previous chapter. Primary antibodies and their dilutions used include: rabbit anti-GFP, also recognizing YFP (Abcam, Ab290; 1:3000), mouse anti-α-Actinin (Sigma, A7811; 1:800), mouse anti-α-SMA (Sigma, A2547; 1:800), rat anti-CD31 (BD Pharmingen; 1:100), rabbit anti-Gata-4 (Santa Cruz, sc9053; 1:100), rabbit anti-Ki67 (Abcam, Ab15580; 1:100), rabbit anti-phospho-Histone H3 (Santa Cruz, sc8656; 1:500), goat anti-Sca1/Ly6 (R&D, AF1226; 1:100), rabbit anti-c-Kit (Santa Cruz, sc5535; 1:50), mouse anti-Cre (Abcam, Ab24607; 1:400), rabbit anti-FSP1 (S100A4) (Abcam,

Ab27957; 1:200), and mouse anti-Snail (Chemicon; 1:600). The nucleophilic dye 4',6-diamidino-2-phenylindole (DAPI; 1:5000; Invitrogen) was used to visualize cellular nuclei. Primary and corresponding secondary antibodies are also listed in **Table 2 (Appendix).**

Imaging and 3-D Reconstruction

A series of confocal images (z-stack) were acquired sequentially and reconstructed 3-dimensionally as described in the previous Chapter.

Tamoxifen Preparation and Administration

For pulse-chase experiments, Cre recombinase was induced in adult, male End-SCL-CreER^{T}-LacZ mice by five intra-peritoneal injections of Tamoxifen as described in the previous Chapter. Furthermore, a continuous 0.8% Tamoxifen chow diet (Harlan) was administered using Tamoxifen citrate salt in sucrose. Tamoxifen chow was freely available to the mice with average consumption of ~1 pellet/mouse/day.

Hematoxylin and Eosin counter-stain of X-gal stained cardiac sections

Paraffin-embedded hearts were cut in 10µm sections, and deparaffinized through Histo-Clear and graded alcohols per standard protocol. Slides were counterstained with Hematoxylin and Eosin (H&E), dehydrated, and mounted in Cytoseal-60 (Fisher).

Epifluorescence analysis

We documented epifluorescence in sections from Tie1-Cre-Confetti mice with direct excitation at 488nm, 515nm, and 561nm to activate nGFP, YFP and RFP, respectively. Sections were stained with DAPI (1:5000).

Quantification of perivascular YFP$^+$ cells

The percentage of coronary arteries containing YFP$^+$ perivascular cells was determined by using cardiac sections from Tie1-Cre-YFP 3-5 month-old, adult males, counterstained with αSMA and CD31. Values were determined by counting the number of arteries with YFP$^+$ perivascular cells compared to total coronary arteries imaged. (N=3 mice, n=57 coronary artery sections). Subsequently, the percentage of YFP$^+$ M cells of total coronary SMCs was quantified by counting the number of YFP$^+$ αSMA$^+$ cells as a percentage of total coronary αSMA$^+$ cells (N=3 mice, n=30 coronary artery sections which contained YFP$^+$ coronary SMCs).

The percentage of Gata4$^+$/YFP$^+$ M and A cells of total YFP$^+$ M and A cells was calculated by counting single and double positive cell numbers around coronary arteries (N=3 mice, n=30 sections). Furthermore, the percentages of Ki67$^+$/YFP$^+$, pH3$^+$/YFP$^+$, Sca1$^+$/YFP$^+$ and c-Kit$^+$/YFP$^+$ cells was also determined by quantification of single and double positive cell numbers (N=3 mice, n=26 sections). 10μm thick transverse sections were used for all image quantification.

RESULTS

Endothelial fate mapping identifies perivascular cell populations

The results of **Figure 19** indicate ECs represent an originating source of CMs, rather than a transient cell type. This model predicts EC lineage tracing will mark intermediate, proliferating cell populations that express early cardiac markers, but have not yet differentiated to CMs. In support of this model, examination of cardiac tissue sections obtained from Tie-Cre-YFP, Tie-Cre-LacZ and End-SCL-CreER^{T}-LacZ mice revealed that besides ECs and CMs, EC fate mapping marked two additional cell types (**Figure 21**).

The first resided in the media layer of coronary arteries and was marked by expression of α Smooth Muscle Actin (**Figure 21A**). YFP^{+}/αSMA^{+} double positive cells in the media layer of coronary vessels, termed M cells (**Figure 21B-E**), also expressed the early cardiac transcription factor Gata4, but lost expression of the EC marker CD31 (**Figure 21B**). The second subpopulation, termed A cells, was found within, or immediately adjacent to the adventitia layer of coronary vessels (**Figure 21B-E**).

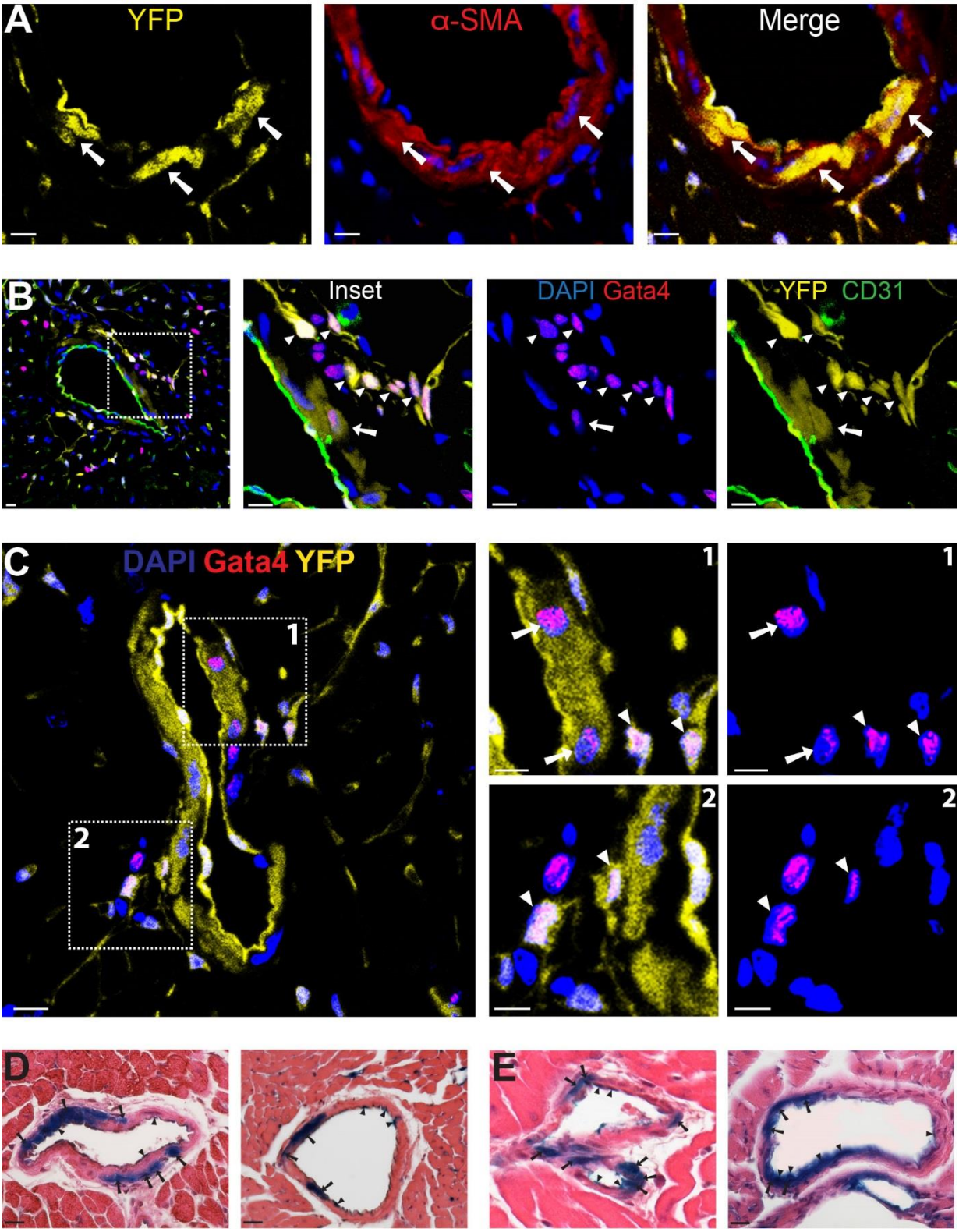

Figure 21. Endothelial fate mapping marks distinct populations of perivascular M and A cells.

Figure 21. Endothelial fate mapping marks distinct populations of perivascular M and A cells. (A-C) IF analysis of cardiac tissue sections from Tie1-Cre-YFP mice. **(A)** $YFP^+/\alpha SMA^+$ cells (termed M cells) are present in the media layer of coronary arteries (arrows). Scale bars 10µm. DAPI was used for nuclear counterstaining in these and subsequent IF images. **(B)** $YFP^+/CD31^-$ cells (termed A cells) are present within, or immediately adjacent to, the adventitia layer of coronary vessels. Magnification inset shows both M (arrows) and A (arrowheads) cells acquire expression of Gata4 protein. Scale bars 10µm. **(C)** IF analysis shows Gata4+ perivascular M cells (arrows) and A cells (arrowheads) in coronary artery medial and adventitial layers. Scale bars 10µm in main panel, 5µm in insets. **(D,E)** Histological analysis of X-gal-stained cardiac tissue sections from (D) Tie1-Cre-LacZ mice, and (E) End-SCL-$CreER^T$-LacZ mice 3 days (top image) or 6 weeks (bottom image) after Tamoxifen administration. Images shows staining of ECs (arrowheads) and perivascular cells (arrows), similar to results in (A-C). Sections were counter-stained with H&E. Scale bars 10µm.

Serial histological analysis revealed that half of the coronary artery sections had M cells, which constituted approximately 30% of the SMC population in those coronary arteries. Moreover, 44% of the $YFP^+/ \alpha SMA^+$ M cells expressed nuclear Gata4 protein (**Figure 22**). Approximately half of the coronary arteries had A cells, and nearly 65% of them expressed Gata4 (**Figure 22**).

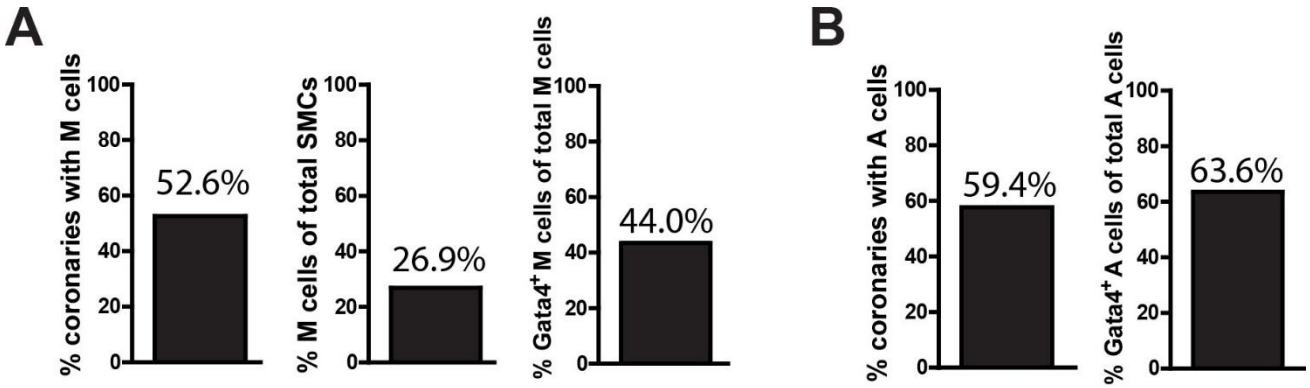

Figure 22. Quantification of perivascular M and A cells. (A) Quantification using cardiac tissue serial sections revealed 52.6% of coronary arteries contain EC-derived M cells (left graph). In those coronaries, ~25% of SMCs are EC-derived M cells (middle) and 44% of M cells express Gata4 (right). **(D)** Quantification using serial sections revealed approximately half of coronary arteries contain endothelial-derived A cells (left graph) and ~65% of A cells express Gata4 (right).

Heterogenous populations of quiescent and proliferating perivascular cells exist in the adult heart

Endothelial cell lineage tracing marks four distinct cells populations: ECs, smooth muscle cells in the media layer of coronary arteries (M cells), adventitial cells immediately surrounding the coronary vessels (A cells), and mature cardiomyocytes. The appearance of M and A cells is also restricted to coronary arteries. Since the microvasculature and veins do not require a smooth muscle layer for support, or contain surrounding adventitial cells, the arteries serve as the only site for observing these unique cell populations.

A cells did not express EC markers, noted by the absence of CD31 expression, and also were negative for mature CM markers such as α-Actinin (**Figure 23A,B**). A cells were often small in size, and found in clusters that stained with antibodies recognizing cell-cycle markers Ki67 and phospho-Histone H3 (pH3) (**Figure 23B,C**). Around 20% of A cells stained positive for proliferation markers (**Figure 23D**).

The proliferative phenotype was a unique property of A cells among all labeled cell types identified in the cell fate mapping experiments. In contrast to the proliferative A cells, M cells were quiescent, as noted by the consistent absence of Ki67 and pH3 staining. M cells were also larger in size than their adjacent adventitial A cells. Furthermore, pulse-chase analysis of ECs using the inducible End-SCL-CreER^{T}-LacZ mouse showed EC-derived perivascular M & A cells can be detected as early as 3 days after the end of the tamoxifen pulse (**Figure 21E**).

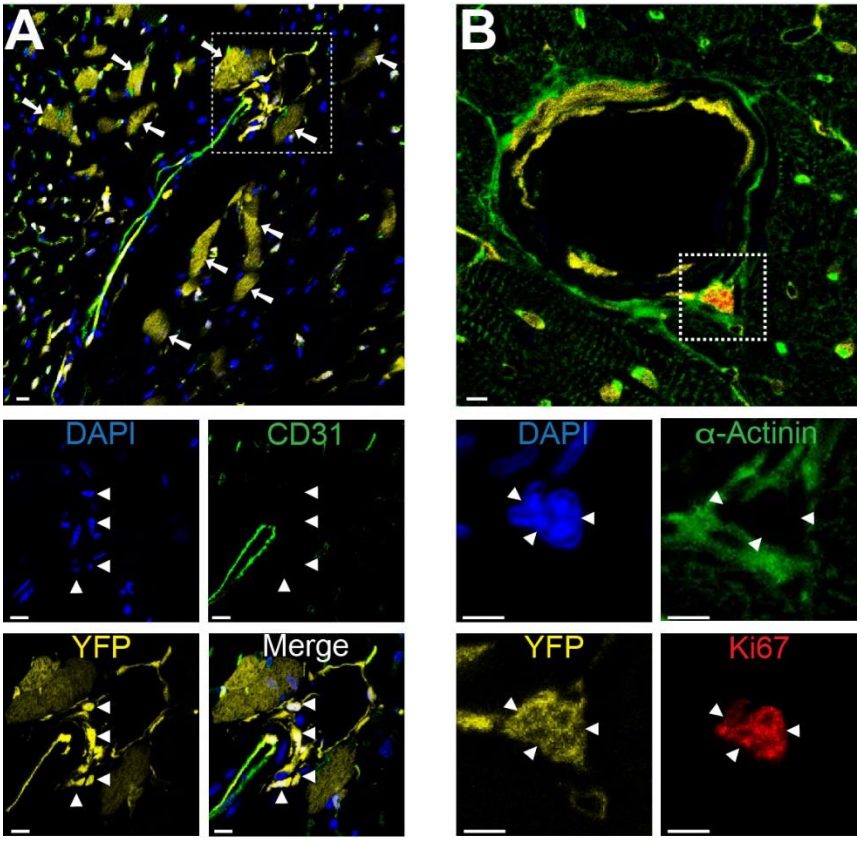

Figure 23. Quiescent M cells and proliferative A cells. (A) A cells are often found in close proximity to YFP$^+$ CMs (arrows). YFP$^+$ A cells lost CD31 expression (arrowheads in magnified boxed areas below). Scale bars 10μm. **(B)** A cells (arrowheads in magnified boxed area) do not express α-Actinin, but stain positive for proliferation marker Ki-67. Scale bars 5μm. **(C)** A cells (arrows in magnified boxed area) stain positive for proliferation marker pH3. Arrowheads indicate YFP$^+$ ECs. Scale bars 5μm. **(D)** Ki-67$^+$ (top graph) and pH3$^+$ (bottom) cells represent ~20% and 16% of A cells, respectively.

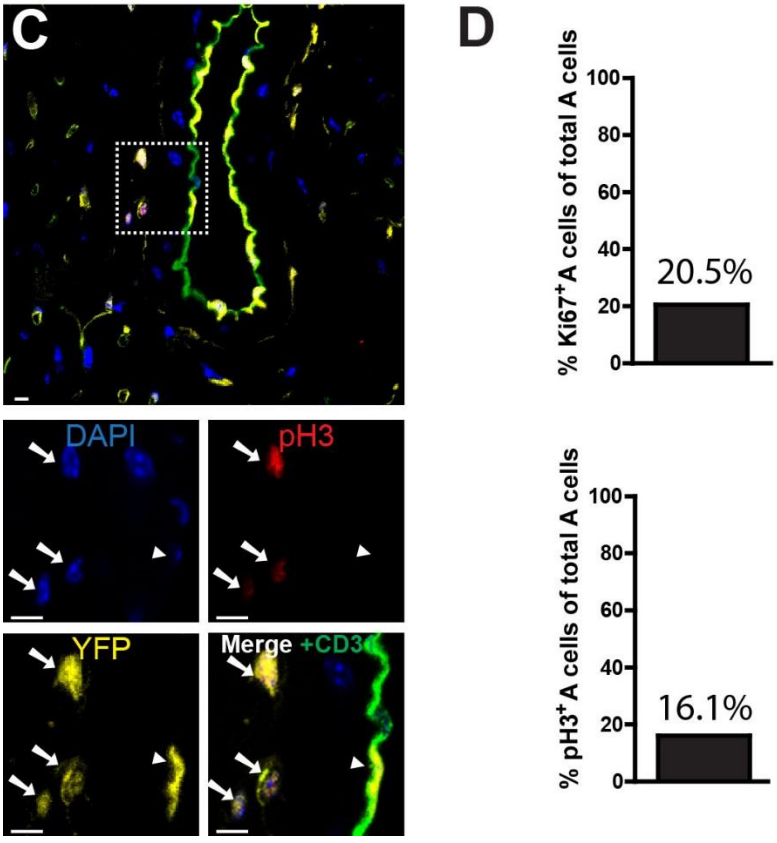

Lineage tracing using Tie1-Cre-Confetti mice indicated coronary ECs and M cells were heterogeneously labeled and expressed different color fluorescent proteins (**Figure 24A,B**). In contrast, A cell clusters were uniformly marked by the same color fluorescent protein (**Figure 24B,C**). This labeling pattern suggests A cell clusters expand from a single cell, consistent with their expression of proliferation markers.

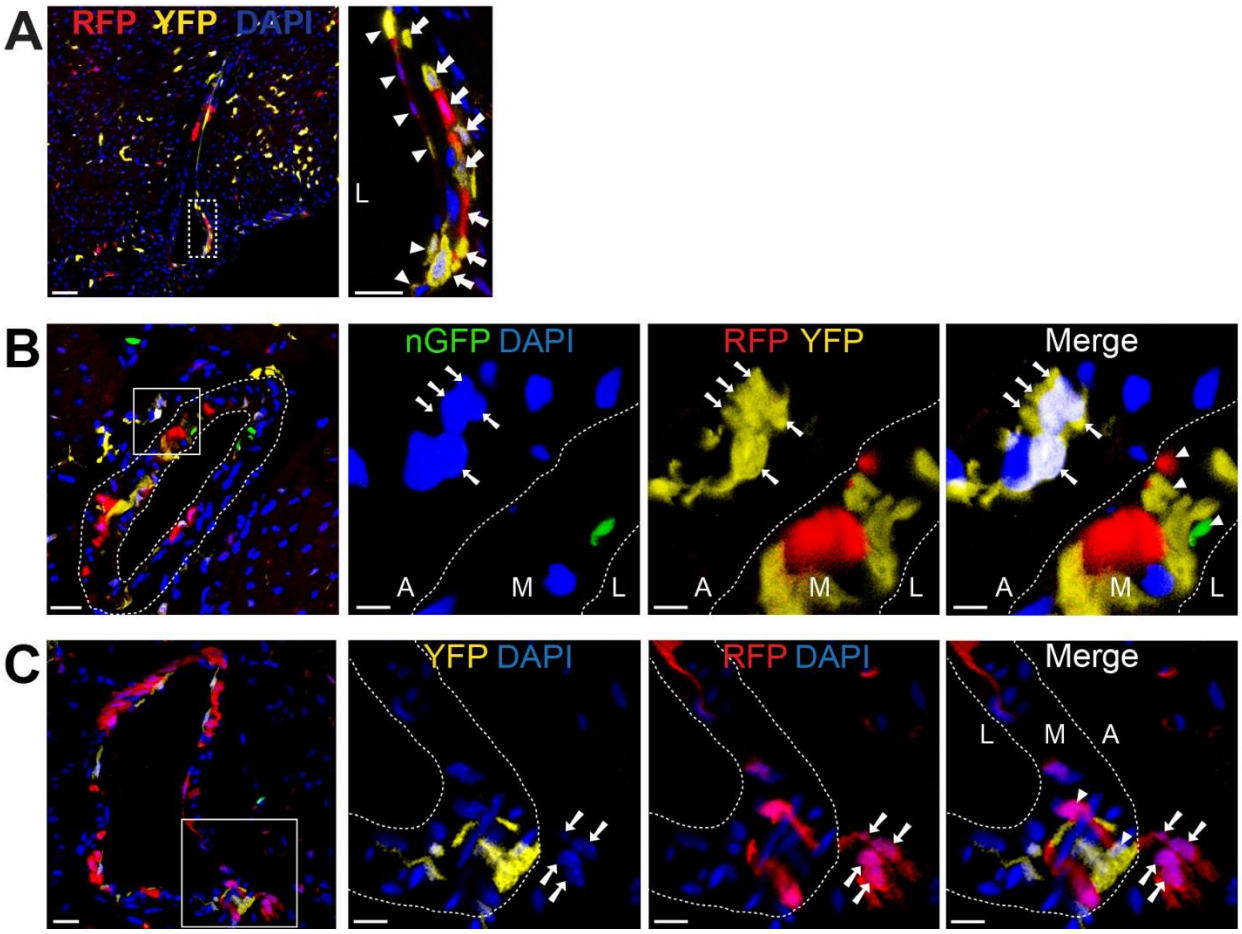

Figure 24. Uniform labeling of A cell clusters suggests single-cell origins. (A-C) Epifluorescence analysis of cardiac sections from Tie1-Cre-Confetti mice. **(A)** Images show heterogeneous labeling of M cells expressing either RFP or YFP (arrows). Arrowheads indicate RFP^+ or YFP^+ ECs. Scale bars, 50μm for original and 20μm for Inset. **(B)** Clusters of A cells are uniformly marked by a single color fluorescent protein (YFP). In the magnified area, arrows point to YFP^+ A cells. Heterogeneous labeling of fluorescent M cells (with RFP, YFP, or nGFP) is seen in the media layer (arrowheads, Merge). Scale bars, 20μm for original, 5μm for Insets. **(C)** Heterogeneous labeling of M cells (RFP and YFP; arrowheads) in contrast to the uniform marking of A cell clusters (RFP, arrows). Scale bars, 20μm for original image, 10μm for insets. Abbreviations: L, M, and A stand for lumen, media, and adventitia, respectively, of the coronary arterial wall.

IF analysis showed no Cre recombinase protein expression in labeled M and A cells, supporting an endothelial origin (**Figure 25A**). Consistent with this possibility, staining of heart tissue sections from Tie1-Cre-YFP and wild-type C57Bl/6 mice with antibodies recognizing mesenchymal markers illustrated that a rare subpopulation of coronary endothelium expresses the mesenchymal marker FSP-1 (Zeisberg *et al.,* 2007) (**Figure 25B-D**). This subpopulation of cells represents approximately 2.5% of coronary ECs (**Figure 25C**).

In addition, proteins known to initiate mesenchymal transformation such as Snail were also observed within rare populations of coronary vasculature (Timmerman *et al*., 2004) (**Figure 25E**). Subcellular Snail localization was observed in both nuclear and cytoplasmic compartments, a pattern that depends on the activation state of Snail (Dominguez *et al*., 2003).

The co-staining of coronary ECs with mesenchymal markers lend support to the idea that labeled perivascular cells of EC origin are derived by EndMT. Rare subpopulations of coronary ECs appear to undergo EndMT and generate αSMA^{+} M cells in the coronary wall. Staining of this cell population with the EndMT-associated transcription factor Snail suggests coronary ECs are capable of generating SMCs.

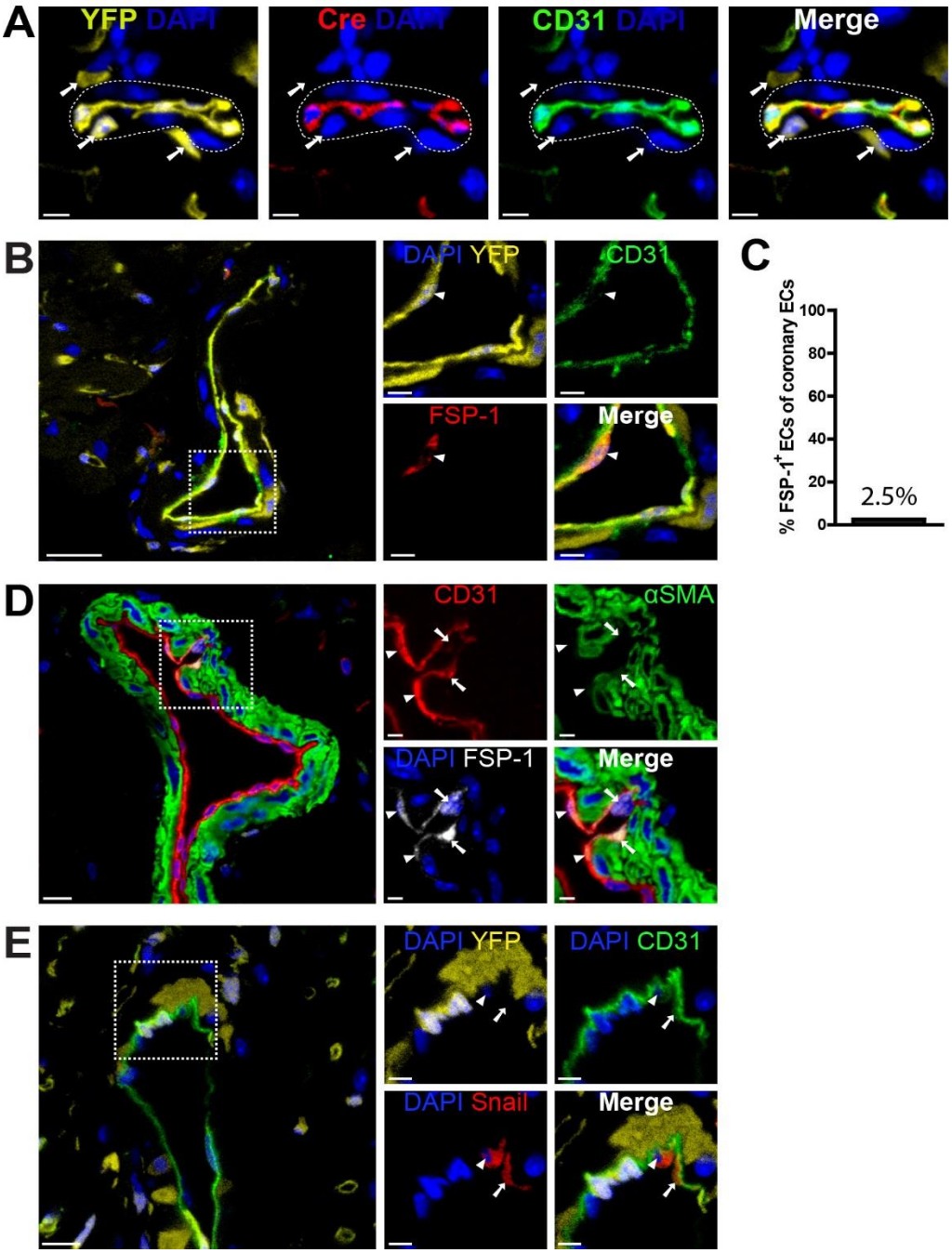

Figure 25. Coronary ECs undergo EndMT to generate M cells. (A,B) Cardiac sections from Tie1-Cre-YFP mice. **(A)** IF analysis with antibodies recognizing Cre recombinase protein show Cre expression is restricted to CD31$^+$ ECs and does not mark YFP$^+$ perivascular cells M and A cells (arrows) within the coronary artery wall. Scale bars, 5μm. **(B) A**ntibodies recognizing the mesenchymal marker FSP-1 indicate rare co-labeling with coronary ECs. Scale bars, 20μm in original, 5μm in insets. **(C)** Approximately 2.5% of coronary ECs co-stain with FSP-1 (N=3 mice, n=16 separate coronary vessels). **(D)** IF analysis of cardiac sections from C57Bl/6 mice indicate a rare population of CD31$^+$/FSP1$^+$ ECs. **(E)** Cardiac sections from Tie1-Cre-YFP mice show a subpopulation of coronary ECs express Snail. Arrowheads indicate nuclear co-staining; arrows indicate cytoplasmic co-staining. Scale Bars, 10μm for originals, 5μm for insets.

Endothelial progeny in perivascular areas include Sca1$^+$ cardiac progenitor cells

The results of the lineage tracing experiments and the identification of EC-derived intermediate cell populations suggested these intermediates represent cardiac progenitor cells. To test this possibility, we stained cardiac tissue sections from Tie1-Cre-YFP mice with antibodies recognizing Sca1 and c-Kit. These two cell surface markers are increasingly used to identify populations of cardiac stem cells.

The results showed M cells did not express either marker. However, 42% of the YFP$^+$ A cells stained positive for Sca1, whereas only a small subset (5%) of A cells stained positive for c-Kit (**Figure 26**). Further histological analysis showed the majority (>70%) of perivascular, Sca1$^+$, CD31$^-$ cells expressed YFP. These results suggest a significant fraction of Sca1$^+$ CSCs are descendants of ECs.

3-D reconstruction of a coronary artery, using z-stack imaging, provided a physical depiction of the spatial arrangement of M and A cells within the coronary niche (**Figures 27A**). ECs, M cells, and A cells are highlighted in gray to showcase their locations within the coronary niche. Single 2-D panels also indicate the locations of these three cell populations (**Figure 27B**), but full reconstruction of a portion of the coronary artery provides a more comprehensive picture of this niche *in vivo*.

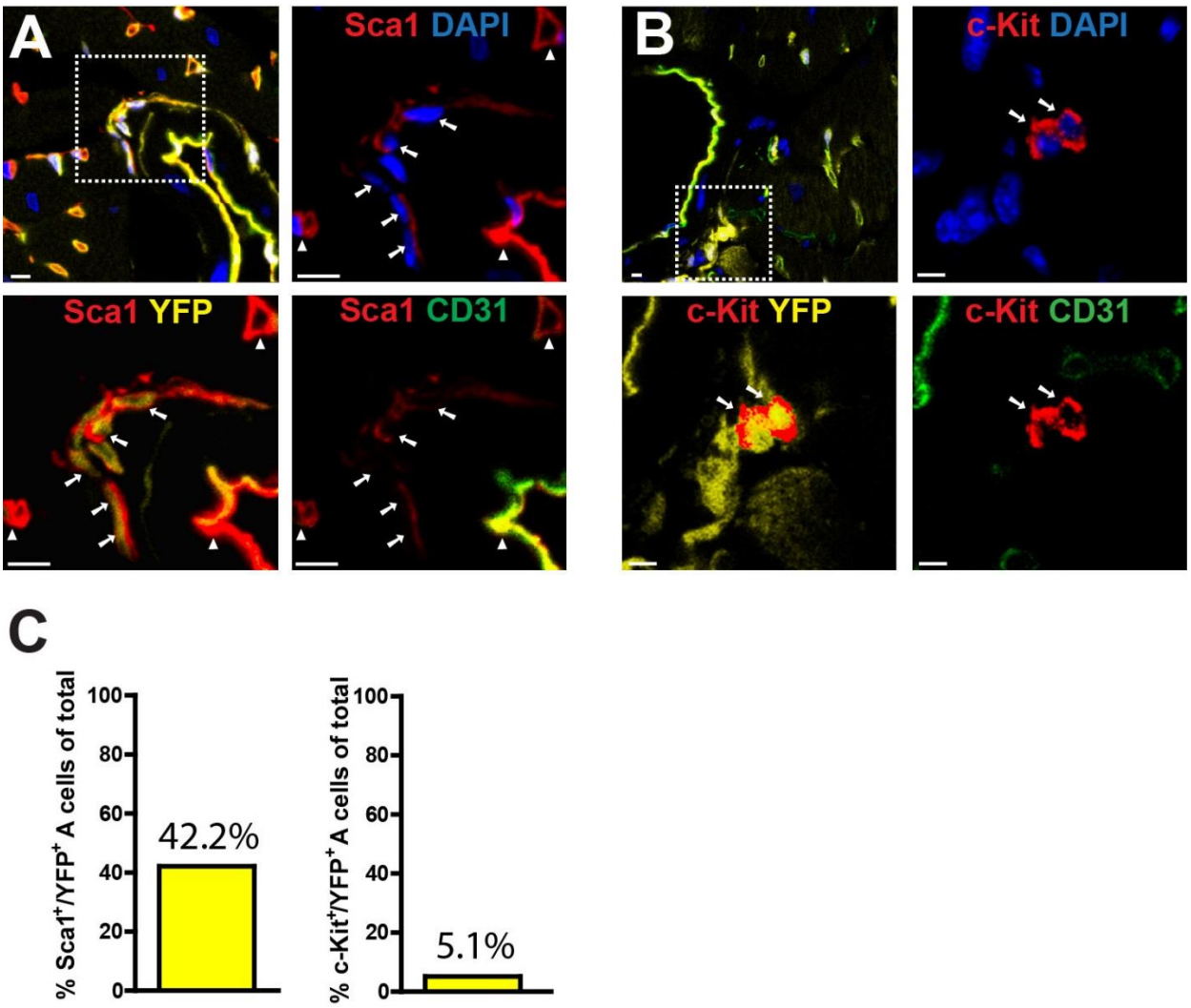

Figure 26. Endothelial fate mapping yields cardiac progenitor cells. (A,B) IF analysis of cardiac tissue sections from Tie1-Cre-YFP mice illustrates $YFP^+/CD31^-$ A cells express Sca1 (panel A) whereas a small subpopulation expresses c-Kit (panel B). Arrows in magnified areas in panel A indicate $YFP^+/Sca1^+$ cells, and arrowheads indicate $Sca1^+$ ECs. Arrows in (B) indicate $cKit^+$ cells in magnified areas. DAPI was used for nuclear counter staining. Scale bars 5µm. **(C)** Serial section analysis of cardiac tissue measured ~40% and 5% of A cells are $Sca1^+$ or $c\text{-}Kit^+$, respectively.

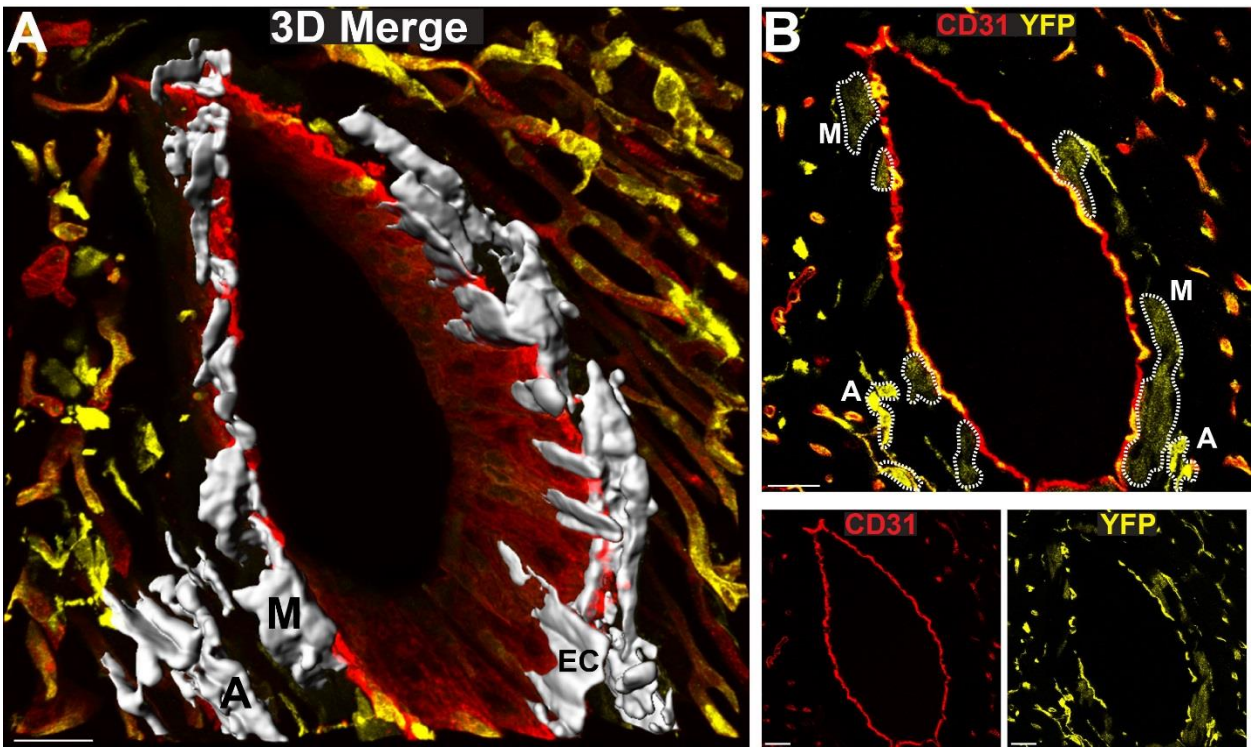

Figure 27. Spatial arrangement of M and A cells within the coronary artery niche. (A) A series of confocal images (z-stack) were acquired sequentially on a 100μm thick cardiac section from a Tie1-Cre-YFP mouse and stained with anti-CD31 antibodies. CD31 (red) and YFP epifluorescence (yellow) marks microvasculature and coronary ECs. Perivascular M and A cells surround the coronary artery (highlighted in white). **(B)** A single cross-section from within the z-stack depicts CD31 (bottom left panel) and YFP (bottom right panel) expression. The merged image (top panel) shows individual M and A cells (outlined with dashed lines) within, and immediately adjacent to, the coronary arterial wall. Abbreviations: EC, endothelial cells; M, M cells; A, A cells.

Considering the results described above and taking into account the cellular spatial relationships, (i.e., distance from coronary endothelium), we propose the following model (**Figure 28**): endothelial, or endothelial-like cells give rise to quiescent, perivascular cells in the coronary wall that lose EC markers and acquire SMC characteristics. These cells, termed M cells, express early cardiac differentiation markers such as Gata4. Further distal to the vascular wall, M cells are replaced by A cells, which lose SMC characteristics, but maintain expression of Gata4, and acquire markers of CSCs such as Sca1^{+}. A cells proliferate, leave the coronary niche, and differentiate to CMs. Thus, EC-derived YFP^{+} M and A perivascular cells within the medial and adventitial layers of coronary vessels likely serve as intermediate populations during generation of adult CMs.

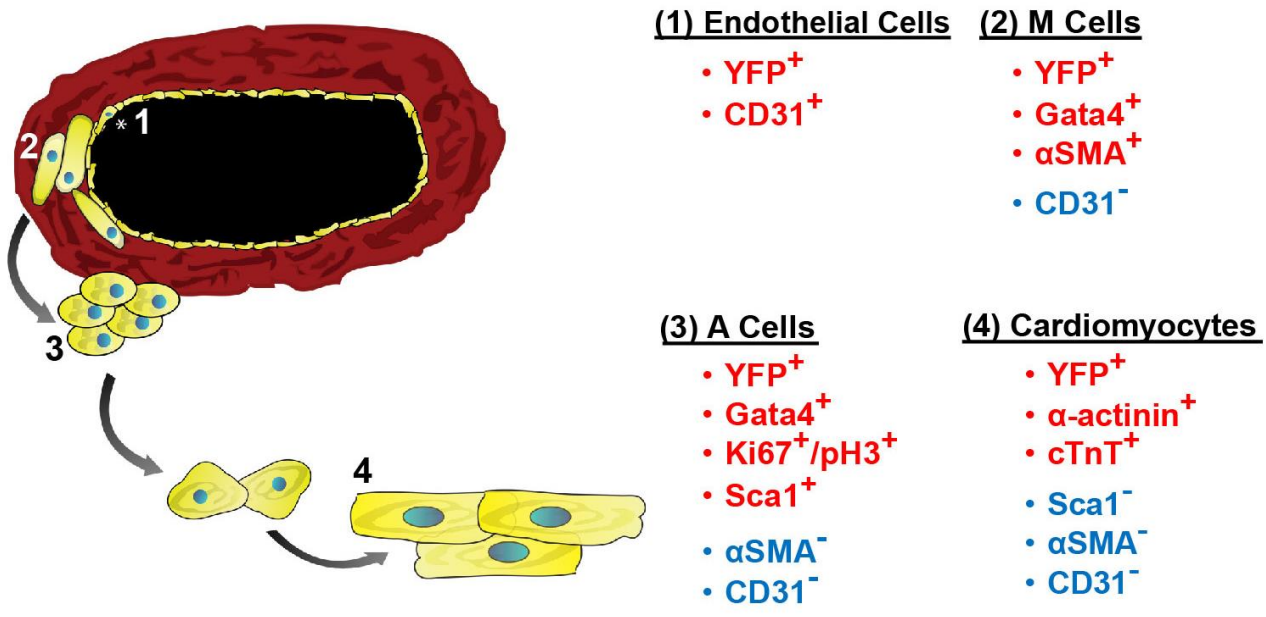

Figure 28. Coronary niche model. Schematic drawing of the cardiac stem cell niche model illustrates the spatial organization of EC progeny. The four unique cell populations marked during endothelial lineage tracing are included with their corresponding expression profiles.

It is important to note that alternative interpretations may also explain the pattern of the lineage tracing results. For instance, low level expression of EC genes in cardiac fibroblasts with cardiogenic potential could account for the observed labeling of cardiomyocytes. Another possibility is that rare proliferating CMs transiently express EC genes, and become labeled before proliferating into labeled clusters. While expression of endothelial markers was not observed in fibroblasts or CMs, the results above cannot fully exclude such possibilities.

DISCUSSION

Current evidence showing low rates of CM apoptosis suggests a renewal mechanism is required to maintain cardiac tissue (Anversa *et al*., 2006; Ellison *et al*., 2007), yet there is little information regarding the native regenerative mechanisms during cardiac homeostasis. Lineage tracing of vascular cells in the healthy adult heart indicates ECs retain cardiogenic potential. The data from this chapter show that 1) the EC-based regenerative mechanism generates both quiescent (M cells) and proliferative (A cells) progeny expressing early stage cardiac differentiation genes such as Gata4, 2) $Sca1^{+}$ cardiac stem cells are EC progeny, and 3) the coronary arteries serve as a structural component of the cardiac stem cell niche, organized in a radial manner.

Although the site of the original cell type with EC characteristics that gives rise to CMs remains currently undetermined, our data provide evidence that the majority (>70%) of $Sca1^{+}$ CSCs are derived from cells with endothelial characteristics. We found EC-derived $Sca1^{+}$ perivascular cells lost endothelial markers and gave rise to $CD31^{neg}$, $Sca1^{+}$ cells. These cells expressed early cardiac markers such as Gata4, but

lacked mature CM characteristics such as sarcomeric structures and α-Actinin expression. In support of this finding, $Sca1^+$ CSCs continuously replace myocardial cells in the adult heart (Uchida *et al.*, 2013). In contrast, we found limited overlap between endothelial-derived YFP^+ cells and c-Kit^+ cells, suggesting the majority of c-Kit^+ cells in the heart belong to a different lineage.

Moreover, the data show EC-derived $Gata4^+$ cells around coronary arteries can be divided into subpopulations based on several criteria (location, size, molecular markers, and proliferation status), indicating the CSC niche is organized in a radial manner with the vasculature at the center. M-cells, closest to the lumenal ECs, are quiescent and combine smooth muscle and early cardiac characteristics, whereas A cells further afield in the adventitia are proliferative and acquire expression of Sca1.

In many respects, the CSC niche shares similarities with the neuronal stem cell niches in the brain. Here, neuronal stem cells in the SVZ give rise to astrocytes (a mesenchymal cell population similar to αSMA^+ cells), which differentiate to groups of proliferating cells before joining the rostral migratory stream (Fuentealba *et al.*, 2012). The cardiac renewal process is also confined to a small subpopulation of mature CMs, similar to the adult brain where renewal is mainly restricted to the olfactory bulb and dentate gyrus.

CHAPTER IV

ENDOTHELIAL CELLS CONTRIBUTE TO MYOCARDIAL REPAIR AFTER CARDIAC INJURY, AT THE EXPENSE OF CARDIOMYOCYTE REGENERATION

INTRODUCTION

After myocardial infarction, current treatment is designed to preserve residual heart function, prevent additional myocyte death through revascularization, and delay ventricular remodeling and heart failure through medical therapy. A number of studies using experimental models and human patients indicate that cardiac function can be improved through injection of stem cells directly into the myocardium, or when delivered through the coronary circulation (Joggerst and Hatzopoulos, 2009). However, the current challenge is to overcome the limited long-term engraftment of stem cells and their minimal differentiation into mature cardiovascular tissue (Bernstein and Srivastava, 2012).

Stem or progenitor cell therapy for treatment of cardiac disease holds the promise of restoring lost cardiac tissue. Enthusiasm for this field began with studies involving transplantation of progenitor cells into various animal models and demonstration of improved cardiac parameters (Segers and Lee, 2008). After muscle injury, skeletal myoblasts were shown to regenerate in mammals (Wagers and Conboy, 2005; Shi and Garry, 2006). Consequently, myoblasts were one of the first cell types transplanted into animal models of cardiac disease, which improved left ventricular function even though they did not fully differentiate into CMs (Reinecke *et al*., 2002).

The potential for tissue regeneration through transplantation of exogenous progenitor cells was studied through a number of government-sponsored clinical trials. One such initiative established by the National Heart Lung and Blood Institute is the Cardiovascular Cell Therapy Research Network (CCTRN) (Simari *et al*., 2010). These studies were based on data indicating that intracoronary delivery of autologous bone marrow mononuclear cells (BMCs) after MI can improve left ventricular function. (Schächinger *et al*., 2006; Janssens *et al*., 2006). One major question about delivery of autologous BMCs was when to administer them following an MI. Consequently, TIME and Late-TIME trials were designed to compare the effects after administration of BMCs in patients with ST-segment elevation MIs at either 3 or 7 days following MI (TIME), or 2 to 3 weeks after MI (Late-TIME) (Traverse *et al*., 2009; Traverse *et al*., 2010). Unfortunately, results from both TIME and Late-TIME trials indicated there was no global or regional improvement in LV function by six months after intracoronary BMC injection at 3 or 7 days following MI (Traverse *et al*., 2012), or 2 to 3 weeks post-MI (Traverse *et al*., 2011).

To date, skeletal myoblasts, bone marrow-derived cells (including BMCs), mesenchymal stem cells, and others have been administered to patients after MI, and produced variable results ranging from no significant effect to improved cardiac ejection fraction or ventricular function (Boudoulas and Hatzopoulos, 2009; Segers and Lee, 2008). Interestingly, after injection of these various cell populations, paracrine effects may actually provide most of the observed benefit by preventing necrosis and promoting healing of the injured myocardium (Gnecchi *et al*., 2005). Specifically, thymosin β4 is known to accelerate wound repair, and the Wnt antagonist secreted frizzled-related

protein 2 (sFRP2) can minimize hypoxia-induced necrosis in myocytes (Mirotsou *et al*., 2007; Hinkel *et al*., 2008; Alfaro *et al*., 2008). These studies implicate the distinct possibility of improving cardiac repair after ischemic injury through the use of biological mediators. Consequently, it is imperative to develop a better understanding of the molecular and cellular mechanisms occurring during the repair process.

Exogenous cell transplantation studies thus far have yet to achieve significant regeneration of cardiac tissue following MI. The inability of transplanted cells to regenerate CMs is primarily due to 1) poor engraftment of the injected cells, 2) the inability to integrate with supportive host cells, and 3) a lack of blood supply. An alternative strategy to transplantation of exogenous progenitor cells involves harnessing the regenerative potential of endogenous cells, which already exist within the myocardium, and are integrated with both vasculature and surrounding cells. Bolstering the natural cardiac regenerative mechanisms of endogenous cardiac progenitors holds great promise for tissue regeneration after injury.

Endogenous populations of CSCs, such as c-Kit$^+$ or Sca1$^+$ cells, represent a viable source for cell-based therapy, but we currently lack knowledge about their origins, and the molecular signaling pathways which regulate their fate after injury. Furthermore, a better understanding of the role of Sca1$^+$ EC-derived cardiac progenitors will provide a novel cell population to target for treatment during cardiac repair. Additional insight into changes in the Sca1$^+$ coronary niche after injury may provide new methods for improving recovery and survival, independently or in combination with stem cell therapy.

EXPERIMENTAL METHODS

Animals

The Tie1-Cre line (Gustafsson *et al*., 2001) and the Tamoxifen-inducible endothelial-SCL-Cre-ER^T line (Göthert *et al*., 2004) were crossed to R26R*stopLacZ* (Soriano, 1999) or R26R*stopYFP* (Srinivas *et al*., 2001) mice to generate double transgenics as described in Chapter II. The Tie1-Cre mouse line was also bred with the multi-fluorescent reporter R26R*stopConfetti* (Snippert *et al*., 2010).

Myocardial infarction

Adult, male mice underwent open chest surgery under anesthesia. During surgery, a 10-0 nylon suture was placed through the myocardium into the anterolateral left ventricular wall around the left anterior descending artery and the vessel was permanently ligated. After surgery, the chest was closed and the animals were allowed to recover. At defined time points after surgery, i.e. 1 and 3 weeks, mice were euthanized and whole hearts were isolated for whole-mount X-gal staining and histological analysis. Sham-operated animals underwent similar procedures without coronary artery ligation. Surgeries were performed in the Vanderbilt Mouse Cardiovascular Pathophysiology and Complications Core.

Angiotensin II infusion via osmotic pump

Tie1-Cre-YFP adult, male mice were implanted with an osmotic minipump (Alzet) containing Angiotensin II (AngII). Hypertension was induced by the infusion of AngII (490 ng-/kg per minute) for ~4 weeks (26 days). Sham mice were implanted with the minipump, but instead received a saline infusion. At the end of the experiment mice

were sacrificed, hearts were perfused with 1X PBS, and frozen in OCT to obtain cryo-sections.

Transverse aortic constriction

Tie1-Cre-LacZ adult, male mice underwent transverse aortic constriction (TAC) surgery to induce hypertension and subsequent cardiac hypertrophy. Control animals underwent the same procedure but did not receive arterial banding. Doppler (flow through) analysis was used to verify a reduction in velocity (mm/s) 1 day after TAC banding in experimental mice compared to controls. Echocardiography analysis was performed to quantify the change in fractional shortening (%FS) at 2 and 3 weeks post-TAC, compared to controls.

Fluorescence activated cell sorting

Suspensions of cardiac cells depleted of myocytes were prepared as follows. Murine hearts were washed to remove blood and aseptically isolated after incision at the base of the aorta. The atria were entirely removed. The ventricles of the heart were minced and digested with 10 mg/ml collagenase II (Worthington), 2.4 U/ml dispase II (Roche Diagnostics), DNase IV (Sigma) in 2.5 mM CaCl2 at 37°C for 20-25 minutes and then passed through a cell strainer. The myocyte-depleted cell suspension was centrifuged at 1500xg for 5 minutes and resuspended in 1X PBS containing 0.5% BSA and 2 mM EDTA.

To prevent non-specific binding, cells were incubated with FcR Blocking Reagent (Miltenyi Biotec). Single-cell suspensions (10^6 cells/ml) were then labeled using FITC-conjugated rabbit anti-GFP (A21311; Invitrogen), Cy7-conjugated anti-mouse Ly-6A/E

(Sca1), phycoerythrin-conjugated anti-mouse CD31 (clone 390; eBioscience), and peridinin-chlorophyll protein-conjugated anti-CD45 (clone 30-F11; eBioscience). Cells were incubated for 20 minutes at 4°C, washed and resuspended in PBS/BSA/EDTA buffer.

Data acquisition was performed on a FACScalibur flow cytometer (BD Immunocytometry Systems) in the Vanderbilt Flow Cytometry Core and the data were analyzed with the WinList 5.0 software. Antigen-negative background binding was defined by the fluorescent intensity of isotype controls.

Whole mount β-gal activity staining assay

Whole mouse hearts were isolated and X-gal stained as described in Chapter II.

Immuno- and epi- fluorescence

Freshly isolated hearts were prepared for cryosectioning as described in the Chapter II. Primary antibodies and their dilutions used include: rabbit anti-GFP, also recognizing YFP (Abcam, Ab290; 1:3000), mouse anti-α-SMA (Sigma, A2547; 1:800), rat anti-CD31 (BD Pharmingen; 1:100), and rabbit anti-FSP1 (S100A4) (Abcam, Ab27957; 1:200). The nucleophilic dye 4’,6-diamidino-2-phenylindole (DAPI; 1:5000; Invitrogen) was used to visualize cellular nuclei. Primary and corresponding secondary antibodies are also listed in **Table 2 (Appendix).**

Tamoxifen Preparation and Administration

For pulse-chase experiments, Cre recombinase was induced in adult, male End-SCL-CreER^T-LacZ mice by five intra-peritoneal injections of Tamoxifen as described in Chapter II.

Hematoxylin and Eosin counter-stain of X-gal stained cardiac sections

Paraffin-embedded hearts were cut in 10µm sections, and deparaffinized through Histo-Clear and graded alcohols per standard protocol. Slides were counterstained with Hematoxylin and Eosin (H&E), dehydrated, and mounted in Cytoseal-60 (Fisher).

Quantification of endothelial-derived CMs per volume of cardiac tissue

Cardiac cross-sections from End-SCL-CreER^T-LacZ mice, previously stained with X-gal for β-gal activity and counterstained with H&E, were analyzed to determine the number of labeled CMs per volume of cardiac tissue as described in Chapter II.

Statistical analysis

All values were reported as mean +/- S.D. Statistical significance was assessed by Student's unpaired two-tailed *t*-test for all statistical analysis comparisons. Statistical significance was expressed as follows: *$p < 0.05$; **$p < 0.01$.

RESULTS

Endothelial cell lineage tracing after acute ischemic injury labels myofibroblasts

The regenerative rates of ECs during homeostasis indicate a low percentage of cardiac tissue is renewed in the adult heart. However, the effects of ischemic injury or fibrosis, such as that caused by myocardial infarction or hypertension, have not been studied on this particular population of cells. The resulting effects on M and A cells, and EC-derived CM regenerative rates, were studied under conditions of acute (MI) and chronic (pressure overload) cardiac injuries.

Adult, male Tie1-Cre-YFP mice underwent experimental MI surgery and were sacrificed one week after infarction. Within the infarct, IF analysis revealed labeling of ECs and myofibroblasts (**Figure 29A**). Quantitative analysis of YFP^+ αSMA^+ cells, which marks reparative myofibroblasts or endothelial origin, indicated approximately 35% of total αSMA^+ cells were derived from ECs (**Figure 29B**). By comparison, sham hearts, which did not receive an infarction, had less than 1% of total αSMA^+ cells that co-expressed YFP. Furthermore, analysis of infarct tissue using a second marker for fibroblasts known as fibroblast specific protein (FSP-1), indicated substantial co-staining of EC-derived myofibroblasts (**Figure 29C**). These myofibroblasts of endothelial origin co-stained with the mesenchymal marker FSP-1, but not with the endothelial marker CD31.

To explore the clonal origins of infarct myofibroblasts, the Tie1-Cre-Confetti mouse line was used. Similar to EC lineage tracing in the uninjured heart, this multi-fluorescent reporter can determine if infarct myofibroblasts are clonally related or independently derived (**Figure 13**). If these repair cells have a clonal origin they will all

express the same color fluorescent protein; however, if they are independently derived, then each cell will randomly express a color. Analysis of infarct tissue from Tie1-Cre-Confetti mice indicated that EC-derived infarct myofibroblasts consisted of a heterogenous population of cells (**Figure 29D**). Expression of nGFP, YFP, and RFP was observed in apparent random fashion throughout the infarct, and clusters of myofibroblasts in which all cells expressed the same color did not appear within the injury tissue.

The granulation tissue repair phase begins around 4-7 days after MI and generally concludes with 21 days (3 weeks) in the mouse. At this point in the repair process, infarct myofibroblasts undergo apoptosis or migrate out of the mature scar tissue. To study the contribution of myofibroblasts within the infarct at 3 weeks after MI, End-SCL-CreER^{T}-LacZ mice were given a series of Tamoxifen injections (pulse) to label ECs, underwent experimental MI, and were sacrificed 3 weeks after surgery. Consistent with the infarct repair timeline, analysis of cardiac tissue from these mice indicated a lack of myofibroblasts; (both EC-derived or originating from other sources) (**Figure 29E**). At this later repair time point, EC lineage tracing marked only ECs of larger vessels and microvasculature. Sham mice, which underwent thoracotomy surgery without ligation and were sacrificed 3 weeks after, also displayed labeling of ECs, but not myofibroblasts.

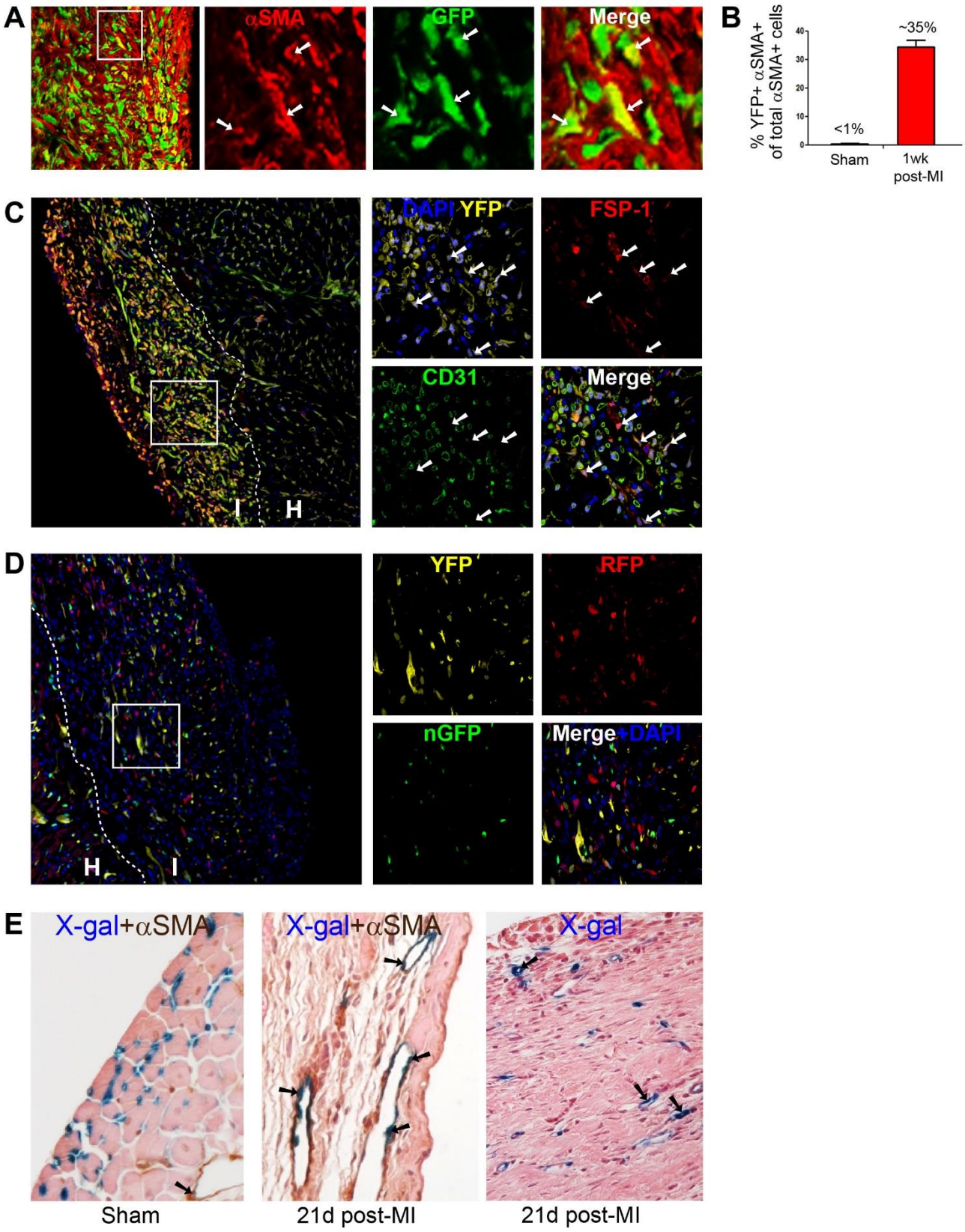

Figure 29. Endothelial fate mapping 1 week after MI marks infarct myofibroblasts.

Figure 29. Endothelial fate mapping 1 week after MI marks infarct myofibroblasts. (A-C) Tie1-Cre-YFP adult, male mice were used for histological analysis 1 week after MI surgery. **(A)** IF analysis of infarct tissue indicated numerous EC-derived myofibroblasts, as determined by co-staining of YFP and the mesenchymal marker, αSMA. Arrows indicate αSMA^{+} GFP^{+} myofibroblasts. **(B)** Serial histological sections were used to quantify numbers of YFP^{+} αSMA^{+} cells, which were compared with the total number of observed αSMA^{+} cells in the infarct tissue. Based on their co-expression of YFP, approximately 35% of total myofibroblasts within the scar tissue were EC-derived. Arrows indicate $FSP\text{-}1^{+}$ YFP^{+} myofibroblasts. **(C)** Within the infarct tissue, a large proportion of repair cells were YFP^{+}, $FSP\text{-}1^{+}$, $CD31^{neg}$, indicating an endothelial origin of these myofibroblasts. Dashed line indicates border between healthy and infarct tissue. **(D)** Tie1-Cre-Confetti mice sacrificed 1 week post-MI show heterogenous labeling of infarct repair cells. Seemingly random expression of nGFP, YFP, and RFP was observed within the tissue. Dashed line indicates border between healthy and infarct tissue. **(E)** Analysis of cardiac tissue from End-SCL-$CreER^{T}$-LacZ mice sacrificed 3 weeks after MI surgery indicated a lack of infarct myofibroblasts. Staining with X-gal, and co-staining with antibodies against αSMA, showed occasional $X\text{-}gal^{+}$ αSMA^{+} perivascular cells. However, as compared to 1 week after MI, a lack of myofibroblasts within the scar was observed at 3 weeks post-MI. Arrows indicate $X\text{-}gal^{+}$ αSMA^{+} perivascular cells (sham and 21days post-MI, middle panel), and $X\text{-}gal^{+}$ vascular cells (21days post-MI, right panel). Abbreviations: H, healthy myocardium; I, infarcted myocardium.

EC lineage tracing in the uninjured heart indicated annual CM regenerative rates of ~0.3%. To determine what affect global ischemic injury had on CM renewal, End-SCL-$CreER^{T}$-LacZ mice were pulsed with Tamoxifen, once every 48 hours, to label ECs. Seven days after the fifth and final injection, mice underwent experimental MI, and were sacrificed at either 1 or 3 weeks after surgery (**Figure 30A**). Rare $X\text{-}gal^{+}$ CMs, identified based on morphology, were observed within the border zone, infarct, and healthy myocardium at both 1 and 3 weeks following MI (**Figure 30B**). Serial histological analysis of infarct tissue indicated a significant reduction in EC-derived cardiomyocytes at 1 and 3 weeks after MI, when compared to sham controls (**Figure 30C**). Furthermore, CM renewal rates did not increase between 1 and 3 weeks after ischemic injury, suggesting the repair process prevents any EC-derived cardiac progenitor cell regenerative response.

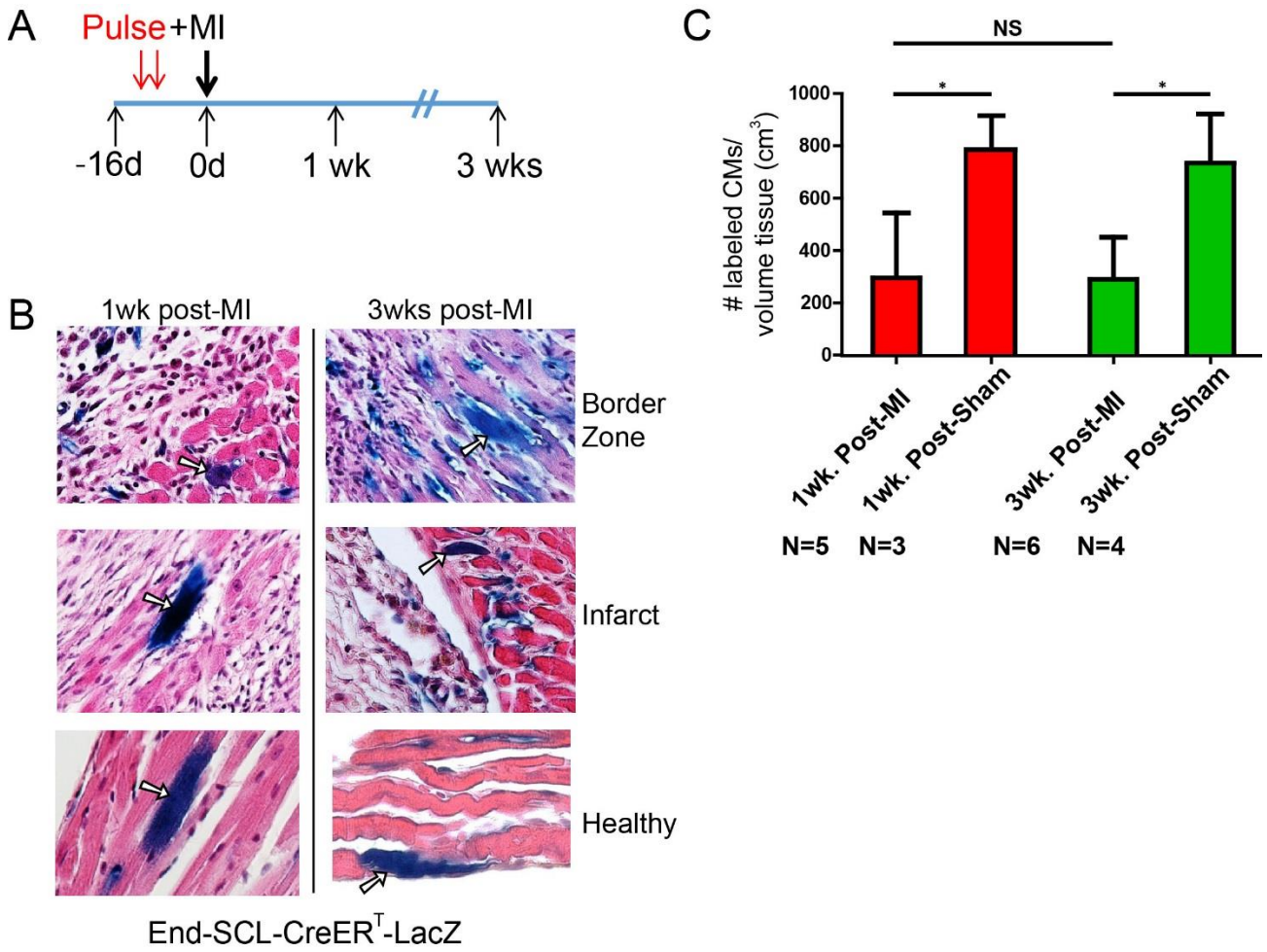

Figure 30. CM renewal rates drop after ischemic injury and have not recovered by 3 weeks post-MI. (A) End-SCL-CreER^T-LacZ mice were given a series of five intraperitoneal Tamoxifen injections to induce labeling of ECs. Seven days after the final injection, mice were given an experimental MI, and sacrificed at either 1 or 3 weeks after surgery. Sham mice underwent thoracotomy surgery but did not have the left anterior descending (LAD) coronary artery ligated. **(B)** Histological sections from End-SCL-CreER^T-LacZ mice sacrificed at 1 or 3 weeks post-MI were stained with H&E, and counter-stained with X-gal to visualize ECs and their derivatives. EC-derived X-gal$^+$ CMs (indicated by arrows) were observed with the border zone and infarct tissues, as well as the healthy myocardium at both time points. **(C)** Histological analysis of cardiac tissue revealed a significant reduction in the number of X-gal$^+$ CMs compared with sham controls at 1 and 3 weeks post-infarction. EC-derived cardiomyocyte renewal rates did not recover by 3 weeks after infarction, the latest time point analyzed.

YFP$^+$ EC and EC-derived populations proliferate 1 week after MI

Myocardial infarction and the subsequent cardiac ischemia induces a significant change in endothelial cell fate. EC lineage tracing after MI marks myofibroblasts contributing to infarct repair. Furthermore, a decline in CM regenerative rates is observed throughout different regions of ventricular tissue, including healthy myocardium, as well as infarct and border zone tissue. Thus, characterizing the changes which occur after MI in specific YFP$^+$ cell populations would provide important insight into the alternative EC fate.

Flow cytometry analysis was used to assess total numbers of cardiac YFP$^+$ cells one week after experimental MI surgery (**Figure 31**). Tie1-Cre-YFP adult, male mice were given an MI and sacrificed 7 days after. Cells were isolated from complete ventricular tissue and analyzed by flow cytometry after excluding cardiomyocytes. Analysis of non-EC, non-hematopoietic cells (CD31^{neg}, CD45^{neg}) showed an increase in the percentage of Sca1$^+$ YFP$^+$ cells after MI, indicating a greater contribution of EC-derived Sca1$^+$ cells in response to injury. (**Figure 31A**). In addition, the percentage of proliferating non-endothelial Sca1$^+$ cells (Sca1$^+$, Ki67$^+$) dramatically increased after MI (**Figure 31B**).

There is also a significant increase in the number of proliferating non-endothelial, non-hematopoietic YFP$^+$ cells 7 days after MI, in comparison to sham controls (**Figure 31C**). **Figure 31A** indicates that roughly one third of non-endothelial YFP$^+$ cells are Sca1$^+$, but does not account for the remaining proportion of YFP$^+$ cells. Alternative populations of EC-derived YFP$^+$ cells, such as myofibroblasts, likely represent the remaining proliferating cells.

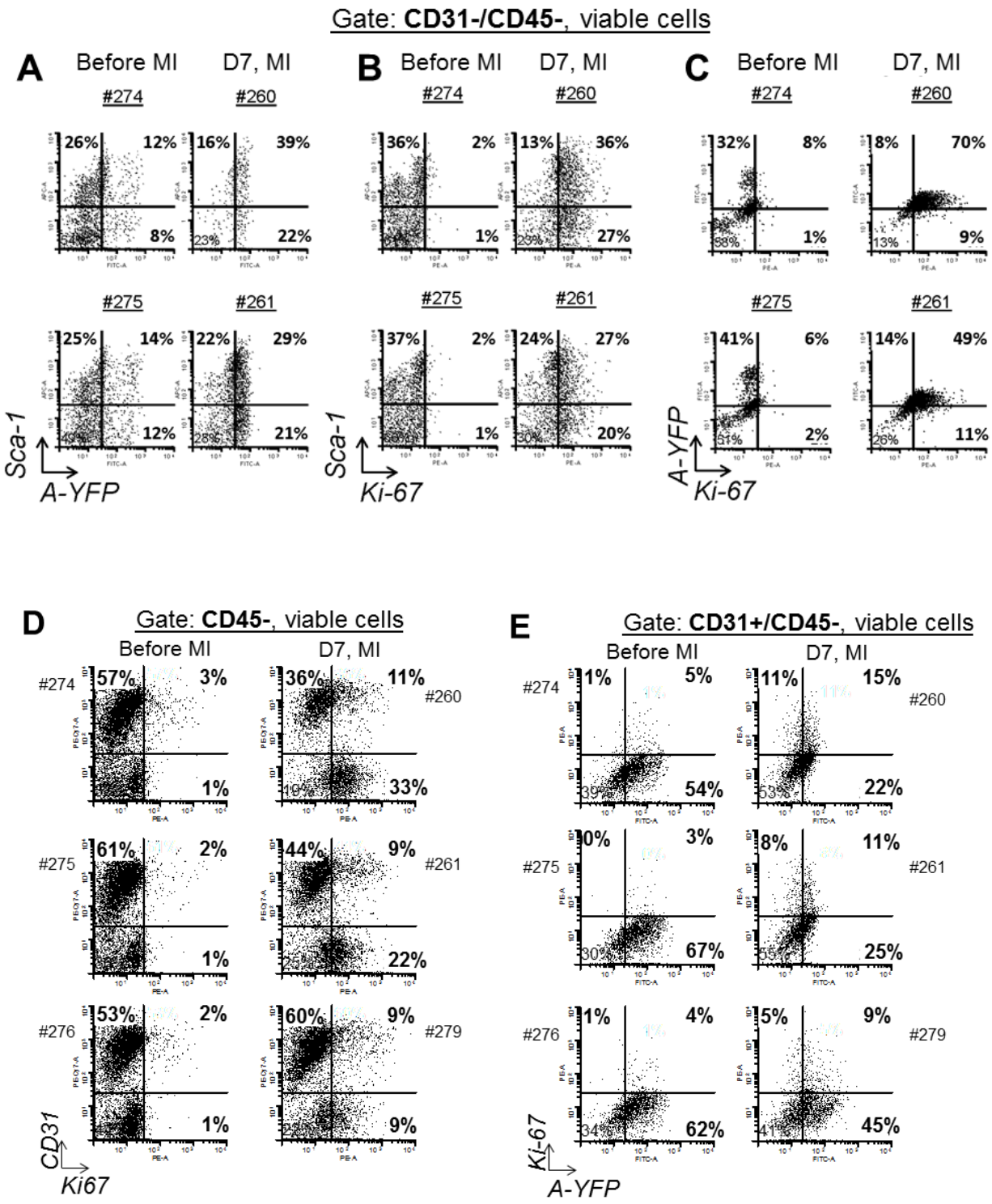

Figure 31. YFP⁺ endothelial cell and non-EC populations proliferate 1 week after MI.

Figure 31. YFP$^+$ endothelial cell and non-EC populations proliferate 1 week after MI. **(A-E)** FACS analysis of Tie1-Cre-YFP adult, male mice was performed one week after infarction to assess the relative percentages of specific YFP$^+$ cell populations in the heart. **(A)** Gating for CD31^{neg}, CD45^{neg} (non-EC, non-hematopoietic cells) reveals an increase in EC-derived Sca1$^+$ cells. **(B)** The same gating parameters as (A) indicate the EC-derived Sca1$^+$ cell population undergoes a significant increase in proliferation. **(C)** A large percentage of YFP$^+$ non-EC, non-hematopoietic cells are revealed to proliferate after MI. Not all of these proliferating YFP$^+$ cells are Sca1$^+$ (see panel A), indicating alternative YFP$^+$ EC-derived cells, such as myofibroblasts, also response to injury by proliferating. **(D)** Analysis of non-hematopoietic (CD45^{neg}) cells illustrates that ~4 fold more ECs proliferate in response to MI. **(E)** Gating for CD31$^+$, non-hematopoietic cells shows YFP$^+$ ECs proliferate after MI.

Gating for non-hematopoietic (CD45^{neg}) cells indicated that a greater proportion of endothelial cells also proliferate after MI (**Figure 31D,E**). Approximately 4 fold more CD31$^+$ cells express the proliferative marker Ki67, and a similar increase in YFP$^+$, CD31$^+$ ECs is observed under more stringent gating conditions. The proliferating ECs may be contributing to angiogenesis, which is actively occurring at this point in the repair process.

The FACS data, analyzing YFP$^+$ cell fate at 1 week after infarction, indicate an alternative fate for ECs and EC-derived cells after ischemic injury. The granulation tissue phase, which is active by 1 week post-infarction, requires extensive angiogenesis and fibrosis. Consequently, the proportion of proliferating ECs at this time during repair increases significantly in comparison with sham controls. Revascularization of the infarct tissue is necessary to provide oxygen and nutrients to repair cells via the blood, and the YFP$^+$ ECs actively participate in this reparative process. There is also an increase in proliferating YFP$^+$ non-endothelial cells at this time point. A large proportion of these EC-derived YFP$^+$ cells are likely myofibroblasts contributing collagen to

strengthen the wound. Flow cytometric analysis of this YFP^+ subpopulation with a fibroblast marker such as αSMA would confirm the identity of these repair cells.

Furthermore, by 1 week post-MI, an increase in the percentage of proliferating YFP^+, $Sca1^+$ cells was observed in comparison to sham controls. While the overall rates of cardiomyocyte regeneration appear to decrease following infarction, it is interesting that the proportion of proliferating $Sca1^+$ cardiac progenitors increases. This finding may reflect an alternative fate for these cells under conditions of cardiac injury, and if so, represents a unique opportunity to stimulate $Sca1^+$ cardiogenic potential, as is observed in the uninjured heart.

Chronic hypertension causes fibroblast production from non-EC populations

Acute ischemic cardiac injury, such as myocardial infarction, causes immediate cell death and invokes a massive reparative response which resolves in a few weeks. In contrast to the abrupt cellular and molecular changes which occur after MI, chronic cardiac injury due to hypertensive heart disease elicits a different reparative response. Chronic hypertension can occur for a variety of reasons, such as diet (i.e.: high in salt), weight, age, or genetics. The consistent pressure and volume overload eventually causes left ventricular hypertrophy (LVH). This type of maladaptive ventricular remodeling often leads to pathological systolic or diastolic dysfunction, and heart failure. The underlying myocardial fibrosis and CM necrosis are associated with substantial rates of morbidity and mortality (Neeland *et al*., 2013).

This type of long-term, less-immediately damaging injury can be experimentally modeled through transverse aortic constriction (TAC) surgery or administration of the

vasoconstrictor Angiotensin II (AngII). The peptide hormone AngII is part of the renin-angiotensin-aldosterone-system (RAAS), and increases blood pressure through vasoconstriction of arteries and veins. AngII also induces release of aldosterone from the adrenal cortex, which further increases blood pressure through promoting retention of sodium. Alternatively, TAC surgery reduces the internal diameter of the aorta through banding, which causes hypertension through pressure overload, and leads to cardiac hypertrophy within several weeks.

Adult, male Tie1-Cre-LacZ mice underwent experimental TAC surgery to induce hypertrophy and determine how the EC-based cardiac regenerative response changes with chronic injury. Sham mice underwent thoracotomy surgery but did not have the aorta banded. Doppler velocity flow rates indicated a significant change in velocity between Baseline and after TAC surgery, as compared with sham controls. (**Figure 32A**). This reduction in velocity (mm/s) was observed only for TAC-operated mice. Three weeks after TAC, evidence of cardiac hypertrophy was obvious between sham and TAC hearts from unstained Tie1-Cre-LacZ mice (**Figure 32B**).

X-gal stained hearts from Tie-Cre-LacZ mice did not show noticeable differences in EC-derived CM labeling patterns, compared with sham controls (**Figure 32C**). While hypertrophy and cardiac remodeling was obvious in TAC-operated mice, the appearance and location of the X-gal^{+} CM clusters did not differ significantly from uninjured controls. As expected, labeling of vasculature was observed in both groups throughout the atria and ventricles.

Ultimately, chronic pressure overload (lasting for 3 weeks) did not appear to affect the EC-derived CM regenerative process. Alternatively, this time period may not have been long enough to cause a significant difference in EC-derived X-gal^{+} CM clusters. To distinguish between these two scenarios, and determine if chronic hypertension and LV remodeling affect coronary niche EC-derived progenitor cells, a TAC experiment of longer duration (between 6-24 weeks) could be performed.

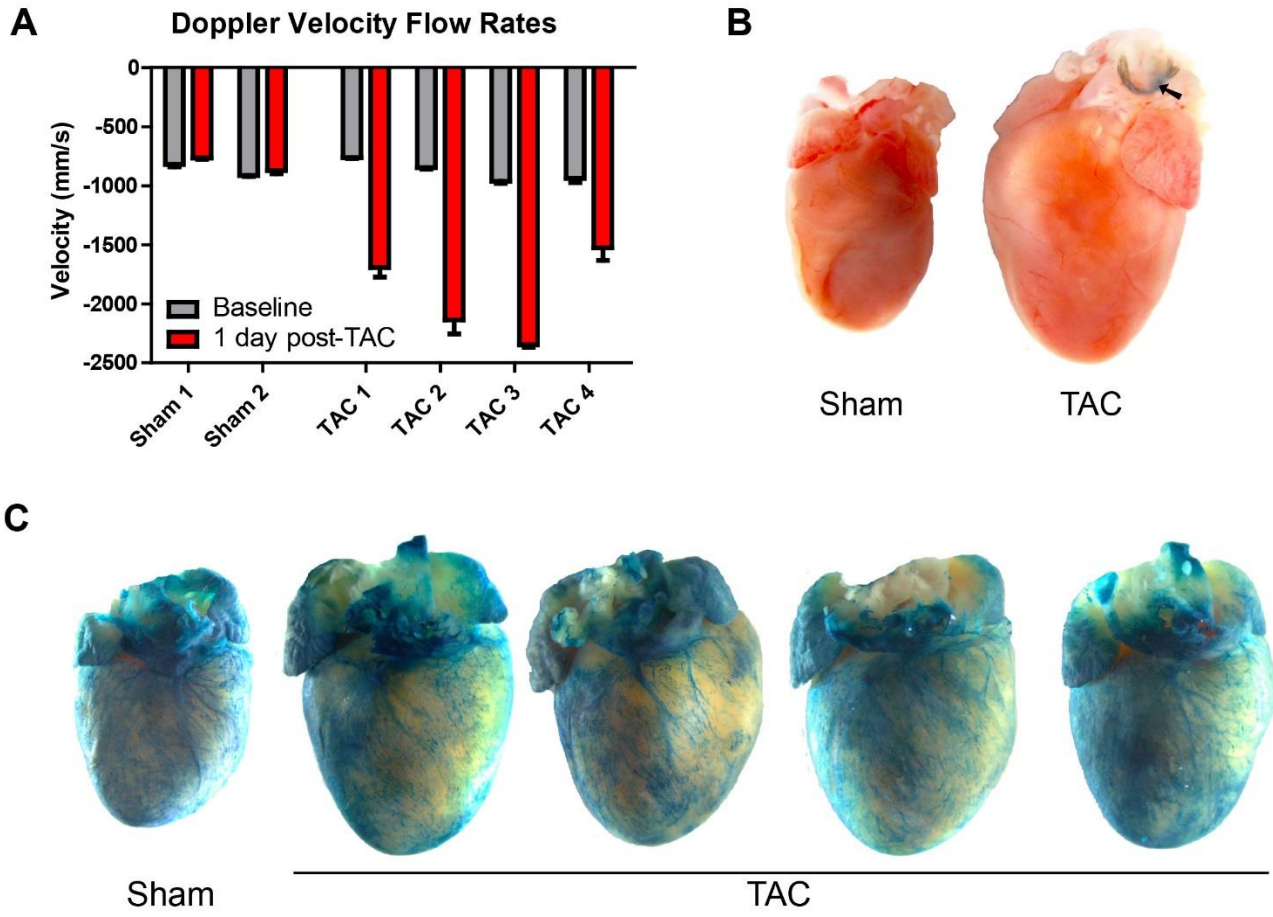

Figure 32. Transverse aortic constriction does not affect EC-derived CM clusters. **(A)** The histogram shows changes in Doppler flow rates (velocity, mm/s) from sham and TAC experimental Tie1-Cre-LacZ mice. **(B)** Hypertrophy of the heart is observed 3 weeks after aortic banding (TAC) in unstained Tie1-Cre-LacZ mouse hearts. Arrow indicates location of the band around the aorta. **(C)** X-gal stained Tie1-Cre-LacZ whole hearts do not show significant differences in EC-derived CM labeling patterns 3 weeks after TAC.

Since EC-derived X-gal^{+} CM clusters were not affected after 3 weeks of pressure overload via TAC, AngII was administered as an alternative method to induce hypertension. The potent effects of AngII, and subsequent increase in aldosterone, act in combination to cause significant systemic vasoconstriction. After 3 or more weeks, these mediators cause cardiac hypertrophy and ventricular remodeling.

To examine the effects of AngII-mediated hypertension on EC-derived myofibroblasts and CM clusters, Tie1-Cre-YFP mice were implanted with an AngII infusing osmotic pump. After approximately 4 weeks (26 days) of receiving AngII, mice were sacrificed and hearts removed. By comparison with sham controls, IF analysis of cardiac sections from mice implanted with the AngII-releasing osmotic pump indicated the number and locations of YFP^{+} CM clusters did not appear to change after AngII treatment (**Figure 33A**). Alternatively, an increase in total fibroblasts was observed in comparison with sham controls. Both EC-derived (YFP^{+}, FSP-1^{+}) and non-EC derived fibroblasts (YFP^{neg}, FSP-1^{+}) were observed within the myocardium and coronary adventitia after chronic AngII.

Fibroblasts within the coronary adventitial layer and ventricular myocardium were quantified (**Figure 33B**). After 26 days of AngII treatment, the proportion of EC derived FSP-1^{+} fibroblasts (YFP^{+}/FSP-1^{+}) was reduced. Conversely, the percentage of non-EC derived fibroblasts (YFP^{neg}/FSP-1^{+}) increased with AngII treatment. This pattern was consistent for both adventitial fibroblasts and the fibroblasts located within ventricular myocardial tissue.

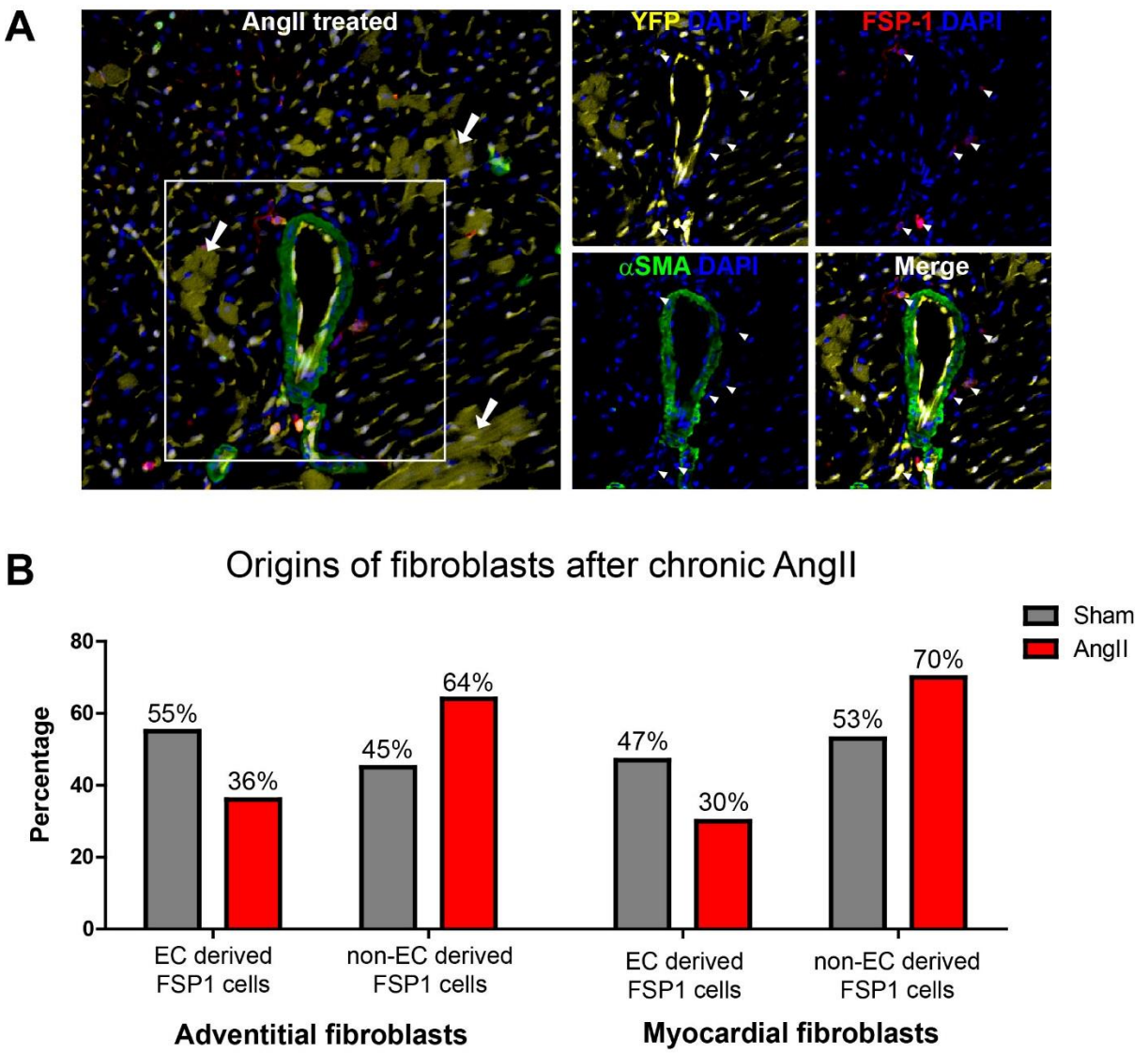

Figure 33. AngII-mediated hypertension increases the proportion of non-EC derived fibroblasts. (A) IF analysis from cardiac sections of Tie1-Cre-YFP mice after 26 day treatment with AngII shows clusters of EC-derived YFP^+ CMs (main panel), similar to sham controls (see Figure 8). Both EC and non-EC derived $FSP\text{-}1^+$ cells were found within the adventitial layer of coronary arteries (arrows, 4 inset panels). **(B)** Cardiac sections from Tie-Cre-YFP mice were used to quantify the proportion of EC or non-EC derived fibroblasts after 26 days of AngII treatment. Numbers of YFP^+, $FSP\text{-}1^+$ positive cells were compared with the total population of $FSP\text{-}1^+$ cells to calculate the percentage of EC-derived fibroblasts in the adventitial layer of coronary arteries ("Adventitial") and within the ventricular myocardial tissue ("Myocardial") in sham or AngII treated mice.

Preliminary IF analysis suggests that chronic administration of AngII does not significantly affect location or numbers of EC-derived CM clusters. However, the total number of fibroblasts within the myocardium and around coronary vessels increases with AngII treatment. Of these cells, the proportion of EC-derived fibroblasts is reduced after 26 days of AngII, while other non-EC derived fibroblast populations alternatively comprise a greater percentage of the FSP-1^{+} population. This outcome suggests that chronic, low-level injury may not stimulate an EC-derived fibrotic response. Instead, resident fibroblasts or BM-derived populations appear to respond to the cardiac hypertrophy and remodeling. Furthermore, EC-derived CM regeneration does not seem to be affected by chronic AngII. These findings are in contrast to the robust EndMT, and reduced CM renewal rates, observed after an acute, traumatic MI.

DISCUSSION

Acute versus chronic cardiac injuries ultimately elicit different reparative responses. Studies using endothelial lineage tracing models to explore the contribution of the vasculature during both of these processes also indicate unique EC responses to different injuries. Induction of acute myocardial infarction or chronic hypertension (pressure overload) in mice were used to explore the changes in coronary M and A cells, EC-derived CM renewal rates, as well as proliferation and origins of myofibroblasts.

After acute MI, a pro-fibrotic repair response is the natural process by which the heart heals, and involves a balance of angiogenesis and fibrosis. One week after MI, endothelial fate mapping using Tie1-Cre and End-SCL-CreER^{T} transgenic mice indicated approximately 35% of the infarct myofibroblasts have been derived through

EndMT. The remaining myofibroblasts originated from activated resident fibroblasts or from bone marrow-derived hematopoietic cells. This endothelial-derived population of myofibroblasts was observed only during the repair phase after cardiac injury, and not under conditions of homeostasis.

Interestingly, the EC-based cardiomyocyte regenerative process observed in the uninjured heart, decreases after MI. Analysis of EC-derived CM numbers within the myocardial tissue indicate a significant decrease compared with sham controls at both 1 and 3 weeks post-MI. Renewal rates have not recovered by 3 weeks after infarction, which may reflect a change in the environment of the coronary artery niche. Conditions of ischemia, and potential exposure to inflammatory mediators, may adversely affect cardiogenic M or A cell proliferation. Any hindrance to these intermediate cardiogenic populations would result in fewer EC-derived cardiomyocytes. Consequently, a better understanding of how injury impedes the EC-derived cardiogenic response could improve tissue regeneration after infarction.

One week after MI, FACS analysis of total cardiac YFP^{+} cell populations (which encompasses both EC and EC-derived cells) indicated a general proliferative response. First, proliferating YFP^{+} ECs were observed, and are likely contributing to angiogenesis within the maturing scar tissue. Without the restoration of blood flow to the wound, no repair cells would survive long enough to heal the injury. Second, the percentage of proliferating YFP^{+}, $CD31^{neg}$ non endothelial cells (A cells) increased, which may correspond to EC-derived myofibroblasts contributing to infarct repair through deposition of collagen. M cells did not appear to be significantly affected within the smooth muscle layer. Finally, there was an increase in the number of proliferating EC-

derived, Sca1^{+} A cells. Combined with the fact that CM regenerative rates decreased after MI, this cardiogenic population may alternatively undergo a fibrotic response and contribute to fibrosis under conditions of ischemia. The ability to repress this type of maladaptive fate change, would counteract the response to injury and might instead lead to formation of healthy cardiac tissue.

Chronic injury, induced through transverse aortic constriction or the vasoconstrictor angiotensin II, elicits a different repair response. Chronic hypertension via TAC did not appear to change the labeling pattern of EC-derived CM clusters. Analysis of whole hearts from Tie1-Cre-LacZ mice 3 weeks after aortic banding indicated X-gal^{+} vasculature and CM clusters were not significantly different than sham controls. This finding suggests artificial pressure overload may not induce enough damage to the myocardium to influence the coronary niche.

However, hypertension and cardiac hypertrophy, achieved through chronic administration of AngII, increased the proportion of non-EC derived fibroblasts in the ventricular myocardium and in the adventitial layer of coronary arteries. This increase in alternatively derived fibroblasts (i.e.: from resident fibroblasts or BM-derived) may have happened independently, or in addition to, a decrease in fibroblast production from EC derived populations. These data indicate low level injury to the myocardium may not affect EC-derived cardiac progenitors (M and A cells), but instead induce a fibrotic response from alternative cell populations.

CHAPTER V

IN VITRO KNOCKDOWN OF SCL/TAL1 INCREASES EXPRESSION OF GENES ASSOCIATED WITH IMMATURE CARDIOMYOCYTES

INTRODUCTION

Lineage tracing using three different endothelial specific promoters indicates endothelial cells retain cardiogenic potential in the adult myocardium. Previous studies have shown that ECs also possess cardiogenic potential during embryonic development. Vascular endothelial growth factor receptor 2 expressing progenitors are multipotent in the developing embryo and give rise to endothelial, smooth muscle, and cardiomyocyte lineages (Kattman *et al*., 2006). Furthermore, floxed removal of the transcriptional regulator SCL/TAL1 during development led to unexpected cardiomyogenesis in the yolk sac vasculature and endocardium (Van Handel *et al*., 2012). Without SCL, the hemogenic endothelium, which naturally generates hematopoietic progenitor cells, alternatively formed ectopic cardiomyocytes. This finding indicates SCL acts as a natural repressor of cardiac fate, in favor of endothelial and hematopoietic lineages.

Based on these data, I hypothesized that subpopulations of adult coronary endothelial cells retain cardiogenic ability, which is observable after down-regulation of SCL. The mouse cardiac endothelial cell (MCEC-1) line consists of immortalized ECs isolated from the hearts of H-2K^{b}-tsA58 mice, and serves as a robust cell line for *in vitro* culture and testing of this hypothesis (Lidington *et al*., 2002). MCECs were isolated from

transgenic mice containing a temperature-sensitive simian virus 40 large T antigen gene (tsA58 TAg), and proliferate under permissive conditions but enhance expression of mature EC characteristics under non-permissive conditions. Since the MCEC-1 line is a heterogenous population of cells, consisting of ECs from the coronary vessels, microvasculature, and endocardium, it is suitable for expansion and testing of the cardiogenic potential in cardiac coronary ECs.

EXPERIMENTAL METHODS

Cell culture

Conditionally immortalized murine cardiac endothelial cells were initially cultured under conditions permissive for proliferation (33^{o}C, with Interferon [IFN] γ). Cells were moved to non-permissive conditions (38^{o}C, no IFNγ) to enhance expression of endothelial characteristics in response to growth factors, and were used for experiments between the first and third passages. MCEC-1 cells were cultured in standard high-glucose DMEM containing 10% FBS, 20mM HEPES, 10 U/mL Heparin, and 30µg/mL EC growth supplement.

Cells were seeded in 12-well plates ($4x10^4$ cells/well), grown for 24 hours, and then transfected with 10pmol of a non-targeting negative control siRNA or with siRNA targeting SCL. The final concentration of siRNA was 10µM in 1mL total volume/well. Cells were treated with Noggin or PRDC at 300ng/mL or 120ng/mL, respectively. MCEC-1 cells were left in the transfection conditions for 48 hours (2 days), at which point the media was replaced and the transfection was continued using fresh reagents.

After 72 hours (3 days) total treatment time, cells were washed with 1X PBS and cultured in a “minimal component media” containing only standard high-glucose DMEM with 10% FBS and 20mM HEPES. After 96 hours (4 days) from the start of the siRNA knock-down experiment, cells were lysed for isolation of RNA.

RNA interference

siRNA gene expression knockdown studies were performed with the Lipofectamine RNAi-MAX Transfection Reagent (Invitrogen) and corresponding protocol. Each 21-mer siRNA was transfected into cells using Opti-MEM (Gibco) following the manufacturer’s guidelines. MISSION siRNA targeting SCL/TAL1 (Sigma; siRNA ID: SASI Mm01 00037684) was designed using the Rosetta Algorithm. The non-coding Silencer Select Negative Control No.1 siRNA (Invitrogen) was used as a negative control. A working concentration of 10μM was used for all experiments.

Real time quantitative RT-PCR

Total RNA was isolated from MCEC-1 cells using the RNeasy Mini Kit (Qiagen) following the manufacturers’ instructions. To reverse-transcribe RNA into cDNA, 3 μg of RNA was mixed with 100 ng oligo$(dT)_{15}$ and incubated for 5 minutes at 65°C. 1 mM dNTPs, 60 mM KCl, 15 mM Tris-Cl, pH 8.4, 3 mM MgCl2, 0.3% Tween 20, 10 mM β-mercaptoethanol, 10 U RNasin (Promega) and 100 U Mo-MLVRT (Invitrogen) were added, and the mix was incubated for 55 minutes at 37°C. The enzyme was inactivated

by incubating at 95°C for 5 minutes. Next, 20 ng cDNA was incubated with Taq DNA polymerase (Promega) and respective primers at 0.25 µM concentration for 35 cycles (1 minute at 95°C, 1 minute 60-65°C, and 1 minute 72°C). *Gapdh* was used as an internal control. Quantitative PCR was performed using the iQ SYBR Green Supermix kit (BioRad) on an iCycler (BioRad). Relative gene expression levels were quantified using the $2^{(-DDCt)}$ formula (Livak and Schmittgen, 2001).

The sequence of primers used for RT-PCR analysis was as follows: SCL/TAL1 5' (GGGATGAGAAGCAGGTCAATGG), 3' (CAAGCTGGATGGATCAACATGG); MLC-2A 5' (AAATCAGACCTGAAGGAGACCTATT), 3' (CAGAGAGACTTGTAGTCAATGTTGC); βMHC 5' (AATGCAGAGTCAGTGAAGGG), 3' (TCTTCCTGTCTTCCTCTGTCT); GapDH 5' (CTCACTCAAGATTGTCAGCAATG), 3' (GAGGGAGATGCTCAGTGTTGG).

RESULTS

Knockdown of SCL in MCECs induces expression of early cardiac genes

To determine if subpopulations of adult cardiac ECs possess cardiogenic potential *in vitro*, MCECs were cultured and treated with siRNA targeting the cardiogenic repressor SCL. MCECs were seeded and grown for 24 hours before transfection with siRNA targeting SCL. After either 2 or 4 days in culture with continuous exposure to the transfection reagent, no morphological differences were observed in the MCECs aside from changes in confluence due to cell proliferation (**Figure 34A**). Nonetheless, gene expression analysis indicated knock-down of SCL at both 2 and 4 days in culture, after transfection with anti-SCL siRNA but not with negative control, non-specific siRNA (**Figure 34B**).

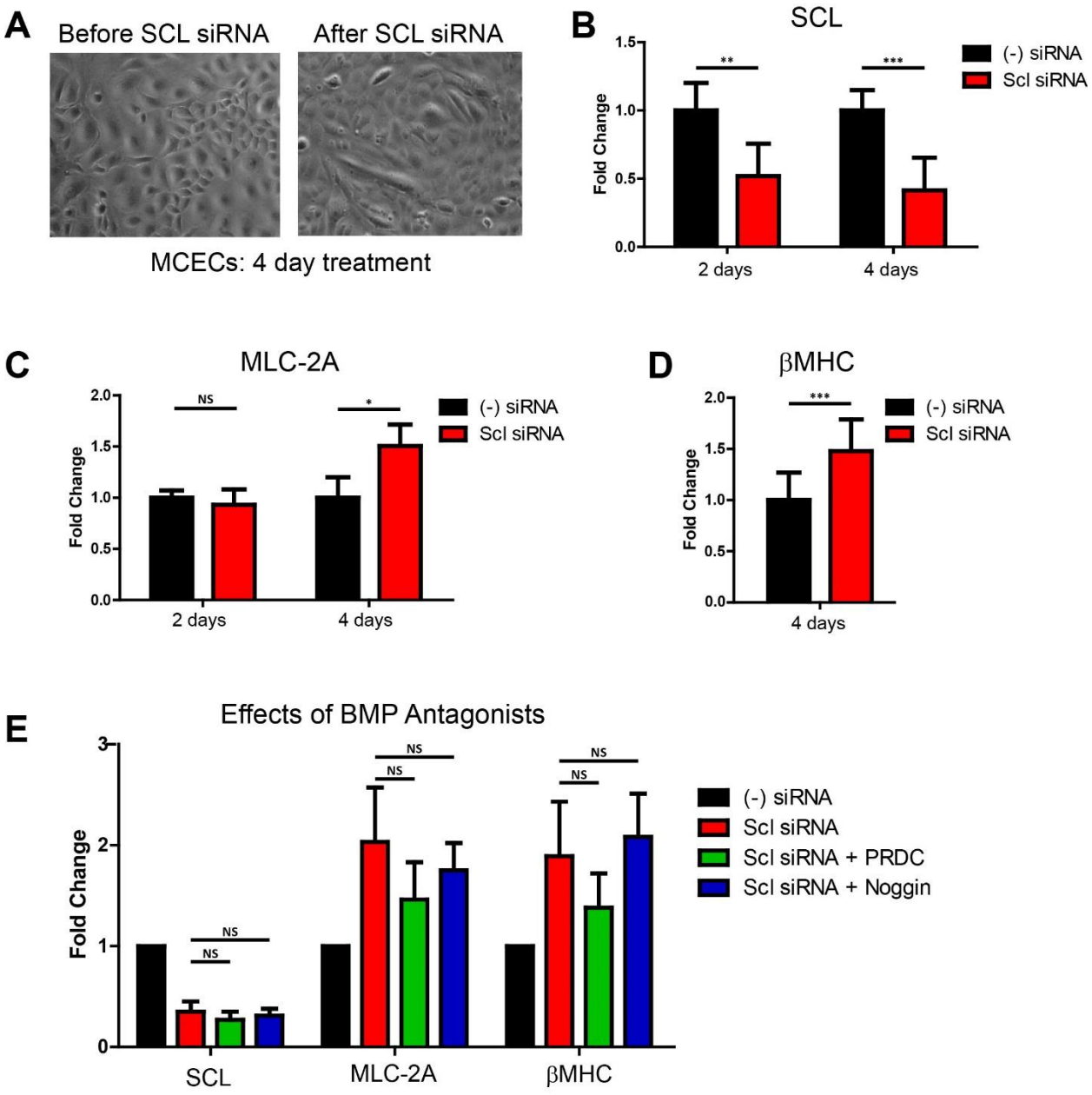

Figure 34. Knockdown of SCL/TAL1 in cultured MCECs induces expression of early cardiac genes. (A) MCECs were treated with siRNA targeting SCL/TAL1. After 96 hours (4 days) of culture, no obvious physical differences were noted in the cultured cells. **(B-D)** Quantitative real time RT-PCR analysis of RNA isolated from MCECs after 2 or 4 days of culture indicated expression levels of SCL/TAL1 decreased two-fold at both time points. Gene expression levels of MLC-2A (Myl7) and βMHC (Myh7) increased by 1.7 fold and 1.5 fold, respectively, after only after 4 days of culture. **(E)** Treatment with the BMP antagonists PRDC or Noggin did not significantly affect expression of SCL/TAL1, MLC-2A, or βMHC after continuous treatment for 96 hours (4 days) in culture.

Gene expression levels of the immature cardiomyocyte genes MLC-2A (Myl7) and βMHC (Myh7) showed a statistically significant increase after treatment with anti-SCL siRNA for 4 days in culture (**Figure 34C,D**). Notably, expression levels of MLC-2A did not rise until after a minimum of 2 days growth under conditions of low levels of SCL. Other mature cardiomyocytes genes (αMHC, α-Actinin, cardiac Troponin T) were not expressed at detectable levels in MCECs treated with anti-SCL or negative control siRNA.

The increase in immature cardiomyocyte gene expression levels after knockdown of SCL indicated MCECs may possess cardiogenic ability. However, analysis of gene expression levels indicated modest fold changes by comparison to controls. In attempt to bolster the cardiogenic response, co-treatment of MCECs with anti-SCL siRNA and a bone morphogenetic protein (BMP) antagonist was performed. The BMP pathway has been shown to maintain quiescence of stem and progenitor cells (Li and Clevers, 2010), and inhibition of this signaling cascade is one method of spurring proliferation of potential cardiogenic ECs.

MCECs were cultured for four days under continuous exposure to siRNA targeting SCL, and either the BMP antagonist Noggin or protein related to DAN and Cerberus (PRDC). While knock down of SCL was achieved in the presence or absence of BMP antagonists, no significant increase in early cardiac genes was observed through blockade of the BMP pathway (**Figure 34E**). Furthermore, while not statistically significant, PRDC appeared to reduce expression of MLC-2A and βMHC compared with untreated controls.

DISCUSSION

Several groups have demonstrated the cardiac potential of various progenitor populations *in vitro*, such as mesenchymal-like stem cells, and stem cells derived from the amniotic fluid or umbilical cord blood (Guan *et al*., 2011; Ryzhov *et al*., 2012; Khattab *et al*., 2013). While transplantation of these progenitor populations may improve cardiac function, oftentimes the positive outcomes are due to paracrine effects and not because of direct differentiation to cardiomyocytes (Hare and Chaparro, 2008). Thus, the ability to induce a novel population of endogenous, endothelial-derived cardiac progenitors to regenerate lost cardiac tissue after injury could have tremendous therapeutic potential. Reaching this goal requires a precise understanding of the molecular mechanisms which regulate this unique endothelial population.

Murine cardiac endothelial cells were found to express low levels of early cardiac genes after knockdown of SCL and four days in culture. While complete knock out of SCL in the developing embryo led to ectopic expression of cardiomyocytes, these results indicate SCL may continue to play a role in repressing cardiogenesis in adult ECs. The current challenge is to demonstrate more robust cardiogenic potential in MCECs, or primary ECs isolated directly from the adult heart. This may be achieved through treatment beyond 4 days, or exposure of the ECs to a more complicated cocktail of mediators (signaling proteins and/or small molecules) which perturb more than one transcriptional regulator or signaling pathway.

Interestingly, in the $SCL^{-/-}$ mouse embryo, MLC-2A (Myl7) was the highest induced cardiac-specific gene (Van Handel *et al*., 2012). Observing a statistically significant induction of this same gene after knockdown of SCL in adult MCECs

suggests it continues to act as a repressor of cardiogenesis. Similarly, upregulation of βMHC (Myh7) was observed after repression of SCL in both the developing mouse embryo and adult MCECs.

Since the BMP pathway maintains quiescence of progenitor cells, it was logical to assume that BMP antagonism would allow for proliferation of cardiogenic endothelial progenitors. However, co-treatment with the BMP antagonist PRDC appeared to repress expression of cardiogenic genes. This result was counterintuitive to the predicted outcome, and may indicate a lack of cardiogenic EC progenitors in the MCEC culture, or the requirement to simultaneously induce EC progenitor proliferation, such as through stimulation via canonical Wnt signaling.

CHAPTER VI

SUMMARY AND CONCLUSIONS

Perspective

Heart disease remains the leading cause of death in the world (Go *et al*., 2013). Current treatment for cardiovascular disease is focused on mitigating the symptoms, minimizing the risk factors, and delaying its progression. Increasing the level of oxygen to the myocardium while simultaneously reducing its oxygen demand helps to minimize stress from the ischemia imposed on the surviving tissue. However, while these techniques may assist with reducing the myocardial burden, they do not lead to regeneration of the lost tissue. Once cardiac tissue has been lost, it cannot be replaced.

Until recently, the heart was regarded as a post-mitotic organ, incapable of additional proliferation and woefully inadequate to replace lost cardiac tissue after injury. However, an increasing number of studies indicate the heart contains CM regenerative capacity and numerous populations of cardiac stem cells have been proposed to contribute to tissue regeneration. Stem cell antigen-1 (Sca1) and c-Kit expressing cells, side population (SP) cells, and cardiosphere-derived progenitor cells have all been shown to possess varying degrees of regenerative capacity (Aguirre *et al*., 2013). These stem/progenitor populations represent a viable source for cell-based therapy, but current methods have yet to achieve substantial rates of CM regeneration, especially in humans. As such, novel methods to improve recovery following ischemic injury are warranted, and may provide a more successful alternative to the less effective, current therapies.

Summary and Implications

These studies indicate endothelial cells serve as a cardiac progenitor population in the adult heart during homeostasis, but generate myofibroblasts for repair after cardiac injury. Lineage tracing using three different endothelial promoters (*Tie1*, *VE-Cadherin*, and endothelial 5'-*Scl*) each independently showed the same labeling pattern. Ultimately, the vasculature plays a dynamic and important role in the adult heart, and is influenced by the degree of myocardial damage and stress.

Using constitutive and inducible fate mapping strategies to track cells expressing endothelial genes in the uninjured adult mouse heart, we discovered ECs generate cells with cardiac stem cell characteristics. EC-derived cells were organized in a radial manner within coronary arteries, with quiescent and proliferative cells residing in the media and adventitia layers, respectively. Distal to the coronary niche, we identified labeled cardiomyocytes organized in clusters of single cell origin. EC pulse-chase experiments demonstrated CM renewal was rapid but spatially restricted. Our data reveal that cells with EC properties are part of the intrinsic cardiac renewal program, and that coronary arteries constitute a structural component of the cardiac stem cell niche.

An important finding of EC lineage tracing during cardiac homeostasis is the emergence of the coronary arteries as the site of the CSC niche. Previous studies show the vasculature is an integral component of most well characterized stem cell niches in various organs, such as the bone marrow and the subventricular zone in the brain (Li and Clevers, 2010). Our data suggest this biological strategy extends to the heart, with

the coronary vessels serving as the CSC niche. In support of this finding, vascular progenitor cells have been observed in the walls of coronary arteries in the human heart (Bearzi *et al*., 2009).

The molecular mechanisms which regulate endothelial progenitor fate within the coronary niche remain to be determined. Our data indicate that ECs, through the process of EndMT, are capable of generating cells with CSC characteristics in the uninjured, adult heart. We and others have shown that TGF-β/BMP and Wnt signaling regulate EndMT after injury, and it is likely these pathways also regulate the process during homeostasis (Zeisberg *et al*., 2007; Aisagbonhi *et al.*, 2011; (Chen *et al*., 2012). In addition, Sonic hedgehog (SHH) signaling has been shown to activate $Sca1^{+}$ cells with stem cell properties residing in the adventitia layer of the arterial wall, and may also influence cardiogenic EC fate (Passman *et al*., 2008).

Furthermore, the mechanisms which direct trafficking of the endothelial-derived cardiac progenitors remain elusive. It is possible that A cells enter the circulation and are recruited to distal heart areas by chemoattractants such as SDF-1, similarly to mesenchymal stem cells (Wynn *et al*., 2004; Laird *et al*., 2008). Alternatively, local gradients of chemoattractants may recruit EC-derived progenitors from their coronary niche.

After acute or chronic cardiac injury, the regenerative fate of endothelial cells changes and they alternatively contribute to repair of the myocardium. It is intriguing that adult ECs give rise to myofibroblasts after cardiac injury (Zeisberg *et al.*, 2007; Aisagbonhi *et al.*, 2011). The striking parallels on the origins of CSCs and

myofibroblasts raise the possibility the two processes are intrinsically linked. Thus, EC-derived CSCs may switch to a pro-fibrotic phenotype in the disease environment after injury, and alter their differentiation from CMs to myofibroblasts to preserve ventricular integrity. This scenario is reminiscent of the situation which occurs in skeletal muscle where myoblasts switch from a regenerative to a pro-fibrotic phenotype with aging (Brack *et al*., 2007).

The ability of endogenous cardiac cells to change fate based on their environment is further supported by an exciting finding which showed after cardiac injury, murine cardiac fibroblasts can be reprogrammed *in vivo* into CMs (Qian *et al*., 2012). Thus, the plasticity of cardiac fibroblasts and endothelial cells may be primarily determined by their environment and exposure to secreted factors. The notion that cell fate is largely determined by environmental signaling suggests it is possible to influence the regenerative capacity of ECs with the right combination of cellular mediators.

Ultimately, endothelial cells within the adult heart respond differently depending on their surrounding environment and overall condition of the myocardium (**Figure 35**). In the uninjured heart, an endothelial-marked cardiac progenitor cell expressing Tie1, VE-Cadherin, SCL, and Flk-1 (Kattman *et al*., 2006), gives rise to both ECs and cardiomyocytes (**Figure 35A**). These CPCs reside within the medial and adventitial layers of coronary arteries throughout the ventricular myocardium, and give rise to clusters of CMs found within both left and right ventricles. Approximately 0.3% of CMs in the entire adult mouse heart are derived from this unique cardiac progenitor source, but rates of regional CM replacement reflect a greater regenerative rate. While the signaling mechanisms regulating this process remain to be determined, a

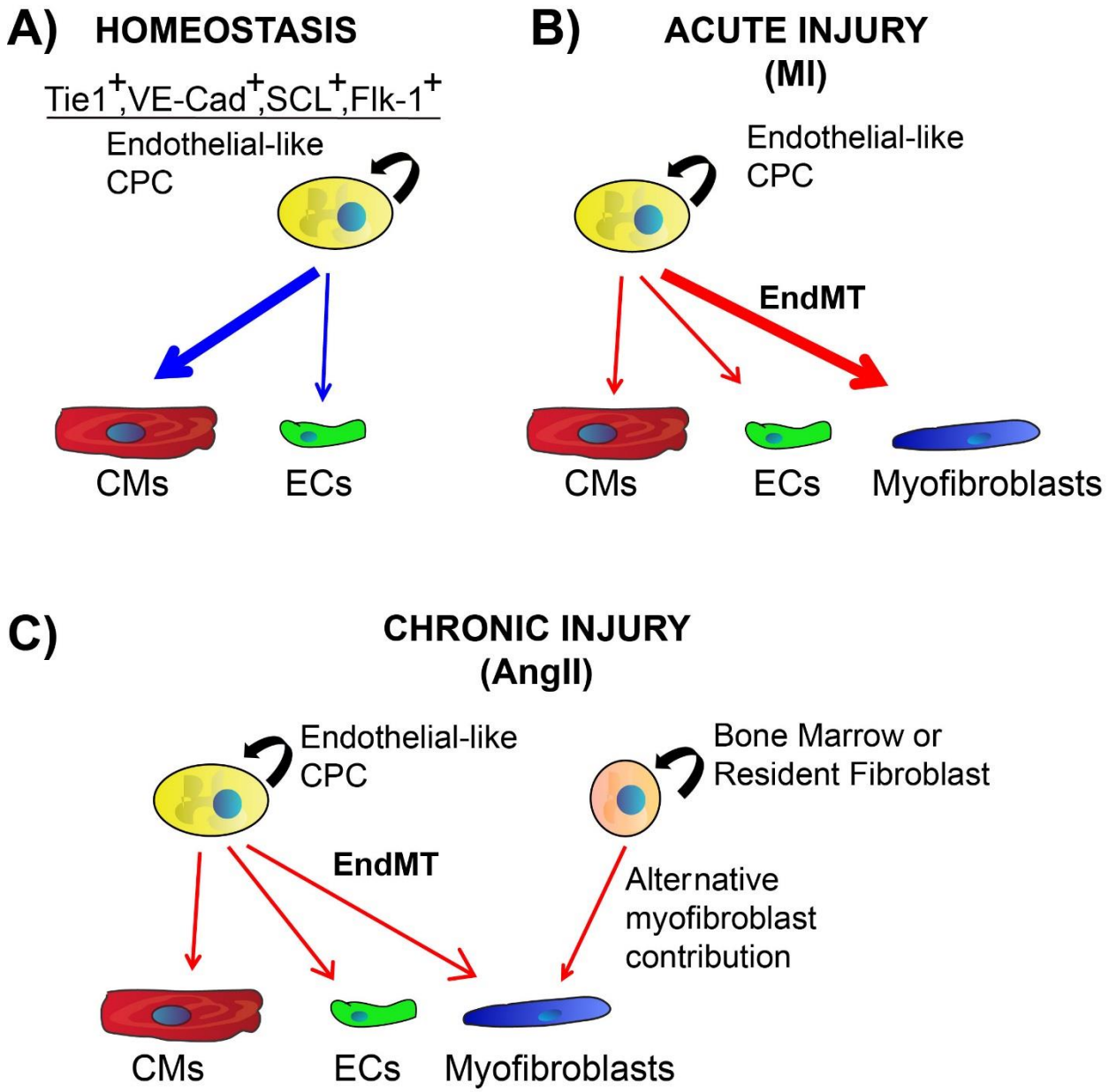

Figure 35, MODEL. Endothelial contribution to cardiac regeneration and repair in the adult heart. (A, Homeostasis) In the uninjured heart, endothelial-derived cardiac progenitor cells expressing Tie1, VE-Cadherin, SCL, and Flk-1 (VEGFR2) generate ECs and CMs (thick blue arrow). **(B, Acute Injury)** After ischemic injury, such as MI, regenerative rates decrease and endothelial cells alternatively generate myofibroblasts (thick red arrow). **(C, Chronic Injury)** Non-ischemic injuries, such as hypertension induced through AngII, reduce the endothelial contribution to myofibroblasts. These cells instead are generated from non-EC sources such as resident fibroblasts or bone marrow-derived cells. Abbreviations: myocardial infarction (MI); transverse aortic constriction (TAC); angiotensin II (AngII).

“cardiogenic EndMT” is the means by which the endothelial-derived CPCs gradually develop into mature cardiomyocytes.

The fate of endothelial cells changes after an ischemic injury such as a myocardial infarction. During the granulation tissue repair phase, ECs alternatively generate myofibroblasts through a “fibrogenic EndMT” (**Figure 35B**). Concurrently, the number of EC-derived CMs decreases. FACS analysis also showed an increase in the percentage of $YFP^+/Sca1^+$ cells (cardiac progenitor A cells). Therefore, EC-derived CPCs may give rise to myofibroblasts instead of CMs after acute ischemic injury.

Considering that approximately 30% of infarct myofibroblasts are derived from an endothelial origin, this EC fate change after MI represents a novel opportunity for improving recovery after ischemic injury. Understanding the molecular mechanisms that regulate the EndMT which generates endothelial-derived fibroblasts could minimize maladaptive fibrosis. Minimizing or inhibiting this EC fibrotic fate switch may instead promote formation of CMs for regeneration of beneficial, contractile myocardial tissue.

Interestingly, ECs respond differently under chronic, non-ischemic injury by comparison with the acute, traumatic injury induced by MI. After AngII-induced hypertension in the adult heart, the proportion of EC-derived fibroblasts in the myocardium and surrounding the coronary arteries decreases in comparison with sham controls (**Figure 35C**). Fibroblasts are instead derived from non-EC sources, such as the bone marrow or resident populations within the myocardium.

Chronic injury induces a less robust “fibrogenic EndMT” in comparison with that caused by MI and its subsequent ischemic damage. Understanding how these two

types of injuries affect the extent of EndMT and the contribution of EC-derived myofibroblasts to the heart will provide greater insight into the role of the vasculature during cardiac repair. These different cellular outcomes, which depend on the type of cardiac injury, may originate based on environmental changes which affect the coronary niche. Here, the fate of M and A cells, and resulting CMs or myofibroblasts, seems to be uniquely regulated based on the specific environment in which they reside.

Our model may also provide novel insight into how coronary arterial disease can lead to heart failure. It is likely that inflammation, oxidative stress, ischemia, calcification, and fibrosis around coronary vessels negatively impact the niche environment, disturbing the normal proliferation and differentiation of CSCs. This effect could compromise cardiac homeostasis, weaken the heart muscle, and eventually lead to hypertrophy and remodeling. Therefore, our findings may open novel opportunities to establish the intrinsic cardiac molecular mechanisms, and identify factors that prevent a pro-fibrotic fate switch after injury in favor of cardiac regeneration.

Limitations

Collectively, the data presented here during cardiac homeostasis, and the results showing ECs contribute to angiogenesis and fibrosis after injury, indicate ECs remain multipotent in the adult. However, it is not clear if this is a universal property of mature cardiac ECs, or confined to specific EC subpopulations within coronary arteries. It is also likely that a multipotent cardiovascular stem cell expressing EC markers exists in the adult and is genetically labeled using EC lineage tracing approaches. Finally, the cardiogenic endothelium may represent one mechanism of cardiac regeneration, but

our findings do not exclude proliferation of resident CMs, or alternative sources of CSCs (Senyo *et al*., 2013; Malliaras *et al*., 2013).

Furthermore, although the proposed model is consistent with the observed data, alternative interpretations may also explain the pattern of the lineage tracing results. For example, low level expression of endothelial genes in cardiac fibroblasts with cardiogenic potential could account for some of the observed labeling patterns. Or, as mentioned above, rare proliferating CMs may transiently express endothelial genes, and thus become labeled before expansion. While we did not observe expression of endothelial markers in fibroblasts and CMs, we cannot fully exclude these possibilities.

Future Directions

While numerous types of cardiac stem cell populations have been identified in the adult heart, they lack a substantial regenerative response after injury. We have identified a subset of endothelial cells in the adult heart which possess cardiogenic potential under conditions of homeostasis. After acute ischemic injury, cardiomyocyte regenerative rates from this cell population decreased significantly. Alternatively, activated myofibroblasts are generated, leading to repair of the injury, at the cost of beneficial regeneration.

To date, there are no effective/robust methods for regenerating myocardial tissue after injury. Myocardial infarction is the most common cause of cardiac injury and results in the permanent loss of cardiomyocytes. This can lead to heart failure and death. Thus, continued studies designed to characterize and enhance the regenerative potential of endogenous cardiac stem cell populations in the adult heart are warranted.

To better understand the unique endothelial-derived CPCs, it will be important to isolate and analyze this population before and after injury. Transcriptional-based profiling of coronary niche M cells (YFP^{+}, $CD31^{neg}$, αSMA^{+}) and A cells (YFP^{+}, $CD31^{neg}$, $Sca1^{+}$) under different conditions will elucidate their distinct genetic profiles in the uninjured heart and after acute or chronic injury. In addition, isolation and *in vitro* culture of these populations will allow for study of the molecular mechanisms used for their regulation. Mediators found to be influential from initial transcriptional screening can be used to direct cell differentiation. Ultimately, any differences in regulatory mediators or signaling pathways may lead to novel treatments to enhance the regenerative response, instead of reparative response, of EC-derived CPCs after injury.

It will also be important to examine how inflammation affects the vascular-derived cardiac progenitor cell population. Inflammatory mediators likely prevent a regenerative response, and instead induce an EC reparative fate through formation of myofibroblasts. *In situ* analysis of the coronary niche M and A cell populations after acute (MI) or chronic (AngII, TAC) injury may identify a 'fork-in-the-road' crucial time period during repair in which these progenitor cells are directed towards a particular maladaptive cell fate.

Finally, to induce significant rates of CM regeneration, it will be necessary to develop a better understanding of the molecular signaling mechanisms and pathways (Wnt, BMP, Notch, SHH, *etc*.) which regulate this progenitor population. Developing mediators, including small molecules or proteins, which directly target the regenerative capacity of the EC-derived CPC populations may provide significant benefit during recovery after cardiac injury. Ultimately, to promote regeneration of lost cardiac tissue

and reduce the risk of cardiac remodeling and heart failure after injury, we must find a way to enhance the rates of CM regeneration from all available cardiac progenitor cell populations.

APPENDIX A

Antibody	Species	Dilution	1º/ 2º	Company	Catalog Number
Anti-α-Actinin	Mouse	1:800	1º	Sigma	A7811
Anti-c-Kit	Rabbit	1:50	1º	Santa Cruz	sc5535
Anti-CD31	Rat	1:100	1º	BD Biosciences	553370
Anti-Collagen-IV	Rabbit	1:500	1º	Abcam	Ab6586
Anti-Connexin43 (GJA1)	Rabbit	1:100	1º	Abcam	Ab11370
Anti-Cre	Mouse	1:400	1º	Abcam	Ab24607
Anti-F4/80	Rat	1:100	1º	Abcam	Ab6640
Anti-FSP1 (S100A4)	Rabbit	1:200	1º	Abcam	Ab27957
Anti-Gata4	Rabbit	1:100	1º	Santa Cruz	sc9053
Anti-GFP#	Rabbit	1:3000	1º	Abcam	Ab290
Anti-phospho Histone H3	Rabbit	1:500	1º	Santa Cruz	sc8656
Anti-Ki67	Rabbit	1:100	1º	Abcam	Ab15580
Anti-N-Cadherin	Mouse	1:100	1º	Sigma	C2542
Anti-Sca1 (Ly6)	Goat	1:100	1º	R&D	AF1226
Anti-α-SMA	Mouse	1:800	1º	Sigma	A2547
Anti-Snail	Mouse	1:600	1º	EMD Millipore	MABE167
Anti-Tie1	Rabbit	1:100	1º	Santa Cruz	sc342
Anti-Rabbit Alexa-Fluor488	Donkey	1:400	2º	Invitrogen	A21206
Anti-Goat Alexa-Fluor488	Donkey	1:400	2º	Invitrogen	A11001
Anti-Rabbit Cy3	Donkey	1:400	2º	Jackson ImmunoResearch	711-165-152
Anti-Mouse Cy3	Goat	1:400	2º	Jackson ImmunoResearch	115-165-146
Anti-Rat Cy3	Donkey	1:400	2º	Jackson ImmunoResearch	712-165-153
Anti-Mouse Cy5	Goat	1:400	2º	Jackson ImmunoResearch	115-176-146
Anti-Rabbit Cy5	Goat	1:400	2º	Jackson ImmunoResearch	111-175-144
Anti-Rat Alexa-Fluor647	Donkey	1:400	2º	Jackson ImmunoResearch	712-605-150

Table 2. Primary and secondary antibodies used for histological analysis. The table includes the species, company, catalog number, and various dilutions of antibodies in blocking solution. To visualize and quantify individual cells, sections were counter-stained nuclei with the nucleophilic dye 4',6-diamidino-2-phenylindole (DAPI; 1:6000; Invitrogen).

REFERENCES

Adler, C.P., Friedburg, H., Herget, G.W., Neuburger, M., and Schwalb, H. (1996). Variability of cardiomyocyte DNA content, ploidy level and nuclear number in mammalian hearts. Virchows Arch. Int. J. Pathol. *429*, 159–164.

Aguirre, A., Sancho-Martinez, I., and Izpisua Belmonte, J.C. (2013). Reprogramming toward Heart Regeneration: Stem Cells and Beyond. Cell Stem Cell *12*, 275–284.

Aisagbonhi, O., Rai, M., Ryzhov, S., Atria, N., Feoktistov, I., and Hatzopoulos, A.K. (2011). Experimental myocardial infarction triggers canonical Wnt signaling and endothelial-to-mesenchymal transition. Dis. Model. Mech. *4*, 469–483.

Alfaro, M.P., Pagni, M., Vincent, A., Atkinson, J., Hill, M.F., Cates, J., Davidson, J.M., Rottman, J., Lee, E., and Young, P.P. (2008). The Wnt modulator sFRP2 enhances mesenchymal stem cell engraftment, granulation tissue formation and myocardial repair. Proc. Natl. Acad. Sci. U. S. A. *105*, 18366–18371.

Alva, J.A., Zovein, A.C., Monvoisin, A., Murphy, T., Salazar, A., Harvey, N.L., Carmeliet, P., and Iruela-Arispe, M.L. (2006). VE-Cadherin-Cre-recombinase transgenic mouse: a tool for lineage analysis and gene deletion in endothelial cells. Dev. Dyn. Off. Publ. Am. Assoc. Anat. *235*, 759–767.

Anversa, P., Kajstura, J., Leri, A., and Bolli, R. (2006). Life and Death of Cardiac Stem Cells A Paradigm Shift in Cardiac Biology. Circulation *113*, 1451–1463.

Arciniegas, E., Frid, M.G., Douglas, I.S., and Stenmark, K.R. (2007). Perspectives on endothelial-to-mesenchymal transition: potential contribution to vascular remodeling in chronic pulmonary hypertension. Am. J. Physiol. - Lung Cell. Mol. Physiol. *293*, L1–L8.

Bearzi, C., Rota, M., Hosoda, T., Tillmanns, J., Nascimbene, A., Angelis, A.D., Yasuzawa-Amano, S., Trofimova, I., Siggins, R.W., LeCapitaine, N., *et al*. (2007). Human cardiac stem cells. Proc. Natl. Acad. Sci. *104*, 14068–14073.

Bearzi, C., Leri, A., Monaco, F.L., Rota, M., Gonzalez, A., Hosoda, T., Pepe, M., Qanud, K., Ojaimi, C., Bardelli, S., *et al*. (2009). Identification of a coronary vascular progenitor cell in the human heart. Proc. Natl. Acad. Sci. pnas.0907622106.

Beltrami, A.P., Urbanek, K., Kajstura, J., Yan, S.-M., Finato, N., Bussani, R., Nadal-Ginard, B., Silvestri, F., Leri, A., Beltrami, C.A., *et al*. (2001). Evidence That Human Cardiac Myocytes Divide after Myocardial Infarction. N. Engl. J. Med. *344*, 1750–1757.

Beltrami, A.P., Barlucchi, L., Torella, D., Baker, M., Limana, F., Chimenti, S., Kasahara, H., Rota, M., Musso, E., Urbanek, K., *et al*. (2003). Adult cardiac stem cells are multipotent and support myocardial regeneration. Cell *114*, 763–776.

Bergmann, O., Bhardwaj, R.D., Bernard, S., Zdunek, S., Barnabé-Heider, F., Walsh, S., Zupicich, J., Alkass, K., Buchholz, B.A., Druid, H., *et al*. (2009). Evidence for cardiomyocyte renewal in humans. Science *324*, 98–102.

Bernstein, H.S., and Srivastava, D. (2012). Stem cell therapy for cardiac disease. Pediatr. Res. *71*, 491–499.

Biernacka, A., and Frangogiannis, N.G. (2011). Aging and Cardiac Fibrosis. Aging Dis. *2*, 158–173.

Boudoulas, K.D., and Hatzopoulos, A.K. (2009). Cardiac repair and regeneration: the Rubik's cube of cell therapy for heart disease. Dis. Model. Mech. *2*, 344–358.

Bowman, A.N., van Amerongen, R., Palmer, T.D., and Nusse, R. (2013). Lineage tracing with Axin2 reveals distinct developmental and adult populations of Wnt/β-catenin-responsive neural stem cells. Proc. Natl. Acad. Sci. U. S. A. *110*, 7324–7329.

Brack, A.S., Conboy, M.J., Roy, S., Lee, M., Kuo, C.J., Keller, C., and Rando, T.A. (2007). Increased Wnt signaling during aging alters muscle stem cell fate and increases fibrosis. Science *317*, 807–810.

Chen, P.-Y., Qin, L., Barnes, C., Charisse, K., Yi, T., Zhang, X., Ali, R., Medina, P.P., Yu, J., Slack, F.J., *et al*. (2012). FGF regulates TGFβ signaling and endothelial-to-mesenchymal transition via control of let-7 miRNA expression. Cell Rep. *2*, 1684–1696.

Decimo, I., Bifari, F., Krampera, M., and Fumagalli, G. (2012). Neural Stem Cell Niches in Health and Diseases. Curr. Pharm. Des. *18*, 1755–1783.

Dey, D., Han, L., Bauer, M., Sanada, F., Oikonomopoulos, A., Hosoda, T., Unno, K., De Almeida, P., Leri, A., and Wu, J.C. (2013). Dissecting the molecular relationship among various cardiogenic progenitor cells. Circ. Res. *112*, 1253–1262.

Doevendans, P.A., Daemen, M.J., Muinck, E.D. de, and Smits, J.F. (1998). Cardiovascular phenotyping in mice. Cardiovasc. Res. *39*, 34–49.

Dominguez, D., Montserrat-Sentis, B., Virgos-Soler, A., Guaita, S., Grueso, J., Porta, M., Puig, I., Baulida, J., Franci, C., and Garcia de Herreros, A. (2003). Phosphorylation Regulates the Subcellular Location and Activity of the Snail Transcriptional Repressor. Mol. Cell. Biol. *23*, 5078–5089.

Ellison, G.M., Torella, D., Karakikes, I., and Nadal-Ginard, B. (2007). Myocyte death and renewal: modern concepts of cardiac cellular homeostasis. Nat. Clin. Pract. Cardiovasc. Med. *4*, S52–S59.

Ellison, G.M., Vicinanza, C., Smith, A.J., Aquila, I., Leone, A., Waring, C.D., Henning, B.J., Stirparo, G.G., Papait, R., Scarfò, M., *et al*. (2013). Adult c-kitpos Cardiac Stem Cells Are Necessary and Sufficient for Functional Cardiac Regeneration and Repair. Cell *154*, 827–842.

Frangogiannis, N.G. (2008). The immune system and cardiac repair. Pharmacol. Res. Off. J. Ital. Pharmacol. Soc. *58*, 88–111.

Frangogiannis, N.G. (2012). Regulation of the inflammatory response in cardiac repair. Circ. Res. *110*, 159–173.

Frangogiannis, N.G. (2014). The inflammatory response in myocardial injury, repair, and remodelling. Nat. Rev. Cardiol. *11*, 255–265.

Fuentealba, L.C., Obernier, K., and Alvarez-Buylla, A. (2012). Adult neural stem cells bridge their niche. Cell Stem Cell *10*, 698–708.

Garcia, J., Sandi, M.J., Cordelier, P., Binétruy, B., Pouysségur, J., Iovanna, J.L., and Tournaire, R. (2012). Tie1 deficiency induces endothelial-mesenchymal transition. EMBO Rep. *13*, 431–439.

Gerhardt, H., Golding, M., Fruttiger, M., Ruhrberg, C., Lundkvist, A., Abramsson, A., Jeltsch, M., Mitchell, C., Alitalo, K., Shima, D., *et al*. (2003). VEGF guides angiogenic sprouting utilizing endothelial tip cell filopodia. J. Cell Biol. *161*, 1163–1177.

Ghosh, A.K., Nagpal, V., Covington, J.W., Michaels, M.A., and Vaughan, D.E. (2012). Molecular basis of cardiac endothelial-to-mesenchymal transition (EndMT): differential expression of microRNAs during EndMT. Cell. Signal. *24*, 1031–1036.

Gnecchi, M., He, H., Liang, O.D., Melo, L.G., Morello, F., Mu, H., Noiseux, N., Zhang, L., Pratt, R.E., Ingwall, J.S., *et al*. (2005). Paracrine action accounts for marked protection of ischemic heart by Akt-modified mesenchymal stem cells. Nat. Med. *11*, 367–368.

Go, A.S., Mozaffarian, D., Roger, V.L., Benjamin, E.J., Berry, J.D., Blaha, M.J., Dai, S., Ford, E.S., Fox, C.S., Franco, S., *et al*. (2013). Heart Disease and Stroke Statistics—2014 Update A Report From the American Heart Association. Circulation 01.cir.0000441139.02102.80.

Göthert, J.R., Gustin, S.E., van Eekelen, J.A.M., Schmidt, U., Hall, M.A., Jane, S.M., Green, A.R., Göttgens, B., Izon, D.J., and Begley, C.G. (2004). Genetically tagging endothelial cells in vivo: bone marrow-derived cells do not contribute to tumor endothelium. Blood *104*, 1769–1777.

Greif, D.M., Kumar, M., Lighthouse, J.K., Hum, J., An, A., Ding, L., Red-Horse, K., Espinoza, F.H., Olson, L., Offermanns, S., *et al*. (2012). Radial construction of an arterial wall. Dev. Cell *23*, 482–493.

Guan, X., Delo, D.M., Atala, A., and Soker, S. (2011). In Vitro Cardiomyogenic Potential of Human Amniotic Fluid Stem Cells. J. Tissue Eng. Regen. Med. *5*, 220–228.

Gustafsson, E., Brakebusch, C., Hietanen, K., and Fässler, R. (2001). Tie-1-directed expression of Cre recombinase in endothelial cells of embryoid bodies and transgenic mice. J. Cell Sci. *114*, 671–676.

Van Handel, B., Montel-Hagen, A., Sasidharan, R., Nakano, H., Ferrari, R., Boogerd, C.J., Schredelseker, J., Wang, Y., Hunter, S., Org, T., *et al*. (2012). Scl represses cardiomyogenesis in prospective hemogenic endothelium and endocardium. Cell *150*, 590–605.

Hare, J.M., and Chaparro, S.V. (2008). Cardiac regeneration and stem cell therapy. Curr. Opin. Organ Transplant. *13*, 536–542.

Hierlihy, A.M., Seale, P., Lobe, C.G., Rudnicki, M.A., and Megeney, L.A. (2002). The post-natal heart contains a myocardial stem cell population. FEBS Lett. *530*, 239–243.

Hinkel, R., El-Aouni, C., Olson, T., Horstkotte, J., Mayer, S., Müller, S., Willhauck, M., Spitzweg, C., Gildehaus, F.-J., Münzing, W., *et al*. (2008). Thymosin beta4 is an essential paracrine factor of embryonic endothelial progenitor cell-mediated cardioprotection. Circulation *117*, 2232–2240.

Hollier, B.G., Evans, K., and Mani, S.A. (2009). The epithelial-to-mesenchymal transition and cancer stem cells: a coalition against cancer therapies. J. Mammary Gland Biol. Neoplasia *14*, 29–43.

Janssens, S., Dubois, C., Bogaert, J., Theunissen, K., Deroose, C., Desmet, W., Kalantzi, M., Herbots, L., Sinnaeve, P., Dens, J., *et al*. (2006). Autologous bone marrow-derived stem-cell transfer in patients with ST-segment elevation myocardial infarction: double-blind, randomised controlled trial. Lancet *367*, 113–121.

Jiang, H., and Edgar, B.A. (2012). Intestinal stem cell function in Drosophila and mice. Curr. Opin. Genet. Dev. *22*, 354–360.

Joggerst, S.J., and Hatzopoulos, A.K. (2009). Stem cell therapy for cardiac repair: benefits and barriers. Expert Rev. Mol. Med. *11*, e20.

Jones, D.L., and Wagers, A.J. (2008). No place like home: anatomy and function of the stem cell niche. Nat. Rev. Mol. Cell Biol. *9*, 11–21.

Kajstura, J., Rota, M., Hosoda, T., Anversa, P., and Leri, A. (2012). Response to Bergmann *et al*: Carbon 14 Birth Dating of Human Cardiomyocytes. Circ. Res. *110*, e19–e21.

Karamitsos, T.D., and Neubauer, S. (2013). The prognostic value of late gadolinium enhancement CMR in nonischemic cardiomyopathies. Curr. Cardiol. Rep. *15*, 326.

Kattman, S.J., Huber, T.L., and Keller, G.M. (2006). Multipotent flk-1+ cardiovascular progenitor cells give rise to the cardiomyocyte, endothelial, and vascular smooth muscle lineages. Dev. Cell *11*, 723–732.

Khattab, R.A.M., Khorshied, M.M.A., Abdel Shafy, S.S., El Ansary, M.S., and Moukhtar, M.S. (2013). In vitro transdifferentiation of umbilical cord stem cells into cardiac myocytes: Role of growth factors. Egypt. J. Crit. Care Med. *1*, 43–50.

Kopinke, D., Brailsford, M., Shea, J.E., Leavitt, R., Scaife, C.L., and Murtaugh, L.C. (2011). Lineage tracing reveals the dynamic contribution of Hes1+ cells to the developing and adult pancreas. Dev. Camb. Engl. *138*, 431–441.

Korhonen, J., Lahtinen, I., Halmekytö, M., Alhonen, L., Jänne, J., Dumont, D., and Alitalo, K. (1995). Endothelial-specific gene expression directed by the tie gene promoter in vivo. Blood *86*, 1828–1835.

Kriegstein, A., and Alvarez-Buylla, A. (2009). The glial nature of embryonic and adult neural stem cells. Annu. Rev. Neurosci. *32*, 149–184.

Laflamme, M.A., and Murry, C.E. (2011). Heart regeneration. Nature *473*, 326–335.

Lahat, G., Zhu, Q.-S., Huang, K.-L., Wang, S., Bolshakov, S., Liu, J., Torres, K., Langley, R.R., Lazar, A.J., Hung, M.C., *et al*. (2010). Vimentin is a novel anti-cancer therapeutic target; insights from in vitro and in vivo mice xenograft studies. PloS One *5*, e10105.

Laird, D.J., von Andrian, U.H., and Wagers, A.J. (2008). Stem cell trafficking in tissue development, growth, and disease. Cell *132*, 612–630.

Lancrin, C., Sroczynska, P., Stephenson, C., Allen, T., Kouskoff, V., and Lacaud, G. (2009). The haemangioblast generates haematopoietic cells through a haemogenic endothelium stage. Nature *457*, 892–895.

Leri, A., Kajstura, J., and Anversa, P. (2011). Role of cardiac stem cells in cardiac pathophysiology: a paradigm shift in human myocardial biology. Circ. Res. *109*, 941–961.

Li, L., and Clevers, H. (2010). Coexistence of Quiescent and Active Adult Stem Cells in Mammals. Science *327*, 542–545.

Lidington, E.A., Rao, R.M., Marelli-Berg, F.M., Jat, P.S., Haskard, D.O., and Mason, J.C. (2002). Conditional immortalization of growth factor-responsive cardiac endothelial cells from H-2K(b)-tsA58 mice. Am. J. Physiol. Cell Physiol. *282*, C67–74.

Livak, K.J., and Schmittgen, T.D. (2001). Analysis of relative gene expression data using real-time quantitative PCR and the 2(-Delta Delta C(T)) Method. Methods San Diego Calif *25*, 402–408.

Lugert, S., Vogt, M., Tchorz, J.S., Müller, M., Giachino, C., and Taylor, V. (2012). Homeostatic neurogenesis in the adult hippocampus does not involve amplification of Ascl1(high) intermediate progenitors. Nat. Commun. *3*, 670.

Malliaras, K., Zhang, Y., Seinfeld, J., Galang, G., Tseliou, E., Cheng, K., Sun, B., Aminzadeh, M., and Marbán, E. (2013). Cardiomyocyte proliferation and progenitor cell recruitment underlie therapeutic regeneration after myocardial infarction in the adult mouse heart. EMBO Mol. Med. *5*, 191–209.

Mani, S.A., Guo, W., Liao, M.-J., Eaton, E.N., Ayyanan, A., Zhou, A.Y., Brooks, M., Reinhard, F., Zhang, C.C., Shipitsin, M., *et al*. (2008). The epithelial-mesenchymal transition generates cells with properties of stem cells. Cell *133*, 704–715.

Martin, C.M., Meeson, A.P., Robertson, S.M., Hawke, T.J., Richardson, J.A., Bates, S., Goetsch, S.C., Gallardo, T.D., and Garry, D.J. (2004). Persistent expression of the ATP-binding cassette transporter, Abcg2, identifies cardiac SP cells in the developing and adult heart. Dev. Biol. *265*, 262–275.

Martin-Puig, S., Wang, Z., and Chien, K.R. (2008). Lives of a Heart Cell: Tracing the Origins of Cardiac Progenitors. Cell Stem Cell *2*, 320–331.

Medici, D., Shore, E.M., Lounev, V.Y., Kaplan, F.S., Kalluri, R., and Olsen, B.R. (2010). Conversion of vascular endothelial cells into multipotent stem-like cells. Nat. Med. *16*, 1400–1406.

Messina, E., De Angelis, L., Frati, G., Morrone, S., Chimenti, S., Fiordaliso, F., Salio, M., Battaglia, M., Latronico, M.V.G., Coletta, M., *et al*. (2004). Isolation and expansion of adult cardiac stem cells from human and murine heart. Circ. Res. *95*, 911–921.

Mirotsou, M., Zhang, Z., Deb, A., Zhang, L., Gnecchi, M., Noiseux, N., Mu, H., Pachori, A., and Dzau, V. (2007). Secreted frizzled related protein 2 (Sfrp2) is the key Akt-mesenchymal stem cell-released paracrine factor mediating myocardial survival and repair. Proc. Natl. Acad. Sci. *104*, 1643–1648.

Moore, K.A., and Lemischka, I.R. (2006). Stem cells and their niches. Science *311*, 1880–1885.

Moorman, A.F.M., Christoffels, V.M., Anderson, R.H., and van den Hoff, M.J.B. (2007). The heart-forming fields: one or multiple? Philos. Trans. R. Soc. Lond. B. Biol. Sci. *362*, 1257–1265.

Mouquet, F., Pfister, O., Jain, M., Oikonomopoulos, A., Ngoy, S., Summer, R., Fine, A., and Liao, R. (2005). Restoration of Cardiac Progenitor Cells After Myocardial Infarction by Self-Proliferation and Selective Homing of Bone Marrow–Derived Stem Cells. Circ. Res. *97*, 1090–1092.

Murphy, E., and Steenbergen, C. (2008). Mechanisms underlying acute protection from cardiac ischemia-reperfusion injury. Physiol. Rev. *88*, 581–609.

Murry, C.E., and Lee, R.T. (2009). Turnover After the Fallout. Science *324*, 47–48.

Murry, C.E., Soonpaa, M.H., Reinecke, H., Nakajima, H., Nakajima, H.O., Rubart, M., Pasumarthi, K.B.S., Virag, J.I., Bartelmez, S.H., Poppa, V., *et al*. (2004). Haematopoietic stem cells do not transdifferentiate into cardiac myocytes in myocardial infarcts. Nature *428*, 664–668.

Nakamura-Ishizu, A., and Suda, T. (2012). Hematopoietic stem cell niche: An interplay among a repertoire of multiple functional niches. Biochim. Biophys. Acta BBA - Gen. Subj.

Neeland, I.J., Drazner, M.H., Berry, J.D., Ayers, C.R., deFilippi, C., Seliger, S.L., Nambi, V., McGuire, D.K., Omland, T., and de Lemos, J.A. (2013). Biomarkers of chronic cardiac injury and hemodynamic stress identify a malignant phenotype of left ventricular hypertrophy in the general population. J. Am. Coll. Cardiol. *61*, 187–195.

Oh, H., Bradfute, S.B., Gallardo, T.D., Nakamura, T., Gaussin, V., Mishina, Y., Pocius, J., Michael, L.H., Behringer, R.R., Garry, D.J., *et al*. (2003). Cardiac progenitor cells from adult myocardium: homing, differentiation, and fusion after infarction. Proc. Natl. Acad. Sci. U. S. A. *100*, 12313–12318.

Okabe, M., Ikawa, M., Kominami, K., Nakanishi, T., and Nishimune, Y. (1997). “Green mice” as a source of ubiquitous green cells. FEBS Lett. *407*, 313–319.

Passman, J.N., Dong, X.R., Wu, S.-P., Maguire, C.T., Hogan, K.A., Bautch, V.L., and Majesky, M.W. (2008). A sonic hedgehog signaling domain in the arterial adventitia supports resident Sca1+ smooth muscle progenitor cells. Proc. Natl. Acad. Sci. U. S. A. *105*, 9349–9354.

Person, A.D., Klewer, S.E., and Runyan, R.B. (2005). Cell biology of cardiac cushion development. Int. Rev. Cytol. *243*, 287–335.

Pfister, O., Mouquet, F., Jain, M., Summer, R., Helmes, M., Fine, A., Colucci, W.S., and Liao, R. (2005). CD31− but Not CD31+ Cardiac Side Population Cells Exhibit Functional Cardiomyogenic Differentiation. Circ. Res. *97*, 52–61.

Qian, L., Huang, Y., Spencer, C.I., Foley, A., Vedantham, V., Liu, L., Conway, S.J., Fu, J., and Srivastava, D. (2012). In vivo reprogramming of murine cardiac fibroblasts into induced cardiomyocytes. Nature *485*, 593–598.

Reinecke, H., Poppa, V., and Murry, C.E. (2002). Skeletal muscle stem cells do not transdifferentiate into cardiomyocytes after cardiac grafting. J. Mol. Cell. Cardiol. *34*, 241–249.

Rota, M., Padin-Iruegas, M.E., Misao, Y., Angelis, A.D., Maestroni, S., Ferreira-Martins, J., Fiumana, E., Rastaldo, R., Arcarese, M.L., Mitchell, T.S., *et al*. (2008). Local Activation or Implantation of Cardiac Progenitor Cells Rescues Scarred Infarcted Myocardium Improving Cardiac Function. Circ. Res. *103*, 107–116.

Ryzhov, S., Goldstein, A.E., Novitskiy, S.V., Blackburn, M.R., Biaggioni, I., and Feoktistov, I. (2012). Role of A2B adenosine receptors in regulation of paracrine functions of stem cell antigen 1-positive cardiac stromal cells. J. Pharmacol. Exp. Ther. *341*, 764–774.

Sangiorgi, E., and Capecchi, M.R. (2008). Bmi1 is expressed in vivo in intestinal stem cells. Nat. Genet. *40*, 915–920.

Scadden, D.T. (2006). The stem-cell niche as an entity of action. Nature *441*, 1075–1079.

Schächinger, V., Erbs, S., Elsässer, A., Haberbosch, W., Hambrecht, R., Hölschermann, H., Yu, J., Corti, R., Mathey, D.G., Hamm, C.W., *et al*. (2006). Intracoronary bone marrow-derived progenitor cells in acute myocardial infarction. N. Engl. J. Med. *355*, 1210–1221.

Schofield, R. (1978). The relationship between the spleen colony-forming cell and the haemopoietic stem cell. Blood Cells *4*, 7–25.

Segers, V.F.M., and Lee, R.T. (2008). Stem-cell therapy for cardiac disease. Nature *451*, 937–942.

Senyo, S.E., Steinhauser, M.L., Pizzimenti, C.L., Yang, V.K., Cai, L., Wang, M., Wu, T.-D., Guerquin-Kern, J.-L., Lechene, C.P., and Lee, R.T. (2013). Mammalian heart renewal by pre-existing cardiomyocytes. Nature *493*, 433–436.

Shi, X., and Garry, D.J. (2006). Muscle stem cells in development, regeneration, and disease. Genes Dev. *20*, 1692–1708.

Simari, R.D., Moyé, L.A., Skarlatos, S.I., Ellis, S.G., Zhao, D.X.M., Willerson, J.T., Henry, T.D., and Pepine, C.J. (2010). Development of a network to test strategies in cardiovascular cell delivery: the NHLBI-sponsored Cardiovascular Cell Therapy Research Network (CCTRN). J Cardiovasc. Transl. Res. *3*, 30–36.

Singh, R.P., Raina, K., Sharma, G., and Agarwal, R. (2008). Silibinin inhibits established prostate tumor growth, progression, invasion, and metastasis and suppresses tumor angiogenesis and epithelial-mesenchymal transition in transgenic adenocarcinoma of the mouse prostate model mice. Clin. Cancer Res. Off. J. Am. Assoc. Cancer Res. *14*, 7773–7780.

Smith, R.R., Barile, L., Cho, H.C., Leppo, M.K., Hare, J.M., Messina, E., Giacomello, A., Abraham, M.R., and Marbán, E. (2007). Regenerative Potential of Cardiosphere-Derived Cells Expanded From Percutaneous Endomyocardial Biopsy Specimens. Circulation *115*, 896–908.

Snider, P., Olaopa, M., Firulli, A.B., and Conway, S.J. (2007). Cardiovascular development and the colonizing cardiac neural crest lineage. ScientificWorldJournal *7*, 1090–1113.

Snippert, H.J., van der Flier, L.G., Sato, T., van Es, J.H., van den Born, M., Kroon-Veenboer, C., Barker, N., Klein, A.M., van Rheenen, J., Simons, B.D., *et al*. (2010). Intestinal Crypt Homeostasis Results from Neutral Competition between Symmetrically Dividing Lgr5 Stem Cells. Cell *143*, 134–144.

Soriano, P. (1999). Generalized lacZ expression with the ROSA26 Cre reporter strain. Nat. Genet. *21*, 70–71.

Srinivas, S., Watanabe, T., Lin, C.-S., William, C.M., Tanabe, Y., Jessell, T.M., and Costantini, F. (2001). Cre reporter strains produced by targeted insertion of EYFP and ECFP into the ROSA26 locus. BMC Dev. Biol. *1*, 4.

Thiery, J.P., Acloque, H., Huang, R.Y.J., and Nieto, M.A. (2009). Epithelial-mesenchymal transitions in development and disease. Cell *139*, 871–890.

Thomson, J.A., Itskovitz-Eldor, J., Shapiro, S.S., Waknitz, M.A., Swiergiel, J.J., Marshall, V.S., and Jones, J.M. (1998). Embryonic stem cell lines derived from human blastocysts. Science *282*, 1145–1147.

Tian, H., Biehs, B., Warming, S., Leong, K.G., Rangell, L., Klein, O.D., and de Sauvage, F.J. (2011). A reserve stem cell population in small intestine renders Lgr5-positive cells dispensable. Nature *478*, 255–259.

Timmerman, L.A., Grego-Bessa, J., Raya, A., Bertran, E., Perez-Pomares, J.M., Diez, J., Aranda, S., Palomo, S., McCormick, F., Izpisua-Belmonte, J.C., *et al*. (2004). Notch promotes epithelial-mesenchymal transition during cardiac development and oncogenic transformation. Genes Dev. *18*, 99–115.

Traverse, J.H., Henry, T.D., Vaughan, D.E., Vaughn, D.E., Ellis, S.G., Pepine, C.J., Willerson, J.T., Zhao, D.X.M., Piller, L.B., Penn, M.S., *et al*. (2009). Rationale and design for TIME: A phase II, randomized, double-blind, placebo-controlled pilot trial evaluating the safety and effect of timing of administration of bone marrow mononuclear cells after acute myocardial infarction. Am. Heart J. *158*, 356–363.

Traverse, J.H., Henry, T.D., Vaughan, D.E., Ellis, S.G., Pepine, C.J., Willerson, J.T., Zhao, D.X.M., Simpson, L.M., Penn, M.S., Byrne, B.J., *et al*. (2010). LateTIME. Tex. Heart Inst. J. *37*, 412–420.

Traverse, J.H., Henry, T.D., Ellis, S.G., Pepine, C.J., Willerson, J.T., Zhao, D.X.M., Forder, J.R., Byrne, B.J., Hatzopoulos, A.K., Penn, M.S., *et al*. (2011). Effect of intracoronary delivery of autologous bone marrow mononuclear cells 2 to 3 weeks following acute myocardial infarction on left ventricular function: the LateTIME randomized trial. JAMA J. Am. Med. Assoc. *306*, 2110–2119.

Traverse, J.H., Henry, T.D., Pepine, C.J., Willerson, J.T., Zhao, D.X.M., Ellis, S.G., Forder, J.R., Anderson, R.D., Hatzopoulos, A.K., Penn, M.S., *et al*. (2012). Effect of the use and timing of bone marrow mononuclear cell delivery on left ventricular function after acute myocardial infarction: the TIME randomized trial. JAMA J. Am. Med. Assoc. *308*, 2380–2389.

Tumbar, T. (2004). Defining the Epithelial Stem Cell Niche in Skin. Science *303*, 359–363.

Uchida, S., De Gaspari, P., Kostin, S., Jenniches, K., Kilic, A., Izumiya, Y., Shiojima, I., grosse Kreymborg, K., Renz, H., Walsh, K., *et al*. (2013). Sca1-Derived Cells Are a Source of Myocardial Renewal in the Murine Adult Heart. Stem Cell Rep. *1*, 397–410.

Vinh, A., Chen, W., Blinder, Y., Weiss, D., Taylor, W.R., Goronzy, J.J., Weyand, C.M., Harrison, D.G., and Guzik, T.J. (2010). Inhibition and genetic ablation of the B7/CD28 T-cell costimulation axis prevents experimental hypertension. Circulation *122*, 2529–2537.

Wada, T., Sakai, N., Sakai, Y., Matsushima, K., Kaneko, S., and Furuichi, K. (2011). Involvement of bone-marrow-derived cells in kidney fibrosis. Clin. Exp. Nephrol. *15*, 8–13.

Wagers, A.J., and Conboy, I.M. (2005). Cellular and Molecular Signatures of Muscle Regeneration: Current Concepts and Controversies in Adult Myogenesis. Cell *122*, 659–667.

Wang, X., Hu, Q., Nakamura, Y., Lee, J., Zhang, G., From, A.H.L., and Zhang, J. (2006). The role of the sca-1+/CD31- cardiac progenitor cell population in postinfarction left ventricular remodeling. Stem Cells Dayt. Ohio *24*, 1779–1788.

Winter, E.M., and Gittenberger-de Groot, A.C. (2007). Epicardium-derived cells in cardiogenesis and cardiac regeneration. Cell. Mol. Life Sci. CMLS *64*, 692–703.

Wynn, T.A. (2008). Cellular and molecular mechanisms of fibrosis. J. Pathol. *214*, 199–210.

Wynn, R.F., Hart, C.A., Corradi-Perini, C., O'Neill, L., Evans, C.A., Wraith, J.E., Fairbairn, L.J., and Bellantuono, I. (2004). A small proportion of mesenchymal stem cells strongly expresses functionally active CXCR4 receptor capable of promoting migration to bone marrow. Blood *104*, 2643–2645.

Zeisberg, E.M., and Kalluri, R. (2010). Origins of Cardiac Fibroblasts. Circ. Res. *107*, 1304–1312.

Zeisberg, E.M., Tarnavski, O., Zeisberg, M., Dorfman, A.L., McMullen, J.R., Gustafsson, E., Chandraker, A., Yuan, X., Pu, W.T., Roberts, A.B., *et al*. (2007). Endothelial-to-mesenchymal transition contributes to cardiac fibrosis. Nat. Med. *13*, 952–961.

Zeisberg, E.M., Potenta, S.E., Sugimoto, H., Zeisberg, M., and Kalluri, R. (2008). Fibroblasts in kidney fibrosis emerge via endothelial-to-mesenchymal transition. J. Am. Soc. Nephrol. JASN *19*, 2282–2287.

Zhu, P., Huang, L., Ge, X., Yan, F., Wu, R., and Ao, Q. (2006). Transdifferentiation of pulmonary arteriolar endothelial cells into smooth muscle-like cells regulated by myocardin involved in hypoxia-induced pulmonary vascular remodelling. Int. J. Exp. Pathol. *87*, 463–474.

Extra References from Fig.3 legend – <u>(will be removed in final pdf document)</u>

(A) HFSC niche: (Tumbar, 2004)
(B) ISC niche: (Moore and Lemischka, 2006); (Jiang and Edgar, 2012); (Sangiorgi and Capecchi, 2008); (Tian *et al*., 2011)
(C) BM niche: (Nakamura-Ishizu and Suda, 2012)
(D) NSC niche (SVZ, SGZ): (Decimo *et al*., 2012); (Fuentealba *et al*., 2012); (Kriegstein and Alvarez-Buylla, 2009); (Lugert *et al*., 2012)